이학박사학위논문

통증 감각의 말초 병태생리 기전

: 세포 기전 및 단일 세포 전사체 프로파일링에 관한 연구

Peripheral Mechanisms of Nociception in Pathophysiological Conditions

: Studies on Cellular Mechanisms and Single-Cell Transcriptional Profiling

2020년 8월

서울대학교 대학원

자연과학대학 뇌인지과학과 전공

이 파 름

ABSTRACT

Peripheral Mechanisms of Nociception in Pathophysiological Conditions : Studies on Cellular Mechanisms and Single-Cell Transcriptional Profiling

Pa Reum Lee
Graduate School of Natural Science
Seoul National University
Brain and Cognitive Sciences Major

Pain sensations experienced in the body, as well as in the orofacial region, convey to the central nervous system (CNS) by peripheral sensory neurons such as the dorsal root ganglion (DRG) and the trigeminal ganglion (TG). Nociceptive pain, called *nociception*, begins at peripheral nerve endings of specialized peripheral sensory neurons known as nociceptors, which exclusively respond to noxious stimuli. Up to date, it has been well studied how the distinct nociceptors respond to various noxious stimuli such as heat, cold, chemical, or mechanical. However, it remains relatively little understood on mechanisms for how innocuous or non-painful stimuli, which would never be considered noxious, can cause pain. In this study, I have explored these polymodalities of nociception that may be elicited by

innocuous stimuli or endogenous mediators of inflammation in several pathophysiological conditions as below.

In the first chapter, I examined the contribution of peripheral γ–aminobutyric acid type A receptor ($GABA_AR$) that may be activated by endogenous GABA produced in the inflamed tissue to inflammatory pain. Using complete Freund's adjuvant (CFA)-induced persistent inflammatory pain mouse model, I demonstrated that CFA-induced spontaneous nociceptive behavior and mechanical hypersensitivity were inhibited by intraplantar (i.pl.) injection of $GABA_AR$ antagonists. Moreover, local blockage of endogenous GABA with injection (i.pl.) of anti-GABA antibody attenuated CFA-induced mechanical hypersensitivity, whereas, i.pl. injection of a positive allosteric modulator of $GABA_AR$ facilitated mechanical allodynia in naïve mice. These findings suggest that peripheral $GABA_AR$ signaling contributes to CFA-induced hypersensitivity, and its modulation can potentially be a therapeutic target for inflammatory pain alleviation.

In the second chapter, I investigated cellular mechanisms by which sweet substances excite dental primary afferent (DPA) neurons, thereby leading dentin hypersensitivity. Sweet substances contain high sugar concentrations so that they cause hyperosmolar conditions at the teeth. I thus demonstrated that the transient receptor potential cation channel, subfamily M, member 8 (TRPM8), a well-known cold- and menthol-receptor, also served as a hyperosmosensor in DPA neurons. By applying a hyperosmolar sucrose solution to the mouse exposed tooth dentin, I investigated whether TRPM8 in DPA neurons mediates upregulation of c-fos expression as a marker of hyperosmolarity-induced nociception in the CNS level. I showed that hyperosmolarity-induced dental nociception was significantly attenuated by

a selective TRPM8 antagonist, implying innocuous stimuli such as sweet substances can be sufficient to result in dental nociception via TRPM8 channels.

In recent years, an increasing number of studies have successfully applied single-cell transcriptomics to characterize a population of cells and to identify rare subtypes or novel therapeutic targets in heterogeneous sensory system. In the third chapter, I thus employed transcriptional profiling using single-cell RNA sequencing (scRNA-seq) and specific gene-expression validation with *in situ* hybridization in order to identify unique molecular signatures in the adult mouse DPA neurons. The single-cell transcriptome analysis detected six distinct clusters of DPA neurons. Interestingly, a particular cluster of DPA neurons was characterized by high expression of a low-threshold mechanosensitive *Piezo2* ion channel and a pain-related neuropeptide *Calca* encoding CGRP (calcitonin gene-related peptide). These findings provide an insight into one of the previously proposed mechanisms underlying dentin hypersensitivity (i.e., hydrodynamic theory; Brännström and Astroem 1964), which is a common occurrence by innocuous mechanical irritations such as brush or air puffs. I further discussed mechanosensitive ion channels that may play critical roles in generating pain within the tooth pulp and their clinical implications.

Keyword: pain; nociceptor; mechanistic study; single-cell RNA-sequencing; $GABA_AR$; TRPM8; dorsal root ganglion neuron; dental primary afferent neuron

Student Number: 2015-22670

CONTENTS

LIST OF FIGURES

Background

CHAPTER 1

CHAPTER 2

CHAPTER 3

LIST OF TABLES

ABBREVIATIONS

3α,5α-THP	3α,5α-tetrahydroprogesterone
AMTB	N-(3-Aminopropyl)-2-[(3-methylphenyl)methoxy]-N-(2-thienylmethyl)benzamide hydrochloride
Bicuculline	1(S),9(R)-(-)-Bicuculline methiodide
CFA	complete Freund's adjuvant
CNS	central nervous system
DiI	1,1′-Dioctadecyl-3,3,3′,3′-tetramethylindocarbocyanine perchlorate
DRG	dorsal root ganglion
DPA	dental primary afferent
GABA	γ–aminobutyric acid
$GABA_AR$	γ–aminobutyric acid type A receptor
GAD	glutamate decarboxylase
KCC2	K-Cl cotransporter 2
NKCC1	Na-K-Cl cotransporter 1
PNS	peripheral nervous system
scRNA-seq	single-cell RNA sequencing
scRT-PCR	single-cell reverse transcription polymerase chain reaction
TG	trigeminal ganglion
TRPM8	transient receptor potential cation channel, subfamily M, member 8

BACKGROUND

1. Pain Sensation and Peripheral Mechanisms of Nociception

Pain sensation experienced in the body, as well as the craniofacial region, comprises four major steps: transduction, transmission, modulation, and perception (**Fig. 1A**). The sensation of pain usually starts from specialized peripheral sensory neurons known as nociceptors, which are subsets of the dorsal root ganglion (DRG) or the trigeminal ganglion (TG). District nociceptors generate action potentials at nerve endings innervating the skin in response to different modalities of noxious stimuli, for example, TRPV1 (> 45℃ heat), ASIC (chemical), TREK-1 (mechanical), and TRPM8 (cold) (**Fig. 1B**). This initial step is referred to the transduction. The pain signals are sequentially carried to the brainstem and the spinal cord (transmission), are perceived as consequences of that inputs in the brain as pain (perception), and are simultaneously regulated by modulatory circuits in the spinal cord (modulation) (Institute of Medicine (US) Committee on Pain 1987, Scholz and Woolf 2002).

Nociceptive pain, called *nociception*, plays fundamental roles in protecting us from dangerous stimuli at the skin so that nociceptors mostly have high thresholds for responses, implying that they are activated by noxious or painful stimuli rather than innocuous or non-painful stimuli (Dubin and Patapoutian 2010, Gold and Gebhart 2010). For example, high-threshold nociceptors are responsible for extremely noxious stimuli, such as

heat, cold, chemical, and mechanical, but not light tactile stimuli such as touch and brush. In contrast, innocuous mechanical stimuli activate low-threshold mechanoreceptors.

Despite these principle roles of nociception, several studies have demonstrated that low-threshold mechanoreceptors are involved in nociception under certain pathophysiological conditions. For example, low-threshold mechanoreceptors can participate in *mechanical allodynia*, a term used to describe pain caused by innocuous stimuli like light touch that would never be considered noxious under normal conditions (Lolignier, Eijkelkamp, and Wood 2015). On the other hand, so-called “silent” high-threshold nociceptors characterized by their complete insensitivity to mechanical stimulation can be activated after only exposure to inflammation or nerve injury (Dubin and Patapoutian 2010, Belmonte and Viana 2009). Therefore, understanding the mechanisms for how innocuous or non-painful stimuli transmit pain signals is necessary to provide therapeutic intervention for pain management.

2. Roles of Peripheral $GABA_A$ Receptors

$GABA_AR$ (γ-aminobutyric acid type A receptor) is an ionotropic receptor and belongs to a subfamily of ligand-gated chloride channels. Its endogenous ligand is GABA (γ–aminobutyric acid), which plays an essential role in regulating neuronal activity as a major inhibitory neurotransmitter in the mammalian brain; it has been primary therapeutic benefits for the treatment of various psychiatric disorders such as anxiety, insomnia, and epilepsy (Uusi-Oukari and Korpi 2010). $GABA_AR$ forms as pentameric assemblies of subunits (**Fig. 2Aa, Ab**), and 19 different subunits have been described to date (α1-6, β1-3, γ1-3, δ, ε, θ, π, and ρ1-3, **Fig. 2Ac**) in humans (Simon et al. 2004) and rodents (Olsen and Sieghart 2008). Importantly, the functional roles of $GABA_ARs$ depend on their subunit composition (**Fig. 2Ad**) and cellular or subcellular location (Olsen and Sieghart 2009, Sieghart 1995). Accordingly, targeting specific subtypes of $GABA_AR$ has been effective therapeutic benefits for developing associated drugs.

It has been demonstrated that $GABA_ARs$ are expressed not only in the CNS but also in the PNS. Their inhibitory actions can be shifted to excitatory in the adult primary sensory neurons (Levy 1977, Price et al. 2009) or under certain pathophysiological conditions such as developmental stage (Ben-Ari 2002) and pathology (Coull et al. 2005). These excitatory effects depend on two major transmembrane cotransporters for controlling intracellular chloride concentration ($[Cl^-]_{in}$) (**Fig. 2B**): NKCC1 (Na-K-Cl cotransporter 1), which accumulates Cl^- intracellularly, and KCC2 (K-Cl cotransporter 2), which extrudes it from the cell (Price et al. 2009, Herbison and Moenter 2011). Since peripheral sensory neurons, such as DRG and TG, maintain a high $[Cl^-]_{in}$ as a result of the higher expression of NKCC1 and lack of KCC2, the activation

of $GABA_AR$ results in peripheral primary afferent depolarization (PAD) in rodents and humans (Price, Hargreaves, and Cervero 2006, Carr et al. 2010, Sung 2000). This phenomenon implies that $GABA_AR$ produces a net excitatory effect rather than inhibition in peripheral sensory neurons.

Interestingly, several reports have suggested that intraplantar injection of a high-dose of $GABA_AR$ agonists, such as GABA and muscimol, can increase pain hypersensitivity in the formalin-induced acute inflammatory pain model (Bravo-Hernandez et al. 2014, Carlton, Zhou, and Coggeshall 1999, Jang et al. 2017). In addition, a previous paper has demonstrated that spinal injection of a $GABA_AR$ antagonist gabazine results in analgesia in the CFA-induced persistent inflammation (Anseloni and Gold 2008), suggesting that $GABA_AR$-mediated signals can be effective toward facilitating pain hypersensitivity in both acute and persistent inflammatory conditions. Furthermore, peripheral $GABA_AR$ is endogenously modulated by a variety of neurosteroids like pregnane steroids (Belelli and Lambert 2005, Magnaghi et al. 2006). Therefore, understanding the shifting roles of $GABA_AR$ in peripheral sensory neurons and their modulatory effects on pain hypersensitivity may offer a way to provide therapeutic strategies for alleviating inflammatory pain.

3. Mechanisms of Dentin Hypersensitivity

Dental nociception, more precisely *dentin hypersensitivity*, is sudden and intense pain. Dentin hypersensitivity occurs when tooth dentin is exposed during eating, drinking, and brushing (Dababneh, Khouri, and Addy 1999). It mostly results from noxious stimuli such as hot and cold temperature; however, it can be frequently followed by innocuous stimuli such as air puffs, water spray, sugar consumption, and sometimes even breath (Dababneh, Khouri, and Addy 1999, Chung, Jung, and Oh 2013). Indeed, tooth or tooth pulp produces only pain regardless of stimulation with noxious or innocuous stimuli.

Dental nociception conveys to the CNS by nociceptors at nerve endings of DPA neurons innervating tooth pulp. It has been revealed that a variety of nociceptors in DPA neurons are responsible for various noxious stimuli, such as thermal (transient receptor potential (TRP) channels), chemical (acid-sensing ion channels (ASICs)), and ATP (P2X purinergic receptors), in humans and rodents (Hossain et al. 2019, Lee et al. 2019). Despite the identification of these nociceptors, understanding the mechanisms of dental nociception is complicated due to the tooth's unique structure (**Fig. 3A**). The tooth dentin is one of the mineralized tissues surrounding tooth pulp and interconnects the nerve endings of DPA neurons with the environment within the dentinal tubules flooded with dentinal fluid. Moreover, odontoblasts, which form the tooth dentin and process into the dentinal tubules from the dental pulp's outer surface, are also able to directly or indirectly affect the DPA neurons (Schuh, Benso, and Aguayo 2019, Chung, Jung, and Oh 2013).

Three main hypotheses have been proposed to understand the dentin hypersensitivity (**Fig. 3B**). Firstly, the *neural theory* refers that nociceptors at

nerve endings of DPA neurons directly detect mostly noxious external stimuli such as hot and cold temperatures. Alternatively, the *hydrodynamic theory* supports that nociceptors are indirectly activated by the fluid movement, which can be induced by various external stimuli, such as thermal, chemical, mechanical, and osmotic, within the dentinal tubules. Finally, the *odontoblast transducer theory* suggests that odontoblasts directly recognize external stimuli or act as mediators in transducing signals to DPA neurons (Chung, Jung, and Oh 2013, Sole-Magdalena et al. 2018).

Among these three hypotheses, the hydrodynamic theory (Brännström and Astroem 1964) is the most commonly accepted because patients with toothache frequently experience pain by not only noxious stimuli but also innocuous stimuli such as water spray, air puffs, and sugar consumption (Chung, Jung, and Oh 2013). Based on this phenomenon, the functional expression of mechanosensitive ion channels, such as PIEZO2 (Won et al. 2017), ASIC3 (Ichikawa and Sugimoto 2002), and TRPV2 (Gibbs, Melnyk, and Basbaum 2011), has been demonstrated in a subset of DPA neurons. Although these findings suggest that low-threshold mechanoreceptors can be involved in dental nociception rather than touch, it remains unclear how DPA neurons detect pure pain sensation without sensing other sensory modalities.

4. Polymodal Roles of TRPM8 Channels

TRPM8 (transient receptor potential cation channel, subfamily M, member 8) is a homotetrameric nonselective cation channel that is activated by mildly cold temperature (15-25℃) or cooling agents from mint such as menthol (Clapham 2002, **Fig. 4A**). It is first identified in a subset of DRG neurons, mostly nociceptive fibers (Peier et al. 2002, McKemy, Neuhausser, and Julius 2002). Its histological and functional expression have been well studied in all somatosensory neurons under normal or pathological conditions. For instance, TRPM8-deficient mice lack not only in detecting normal cold temperatures (Dhaka et al. 2007) but also tissue inflammation- or nerve injury-induced hypersensitivity to innocuous cooling (Colburn et al. 2007).

Interestingly, TRPM8 is engaged in transducing stimuli of innocuous cool temperature and noxious cold temperature, so it is not apparent to define the TRPM8 as a nociceptor (Julius 2013). In addition, TRPM8 is directly able to detect pH (Andersson, Chase, and Bevan 2004) and mediates menthol-induced analgesia in animal models of chronic neuropathic pain or inflammatory pain (Liu et al. 2013, Proudfoot et al. 2006). Recently, several studies have demonstrated that TRPM8 serves as an osmosensor that is sensitive to the extracellular hyperosmolar environment, such as dry eye, to mediate eye blinking in corneal afferent neurons (Quallo et al. 2015, Bereiter et al. 2018).

TRPM8 expression has been molecularly and functionally detected in a subset of DPA neurons (**Fig. 4Ba-Bc**), encompassing nociceptive fibers with TRPV1 (transient receptor potential cation channel, subfamily V, member 1), TRPA1 (transient receptor potential cation channel, subfamily A, member 1) (Park et al. 2006, Chung, Jung, and Oh 2013), and VGLUT2 (vesicular

glutamate transporter 2; Kim et al. 2015). These studies demonstrate the mechanisms underlying dentin hypersensitivity frequently evoked by cold stimulation to the exposed dentin of teeth.

5. Identifying Somatosensory System with Single-Cell RNA Sequencing

The somatosensory systems are the largest sensory system in mammalian and are composed of heterogeneous cell types, participating in various sensory modalities such as thermoception, mechanoreception, pruritoception, and proprioception (Li et al. 2018, Le Pichon and Chesler 2014). Using anatomical and physiological parameters, such as histological staining with markers, degree of myelination, and electrophysiological properties, somatosensory neurons have been classified into four general fiber types: C (unmyelinated nociceptive fiber), Aδ (myelinated nociceptive fiber), Aβ (myelinated mechanosensitive fiber), and Aα (myelinated proprioceptive fiber) (Le Pichon and Chesler 2014).

With the recent rapid development of biological technologies, it has been possible to dissect somatosensory neurons at the single-cell level. For example, the identity of a cell can be determined by whole transcriptome profiling via single-cell RNA-sequencing (scRNA-seq) (Li et al. 2016, Shrestha et al. 2018, Usoskin et al. 2015). An increasing number of studies have applied scRNA-seq to identify rare cell types in mixed cell populations of tissues or novel marker genes that may be an effective therapeutic target. Accordingly, several pioneering works have successfully verified well-known molecular phenotypes of subpopulations, such as C-fibers (peptidergic or non-peptidergic) and A-fibers (Aδ, Aβ, and Aα), as well as revealed novel marker genes in DRG (Usoskin et al. 2015, Li et al. 2016) and TG (Nguyen et al. 2017).

These novel findings are required for new unbiased computational

methods for single-cell transcriptome analysis (Usoskin et al. 2015). Furthermore, the scRNA-seq technique has been advanced with various combined approaches of genetically labeling (Megat et al. 2019, Chiu et al. 2014, Goswami et al. 2014, Thakur et al. 2014) and electrophysiological techniques (Li et al. 2016) to reveal molecular and functional changes across neuronal populations by developmental states (Sharma et al. 2020) or pathological conditions (Hu et al. 2016). Therefore, scRNA-seq has been a remarkable strategy to elucidate heterogeneity of the somatosensory system and its novel cell types or marker genes.

Figure 1.

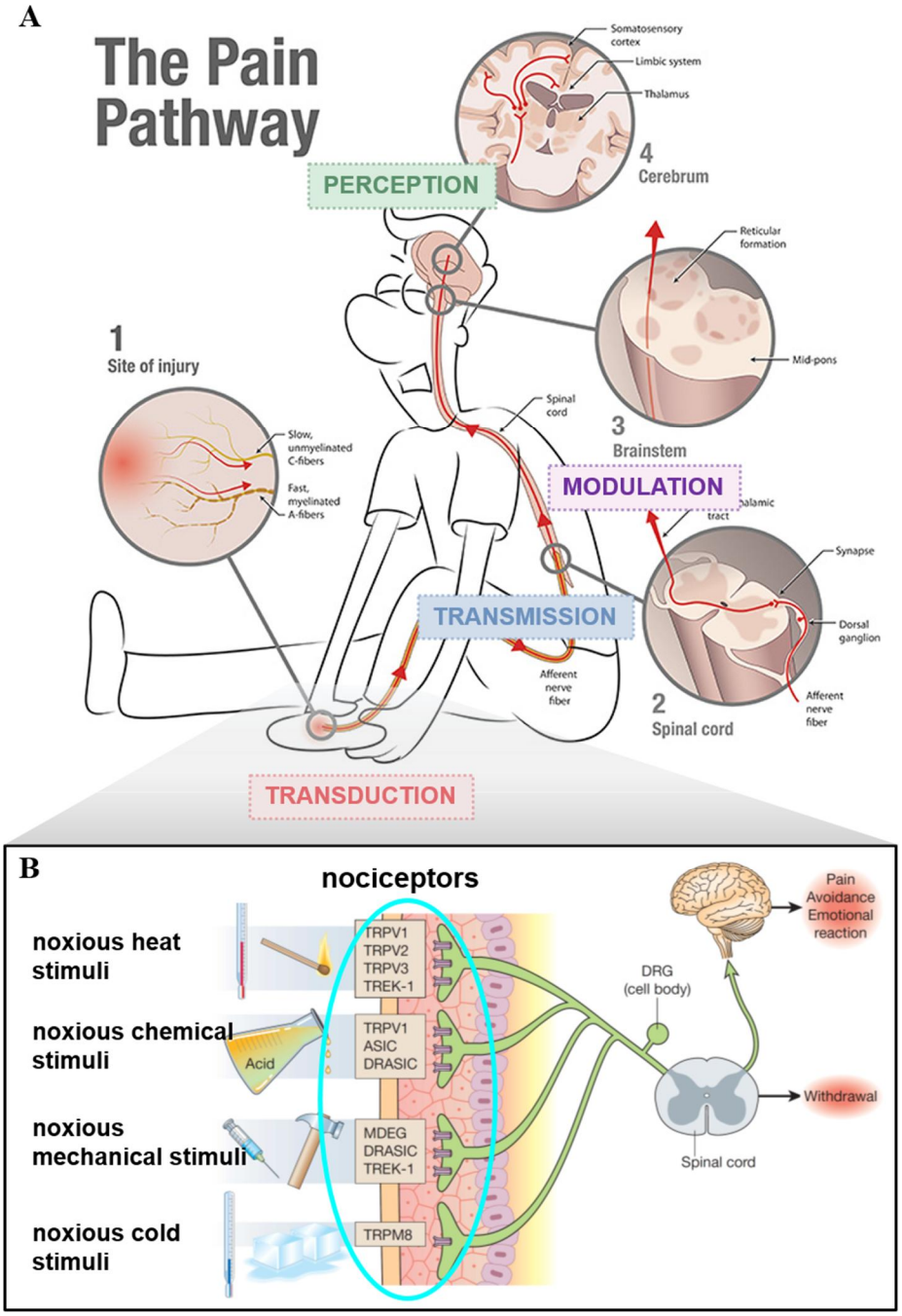
A
The Pain Pathway
Somatosensory cortex
Limbic system
Thalamus
4
Cerebrum
PERCEPTION
Reticular formation
Mid-pons
3
Brainstem
1
Site of injury
Spinal cord
Slow, unmyelinated C-fibers
Fast, myelinated A-fibers
MODULATION
tract
Synapse
Dorsal ganglion
TRANSMISSION
Afferent nerve fiber
2
Spinal cord
Afferent nerve fiber
TRANSDUCTION
B
nociceptors
noxious heat stimuli
TRPV1
TRPV2
TRPV3
TREK-1
noxious chemical stimuli
Acid
TRPV1
ASIC
DRASIC
noxious mechanical stimuli
MDEG
DRASIC
TREK-1
noxious cold stimuli
TRPM8
DRG (cell body)
Pain
Avoidance
Emotional reaction
Withdrawal
Spinal cord

Figure 1. Pain pathway and nociceptors

(**A**) Schematic drawing of four major processes of the pain pathway: transduction, transmission, modulation, and perception. (**B**) The functionally distinct nociceptors in response to their adequate noxious stimuli, including heat, chemical, mechanical, and cold.

Fig. 1A *modified from Muench 2015*

Fig. 1B *modified from Scholz and Woolf 2002*

Figure 2.

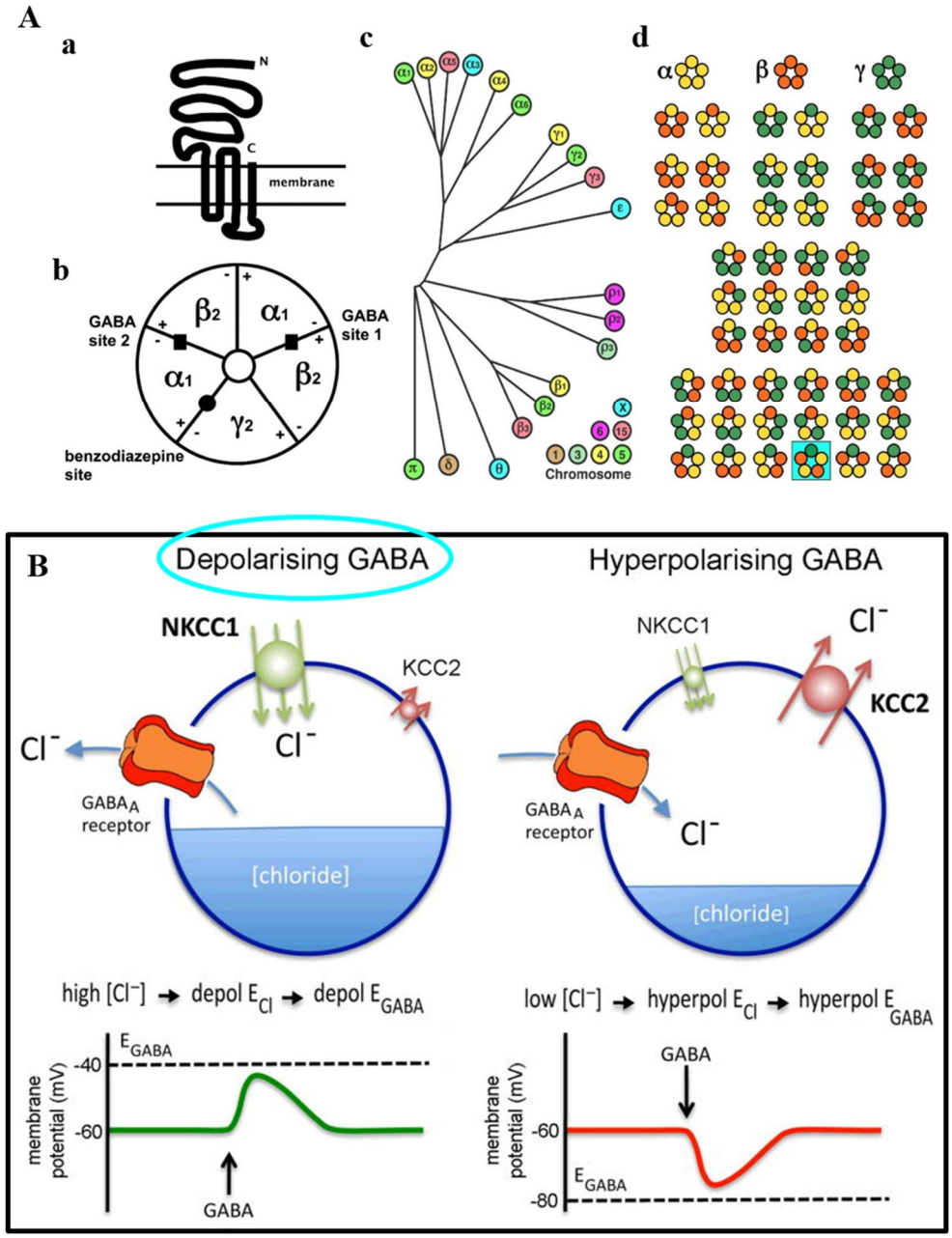
A
a
N
C
membrane
b
GABA site 2
GABA site 1
β2
α1
α1
β2
γ2
benzodiazepine site
c
Chromosome
d
α
β
γ
B
Depolarising GABA
Hyperpolarising GABA
NKCC1
KCC2
Cl⁻
GABA A receptor
[chloride]
high [Cl⁻] → depol E Cl → depol E GABA
low [Cl⁻] → hyperpol E Cl → hyperpol E GABA
membrane potential (mV)
E GABA
-40
-60
-80
GABA

Figure 2. Structure and functional shifts of $GABA_A$ receptors

(**Aa-Ad**) Representative illustrations of the transmembrane structure of $GABA_AR$ (**Aa**) comprising heteropentamers, α1β2γ2 as the major isoforms (**Ab**), 19 genes encoding $GABA_AR$ subunits described to date in humans and rodents (**Ac**), and possible compositions of three different subunits, α (yellow), β (red), and γ (green) (**Ad**). (**B**) Schematic drawings of $GABA_AR$ functions of depolarization or hyperpolarization depending on intracellular chloride concentration affected by expression levels of chloride transporters.

Fig. 2A *adopted from Sieghart 1995*

Fig. 2B *adopted from Herbison and Moenter 2011*

Figure 3.

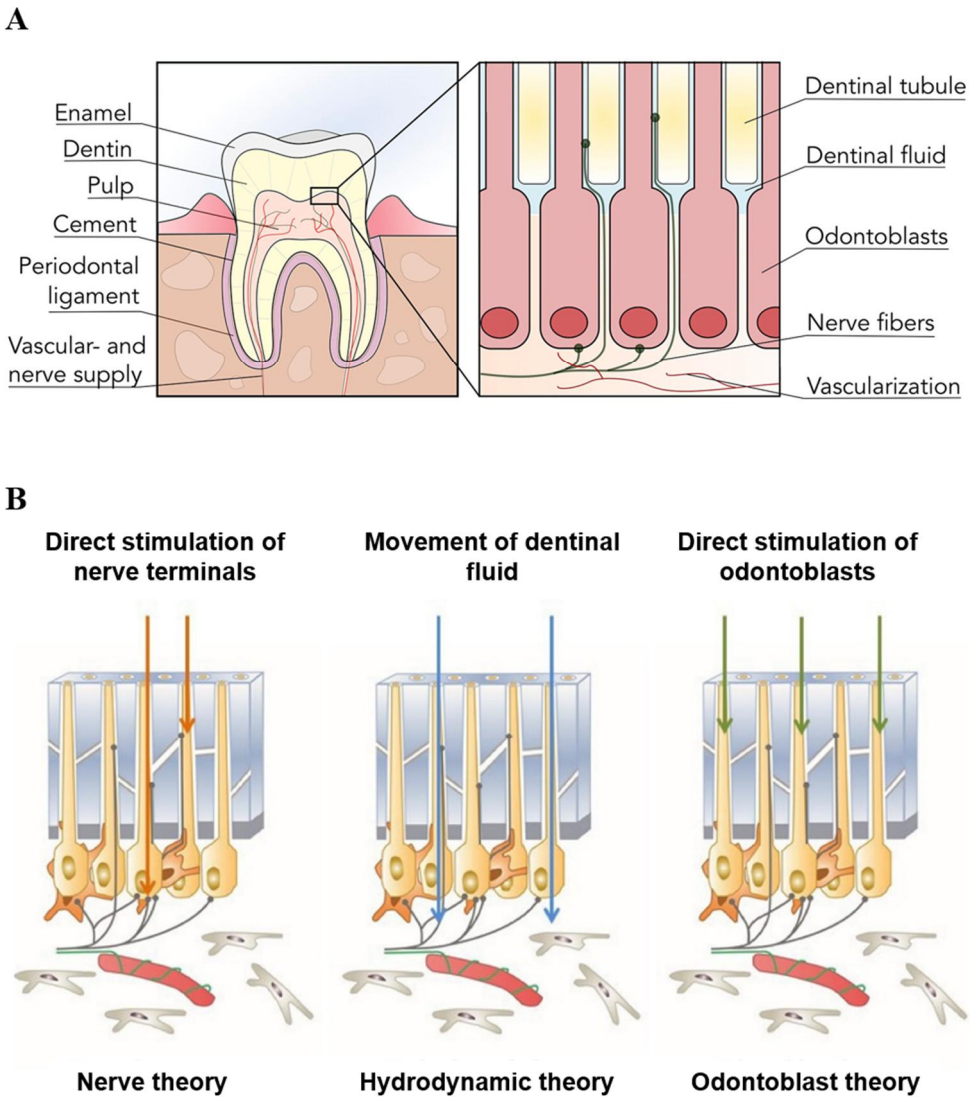
A
Enamel
Dentin
Pulp
Cement
Periodontal ligament
Vascular- and nerve supply
Dentinal tubule
Dentinal fluid
Odontoblasts
Nerve fibers
Vascularization
B
Direct stimulation of nerve terminals
Movement of dentinal fluid
Direct stimulation of odontoblasts
Nerve theory
Hydrodynamic theory
Odontoblast theory

Figure 3. Teeth anatomy and mechanisms of dentin hypersensitivity

(**A**) The structure of a tooth consists of enamel, dentin, dental pulp, etc. The dentin surrounding tooth pulp interconnects DPA neurons' nerve endings with the environment within the dentinal tubules flooded with dentinal fluid. (**B**) Three major hypotheses underlying the development of dentin hypersensitivity.

Fig. 3A *adopted from Schuh, Benso, and Aguayo 2019*

Fig. 3B *adopted from Sole-Magdalena et al. 2018*

Figure 4.

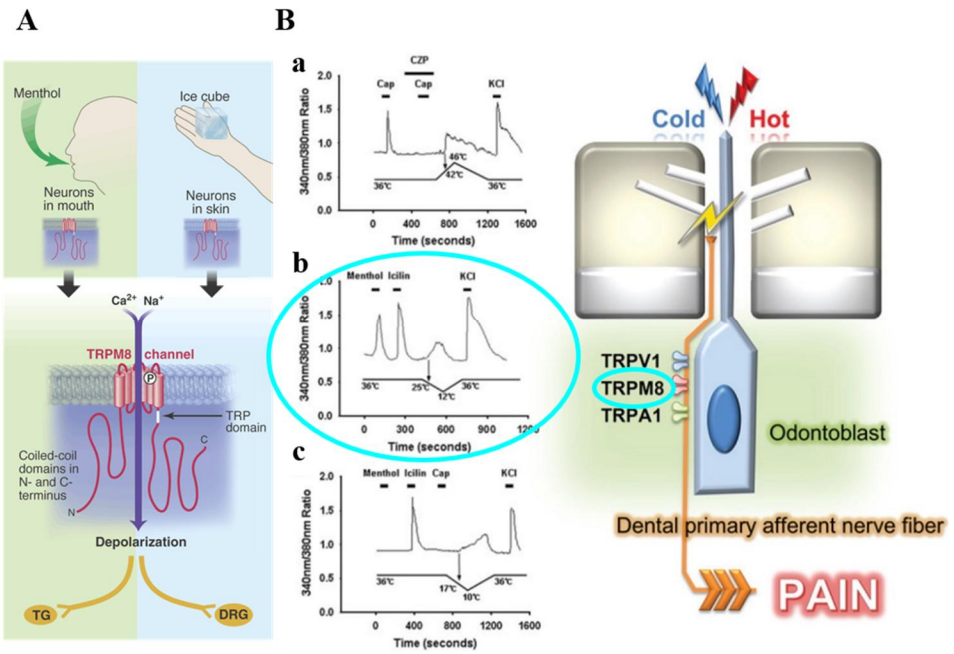
A
B
Menthol
Ice cube
Neurons in mouth
Neurons in skin
Ca2+ Na+
TRPM8 channel
TRP domain
Coiled-coil domains in N- and C-terminus
Depolarization
TG
DRG
a
b
c
CZP
Cap
KCl
Menthol
Icilin
340nm/380nm Ratio
Time (seconds)
Cold
Hot
TRPV1
TRPM8
TRPA1
Odontoblast
Dental primary afferent nerve fiber
PAIN

Figure 4. Polymodal functions of TRPM8 channels

(**A**) Schematic drawing of polymodal functions of TRPM8 in response to mildly cold temperature (15-25℃) and a cooling agent such as menthol. (**Ba-Bc**) The confirmation of functional expression of TRPM8 in DPA neurons in response to both TRPM8 agonists, which are menthol and icilin, and cold stimulation (below 25℃) using a calcium imaging technique (Park et al. 2006, **Bb**).

Fig. 4A *adopted from Clapham 2002*

Fig. 4B *adopted from Chung, Jung, and Oh 2013*

PURPOSE

Although identifications of distinct nociceptors in response to different modalities of noxious or painful stimuli are well known, it remains elusive how innocuous or non-painful stimuli transmit pain signals under pathophysiological conditions. Here, I have explored these polymodalities of nociceptors that may be activated by innocuous stimuli or endogenous mediators of inflammation. I have focused research on the level of cellular, molecular biology, and the behavioral level using dorsal root ganglion (DRG) neurons and dental primary afferent (DPA) neurons.

- To examine the contribution of peripheral $GABA_A$ receptors that may be activated by endogenous GABA to persistent inflammatory hypersensitivity

- To investigate cellular mechanisms on how TRPM8 channels in DPA neurons can detect sweet substances as dentin hypersensitivity

- To identify molecularly distinct subtypes and gene-expression signatures of DPA neurons using scRNA-seq

CHAPTER 1:
Functional Roles of Peripheral $GABA_A$ Receptors in Persistent Inflammatory Hypersensitivity

* This chapter has been reproduced from the article published by Pa Reum Lee, Seo-Yeon Yoon, Hyoung Woo Kim, Ji–Hee Yeo, Yong Ho Kim, Seog Bae Oh. Peripheral $GABA_A$ receptor-mediated signaling facilitates persistent inflammatory hypersensitivity. Neuropharmacology, 2018, Jun;135:572-580. doi: 10.1016/j.neuropharm.2018.04.009.

ABSTRACT

Unlike in the central nervous system (CNS), in the adult peripheral nervous system (PNS), activation of $GABA_A$ receptors ($GABA_AR$) is excitatory due to the relatively high concentration of intracellular chloride in these neurons. Indeed, exogenous GABA and muscimol, $GABA_AR$ agonists, exacerbate acute inflammatory hypersensitivity in rodents. However, it remains unclear whether peripheral $GABA_AR$ and the endogenous GABA play an important role in persistent inflammatory hypersensitivity. In this study, I thus investigated how peripheral $GABA_AR$ affects pain hypersensitivity by using the complete Freund's adjuvant (CFA)-induced persistent inflammatory pain mouse model. I found that intraplantar (i.pl.) administration of $GABA_AR$ antagonists, picrotoxin, and 1(S),9(R)-(-)-bicuculline methiodide (bicuculline) significantly inhibited both spontaneous nociceptive (paw licking and flinching) behavior and mechanical hypersensitivity in CFA-injected mice at day 3 (D3), but not in naïve mice. Interestingly, CFA-induced mechanical hypersensitivity was significantly reversed by anti-GABA antibody (anti-GABA, i.pl.). In addition, RT-qPCR revealed that glutamate decarboxylase *Gad1* (GAD 67) and *Gad2* (GAD 65) mRNA expression levels were also upregulated in the ipsilateral hind paw of CFA-injected mice at D3. Finally, 5α-pregnan-3α-ol-20-one (3α,5α-THP), a selective positive allosteric modulator of $GABA_AR$, produced mechanical allodynia in naïve mice in a dose-dependent manner. Taken together, these results indicate that peripheral $GABA_AR$ and endogenous GABA, possibly produced by the inflamed tissue, potentiate CFA-induced persistent inflammatory hypersensitivity, suggesting

that they can be used as a therapeutic target for alleviating inflammatory pain.

INTRODUCTION

Unlike in most central nervous system (CNS), γ-aminobutyric acid (GABA) generates excitatory effects in the adult peripheral nervous system (PNS), through ligand-gated $GABA_A$ receptors ($GABA_AR$) (Levy 1977, Price et al. 2009). For $GABA_AR$, these excitatory actions depend on two major transmembrane cotransporters for controlling intracellular chloride concentration ($[Cl^-]_{in}$); the Na-K-Cl cotransporter NKCC1, which accumulates Cl^- intracellularly, and the K-Cl cotransporter KCC2, which extrudes it from the cell (Price et al. 2009). Since primary afferent neurons, such as those of the dorsal root ganglion (DRG) and the trigeminal ganglion (TG), maintain a high $[Cl^-]_{in}$ as a result of the higher expression of NKCC1 and lack of KCC2, the activation of $GABA_AR$ results in peripheral primary afferent depolarization (PAD) (Alvarez-Leefmans et al. 2001, Kanaka et al. 2001, Price, Hargreaves, and Cervero 2006, Sung 2000, Toyoda et al. 2005).

It has been reported that intrathecal injection of $GABA_AR$ agonist produces an analgesic effect (Yamamoto and Yaksh 1991), while spinal application of $GABA_AR$ antagonist induces pain hypersensitivity (Yamamoto and Yaksh 1993). These findings suggest that spinal inhibition, including the presynaptic inhibition of primary afferent terminals via $GABA_AR$ signaling, contributes to the regulation of nociceptive signaling. In addition, a recent report demonstrated that administration of GABA to sensory ganglia produces a net inhibitory effect on acute nociceptive transmission (Du et al. 2017). Surprisingly, however, the enhancement of PAD, mediated by the activation of peripheral $GABA_AR$ (i.e., on peripheral nerve endings), can lead

to the generation of action potentials, indicating a net excitatory effect rather than inhibition, in peripheral sensory neurons (Carr et al. 2010, Price et al. 2009).

It has been demonstrated that intraplantar (i.pl.) injection of a high-dose of $GABA_AR$ agonists, GABA and muscimol, can increase pain hypersensitivity in the formalin-induced acute inflammatory pain model (Bravo-Hernandez et al. 2014, Carlton, Zhou, and Coggeshall 1999, Jang et al. 2017). Interestingly, several reports have also suggested that $GABA_AR$-mediated signals on pain modulation can change in complete Freund's adjuvant (CFA)-induced persistent inflammation. For example, the intrathecal administration of muscimol potentiates CFA-induced pain hypersensitivity, whereas the $GABA_AR$ antagonist gabazine produces an analgesic effect (Anseloni and Gold 2008). Furthermore, persistent inflammation by CFA facilitates GABA-induced depolarization through $GABA_AR$ in cultured mouse DRG neurons (Zhu, Dua, and Gold 2012, Zhu, Lu, and Gold 2012), and inflammatory mediators also potentiate GABA-induced currents in human sensory neurons (Zhang et al. 2015). However, it is not completely understood how the GABA signaling, which is mediated by $GABA_AR$ and endogenous GABA, works on the nociception at peripheral sensory terminals under persistent inflammatory conditions.

In this study, I thus investigated the role of peripheral $GABA_AR$ signaling on pain hypersensitivity by using the CFA-induced persistent inflammatory pain model in mice. I found that peripheral $GABA_AR$ signaling contributes to CFA-induced hypersensitivity, and its modulation can potentially be a novel therapeutic target for inflammatory pain alleviation.

MATERIALS AND METHODS

Animals

Adult male C57BL/6 mice (6 to 10 weeks old) were used in this study. Mice were housed by 4 to 6 per cage in a temperature controlled room (23 ± 1°C, 12 h/12 h light/dark cycle) and were maintained with free access to food and water. All surgical and experimental procedures were in accordance with the Institutional Animal Care and Use Committee (IACUC) at Seoul National University.

Reagents and drug administration

The following materials were used: 1x phosphate buffered saline (PBS, pH 7.4; Life technologies); rabbit anti-GABA antibody (Cat. 20094, Immunostar); picrotoxin, 1(S),9(R)-(-)-bicuculline methiodide (bicuculline), 5α-pregnan-3α-ol-20one (3α,5α-THP), CFA, and dimethyl sulfoxide (DMSO) (Sigma).

For generating persistent inflammatory pain model, undiluted CFA (20 μL) was injected into the plantar surface of the left hind paw, and then animals were returned to their home cages. All other drugs were administered by i.pl. injection in a volume of 10 μL, unless otherwise indicated. The following drug concentrations were used; 1, 3, and 5 mM picrotoxin; 3 mM bicuculline; anti-GABA antibody, 1/100 dilution in PBS; and 1, 10, and 100 mM 3α,5α-THP. The dose of picrotoxin and bicuculline was determined based on previous studies (Carlton, Zhou, and Coggeshall 1999, Jang et al. 2017). Vehicle was injected as follows; 1% DMSO in PBS, in the case of picrotoxin; PBS, in the case of bicuculline; heat-inactivated anti-GABA antibody for the

respective antibody experiments; and PBS in the case of 3α,5α-THP. The anti-GABA antibody was heat- inactivated at 60℃ for 20 min.

Behavioral tests

Mice were acclimated in a cage at least for a week and then were habituated in acrylic observation chambers with wire grid floors (size ranges 12 x 12 x 12 cm) for at least 3 h, three times before the experiment. Behavioral testing was performed under blind conditions for all experiments. The treatments were randomized with either vehicle or drug (picrotoxin, bicuculline, anti-GABA antibody, or 3α,5α-THP), and observer was unaware of which treatment each animal had received until after the behavioral experiments and measurements were over. CFA-induced spontaneous nociceptive behavior was observed for a period of 14 days (D0-D14) following CFA injection on D0. To test drug effects, naïve or CFA-injected mice at D3 received an i.pl. injection of vehicle or drug, and were video-recorded for 30 min before drug administration (pre-injection), to set a baseline, and for 30 min after (post-injection). The CFA-induced spontaneous nociceptive behavior was analyzed by measuring the time spent licking and flinching of the injected hind paw in the 30 min period pre- or post-injection. To test mechanical hypersensitivity/allodynia, I measured both the 50% paw withdrawal threshold and paw withdrawal frequency after stimulating the hind paw of the animals with a series of von Frey filaments. The 50% paw withdrawal threshold was determined based on the up-down method (Dixon 1991), while the response frequency was used to assess the paw withdrawal frequency to the repeated application of a single von Frey filament (0.16-g or 0.6-g, ten times each).

Quantitative reverse transcription polymerase chain reaction (RT-qPCR)

The ipsilateral and contralateral hind paw tissue were harvested at D3 after PBS (20 µL) or CFA (20 µL) injections using 4-mm biopsy punches (Kai medical). Tissues were immediately frozen in liquid nitrogen and were stored at -80°C. Total RNA was extracted by using the RNeasy Mini Plus Kit (Qiagen), and 0.5 to 1 mg of the total RNA was used for cDNA synthesis with the M-MLV Reverse Transcriptase (Invitrogen) according to the manufacturer's instructions. For quantitative PCR, each sample containing 20 ng of cDNA was run in triplicate with primer pairs (*Gad1*, *Gad2*, and *Gapdh*, **Table 1**) and SYBR Green PCR Master Mix Kit (Applied Biosystems). The quantitative PCR was performed using a 7500 Real-Time PCR system (Applied Biosystems) under the following conditions: 50°C for 2 min, 95°C for 10 min, 40 cycles of 95°C for 15 sec and 60°C for 1 min, followed by a dissociation stage. The expression of *Gad1* and *Gad2* in the PBS group and the CFA group relative to the Naïve control group was calculated by the ΔΔCT method using *Gapdh* as the reference gene.

Statistical analysis

Results are representative of n = 4 to 30 mice per each group, depending on the experiment. All data are presented as mean ± SEM. A statistical analysis was performed using the GraphPad Prism software (version 6.01, Graphpad Software Inc.). The differences between two groups were assessed by the unpaired two-tailed Student's t-test, in order to analyze the expression of *Gad1* and *Gad2*. For multiple comparisons, data were analyzed with one- or two-way analysis of variance (ANOVA) followed by Bonferroni post hoc test.

Statistical differences were considered to be significant at $p < 0.05$.

TABLES

Table 1. List of primer pairs used

Target Gene (bp)	Primer Sequences	GeneBank No.	Reference
Gad1 (118)	(F) GTGACTGTGGCTTAGTCCTAGA (R) ATACCATCCGCCCTGTAGTT	NM_008077.5	
Gad2 (80)	(F) AGTAGGTCAGCACTCCCTAATG (R) GGGCAGCTGCATATTTACTCTC	NM_008078.2	
Gapdh (317)	(F) AGGTCATCCCAGAGCTGAACG (R) CACCCTGTTGCTGTAGCCGTAT	NM_001289726.1 NM_008084.3	(Kim, You, et al. 2011)

RESULTS

Intraplantar application of $GABA_A$ receptor antagonists inhibits CFA-induced spontaneous nociceptive behavior

To address the role of peripheral $GABA_AR$, I used CFA to generate persistent inflammatory pain model in adult mice. First, I examined CFA-induced spontaneous nociceptive behavior at D0 to D14 following CFA injection. I measured the time spent in paw licking and flinching in a period of 30 min before (pre-injection group) or after (post-injection group) an injection of PBS (20 μL, i.pl.). CFA injection induced significant spontaneous nociceptive behavior at D3 and D7 in both groups, compared to D0 (D0 *vs* D3, $p = 0.0009$ and D0 *vs* D7, $p = 0.0056$, pre-injection group; D0 *vs* D3, $p = 0.0004$ and D0 *vs* D7, $p = 0.0281$, post-injection group, **Fig. 5A**). In contrast, PBS administration did not affect nociceptive behavior in CFA-injected mice at any time point (**Fig. 5A**).

Next, I tested the effects of $GABA_AR$ antagonists on CFA-induced spontaneous/ongoing nociceptive behavior. I used picrotoxin, a noncompetitive $GABA_AR$ inhibitor, and bicuculline, a competitive inhibitor unable to cross the blood-brain barrier (Johnston 2013). I administered picrotoxin and bicuculline by i.pl. injection in naïve or CFA-injected mice at D3, according to the experimental protocol shown in **Fig. 5B**. Paw licking and flinching behavior was significantly inhibited by administration of picrotoxin (3 mM, 10 μL) compared to vehicle (1% DMSO in PBS, 10 μL, $p < 0.0001$, **Fig. 5C**) in CFA-injected mice, but there were no significant effects in naïve mice. The vehicle injection (1% DMSO) also exhibited nociceptive

behavior in CFA-injected mice ($p = 0.0008$, **Fig. 5C**).

To confirm the analgesic effects of picrotoxin via blockade of peripheral $GABA_AR$ in inflamed tissue, the competitive $GABA_AR$ antagonist bicuculline was applied in the hind paw of naïve or CFA-injected mice (at D3 post-CFA). The spontaneous nociceptive behavior of CFA-injected but not of naïve mice was also significantly reduced by bicuculline (3 mM, 10 μL, i.pl., $p = 0.0013$, **Fig. 5D**) compared to the vehicle (PBS, 10 μL). Vehicle (PBS) injection also exhibited nociceptive behavior in CFA-injected mice ($p = 0.0001$, **Fig. 5D**). In addition, CFA-induced spontaneous nociceptive behavior was dose-dependently attenuated by injection of 1 mM ($p = 0.1855$), 3 mM ($p < 0.0001$), and 5 mM ($p < 0.0001$) picrotoxin compared to the vehicle (**Fig. 5E**).

Intraplantar application of $GABA_A$ receptor antagonists alleviates CFA-induced mechanical hypersensitivity

It has been reported that i.pl. injection of CFA induces mechanical hypersensitivity in rodents (Gao et al. 2010, Ren 1999, Ren and Dubner 1993). I measured both 50% paw withdrawal threshold and frequency using von Frey filaments (0.16-g or 0.6-g, ten times each) in naïve or CFA-injected mice, administered with picrotoxin at D3 post-CFA (**Fig. 6A-C**). In the 0.5 h post-injection group, picrotoxin (3 mM, 10 μL) significantly reduced mechanical hypersensitivity compared to the vehicle injection (1% DMSO in PBS, 10 μL) in CFA-injected mice ($p = 0.0009$ for the 50% paw withdrawal threshold, **Fig. 6A**; for paw withdrawal frequency, $p = 0.0001$ using the 0.16-g filament; $p < 0.0001$ using the 0.6-g filament, **Fig. 6B, C**), but not in naïve mice. Picrotoxin also significantly reduced mechanical hypersensitivity in CFA-injected mice

compared to the baseline (p = 0.0039 for the 50% paw withdrawal threshold, **Fig. 6A**; for paw withdrawal frequency; p = 0.0002 using the 0.16-g filament and p < 0.0001 using the 0.6-g filament, **Fig. 6B, C**). The CFA-induced mechanical hypersensitivity was dose-dependently inhibited by i.pl. injection of 1 mM (p = 0.3013), 3 mM (p < 0.0001), and 5 mM (p < 0.0001) picrotoxin compared to the vehicle, in CFA-injected mice (**Fig. 6G-I**).

Bicuculline (3 mM, 10 μL) also significantly attenuated mechanical hypersensitivity in the 0.5 h post-injection group, compared to the vehicle (PBS, 10 μL), in CFA-injected mice (p = 0.0361 for the 50% paw withdrawal threshold, **Fig. 6D**; for paw withdrawal frequency, p = 0.0028 using the 0.16-g filament and p = 0.0001 using the 0.6-g filament, **Fig. 6E, F**), but not in naïve mice. Injection of bicuculline also significantly reduced the mechanical hypersensitivity in CFA-injected mice compared to the baseline (p = 0.0062 for the 50% paw withdrawal threshold, **Fig. 6D**; for paw withdrawal frequency, p = 0.0056 using the 0.16-g filament and p < 0.0001 using the 0.6-g filament, **Fig. 6E, F**). Taken together, these results indicate that local administration of the $GABA_AR$ antagonists, picrotoxin and bicuculline, in peripheral inflamed tissue, can alleviate CFA-induced mechanical hypersensitivity.

Intraplantar application of anti-GABA antibody attenuates CFA-induced mechanical hypersensitivity

Attenuation of spontaneous nociceptive behavior and mechanical hypersensitivity by $GABA_AR$ antagonists in the CFA-induced inflammatory pain model suggests that endogenous GABA plays an important role in peripheral inflamed tissue by activating peripheral $GABA_AR$ and nociceptive fibers under persistent inflammation. Thus, I tested whether CFA-induced

persistent mechanical hypersensitivity can be inhibited by i.pl. application of anti-GABA which can accomplish a functional blockade of GABA in the inflamed tissue (**Fig. 7**). The timeline for application was as shown in **Fig. 5B**, except I also tested the effects of anti-GABA 1 h and 3 h post-injection. Administration of anti-GABA (1/100 dilution in PBS, 10 μL) significantly reversed the CFA-induced mechanical hypersensitivity in CFA-injected mice (0.5 h post-injection group), compared to heat-inactivated anti-GABA, which was injected as a control ($p = 0.0008$ for the 50% paw withdrawal threshold, **Fig. 7A**; for paw withdrawal frequency, $p < 0.0001$ using the 0.16-g filament and $p < 0.0001$ using the 0.6-g filament, **Fig. 7B, C**). Anti-GABA did not affect mechanical sensitivity in naïve mice. Injection of anti-GABA also significantly reduced mechanical hypersensitivity at 0.5 h compared to the baseline, in CFA-injected mice ($p = 0.0026$ for the 50% paw withdrawal threshold, **Fig. 7A**; for paw withdrawal frequency, $p = 0.0004$ using the 0.16-g filament and $p = 0.0003$ using the 0.6-g filament, **Fig. 7B, C**). Among the three time points tested, the analgesic effects of anti-GABA on CFA-induced mechanical allodynia were significantly observed at the 0.5 h post-injection, compared to the control ($p < 0.0001$, **Fig. 7D**), while no significant differences were observed in naïve mice at any time point (**Fig. 7E**). Moreover, anti-GABA significantly reversed paw withdrawal threshold in CFA-injected mice, compared to the baseline at D3 ($p = 0.0002$, **Fig. 7D**), but not in naïve mice (**Fig. 7E**). In order to confirm the efficient neutralization of GABA by the blocking antibody, whole-cell patch clamp recordings were used in cultured mouse DRG neurons. GABA (100 mM)-induced currents were significantly reduced by anti-GABA co-application (1/100 dilution in the extracellular solution), but not by the vehicle control solution (data not

shown). These results indicate that endogenous GABA in inflamed tissue contributes to the facilitation of inflammatory mechanical hypersensitivity.

***Gad1* and *Gad2* expression levels increase in the CFA-inflamed hind paw**

Since I found an important role of endogenous GABA in CFA-induced mechanical hypersensitivity, I investigated whether GABA production increases in the inflamed tissue, by examining changes in the expression levels of GADs, the GABA synthesizing enzymes. Mammalian species express two isoforms of GADs to synthesize the transmitter GABA. GAD 67, encoded by the *Gad1* gene, preferentially synthesizes cytoplasmic GABA, whereas GAD 65, encoded by *Gad2*, preferentially synthesizes GABA for vesicular release (Soghomonian and Martin 1998, Tian et al. 1999). To address the regulation of GABA synthesis in inflammation, I tested *Gad1* and *Gad2* mRNA expression levels in the ipsilateral and contralateral hind paws of PBS- and CFA-injected mice using the RT-qPCR. Both *Gad1* and *Gad2* mRNAs were significantly higher in the ipsilateral hind paw of CFA-injected mice than of the PBS-injected mice ($p = 0.0022$ for *Gad1*, **Fig. 8A**; $p = 0.0077$ for *Gad2*, **Fig. 8C**), while there were no differences in the contralateral hind paw ($p = 0.4607$ for *Gad1*, **Fig. 8B**; $p = 0.5474$ for *Gad2*, **Fig. 8D**). These results show that levels of GADs were upregulated upon CFA-induced inflammation.

Intraplantar application of 3α,5α-THP is sufficient to induce mechanical allodynia through $GABA_AR$ in naïve mice

To address whether peripheral $GABA_AR$-mediated signaling is sufficient for the development of mechanical allodynia, I employed 3α,5α-THP, a neurosteroid that acts as a selective positive allosteric modulator of $GABA_AR$

(Lambert et al. 2001, Majewska 1990). Thirty minutes after administration, the 50% paw withdrawal threshold was dose-dependently reduced by 1 mM ($p = 0.0027$), 10 mM ($p = 0.0004$), and 100 mM ($p < 0.0001$) 3α,5α-THP (20 μL, i.pl.), compared to the baseline (**Fig. 9A**). The paw withdrawal frequency using a 0.16-g filament was instead dose-dependently increased by 1 mM ($p = 0.2053$), 10 mM ($p = 0.0282$), and 100 mM ($p < 0.0001$) 3 α,5α-THP (20 μL, i.pl.) compared to the baseline (**Fig. 9B**). To confirm $GABA_AR$ dependency on 3α,5α-THP inducing mechanical allodynia, I used the $GABA_A$ antagonist picrotoxin. The effects of the high dose of 3α,5α-THP (100 mM, 20 μL, i.pl.) were significantly reversed by co-injection of 3α,5α-THP (100 mM, 20 μL) with picrotoxin (3 mM) on paw withdrawal frequency ($p < 0.0001$, **Fig. 9D**), but not the paw withdrawal threshold ($p = 0.4508$, **Fig. 9C**). These results indicate that potentiated peripheral $GABA_AR$-mediated signaling is sufficient to produce mechanical allodynia in naïve animals.

Figure 5.

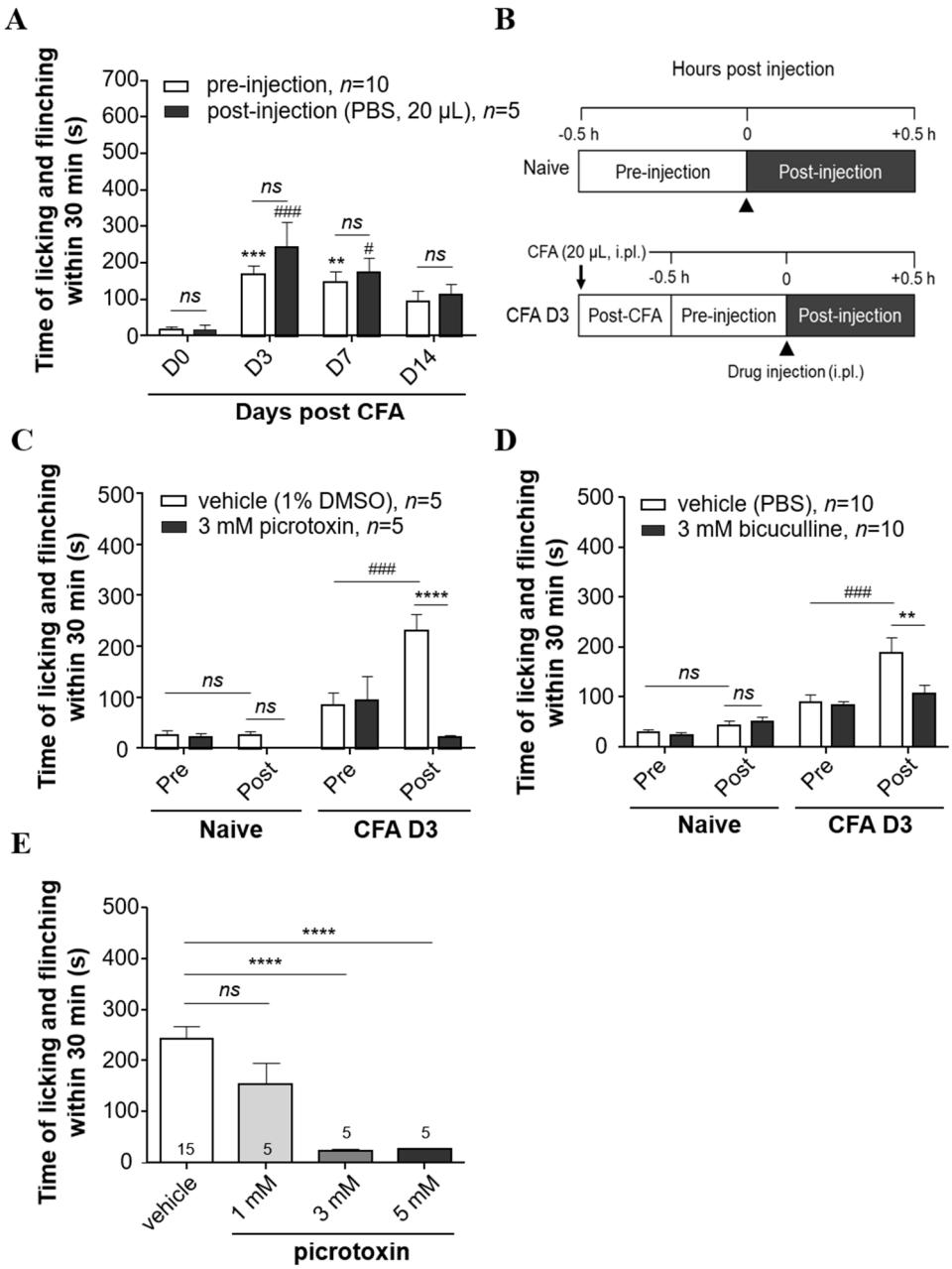
A
Time of licking and flinching within 30 min (s)
pre-injection, n=10
post-injection (PBS, 20 μL), n=5
ns
###
***
**
#
D0
D3
D7
D14
Days post CFA
B
Hours post injection
-0.5 h
0
+0.5 h
Naive
Pre-injection
Post-injection
CFA (20 μL, i.pl.)
CFA D3
Post-CFA
Drug injection (i.pl.)
C
vehicle (1% DMSO), n=5
3 mM picrotoxin, n=5
****
Pre
Post
Naive
CFA D3
D
vehicle (PBS), n=10
3 mM bicuculline, n=10
E
15
5
picrotoxin
vehicle
1 mM
3 mM
5 mM

Figure 5. Inhibition of CFA-induced spontaneous nociceptive behavior by application (i.pl.) of $GABA_AR$ antagonists

(**A**) Quantification of time spent paw licking and flinching in a period of 30 min before (pre-injection) and after (post-injection) injection of PBS (20 μL, i.pl.) in CFA (20 μL, i.pl.) injected mice at 0-14 days (D0-D14). Data are expressed as mean ± SEM and analyzed by two-way ANOVA and Bonferroni post hoc test. $^{**}p < 0.01$ and $^{***}p < 0.001$ *vs* D0 pre-injection group, $^{\#}p < 0.05$ and $^{\#\#\#}p < 0.001$ *vs* D0 post-injection group. (**B**) Experimental protocol for measuring CFA-induced spontaneous nociceptive behavior in naive mice and CFA-injected mice at D3. (**C-D**) Quantification of time spent paw licking and flinching in a period of 30 min before (pre-injection, pre) and after (post-injection, post) injection of the noncompetitive $GABA_AR$ antagonist picrotoxin (3 mM,10 μL, i.pl., **C**), the competitive $GABA_AR$ antagonist bicuculline (3 mM,10 μL, i.pl., **D**), or vehicle (10 μL, i.pl., 1% DMSO in PBS or PBS for picrotoxin and bicuculline, respectively) in CFA-injected (CFA D3) or naïve mice, as indicated. Note; the inhibition of CFA-induced spontaneous nociceptive behavior after drug administration. For all groups, $n = 5$ to 10 mice, as indicated. Data are expressed as mean ± SEM. $^{**}p < 0.01$ and $^{****}p < 0.0001$, two-way ANOVA with Bonferroni post hoc test; $^{\#\#\#}p < 0.001$, one-way ANOVA with Bonferroni post hoc test. *ns*, not significant. (**E**) Quantification of time spent paw licking and flinching after injection of picrotoxin (1, 3, and 5 mM, 10 μL, i.pl.) or vehicle (1% DMSO in PBS, 10 μL, i.pl.) in CFA-injected mice at D3. (**F-H**) Quantification of the paw withdrawal threshold **(F)** and paw withdrawal frequency of in CFA-injected mice at D3

in response to the 0.16-g (**G**) or 0.6-g (**H**) von Frey filaments, after injections of picrotoxin (1, 3, and 5 mM, 10 µL, i.pl.) or vehicle (1% DMSO in PBS, 10 µL, i.pl.). n = 5 to 30 mice. Data are expressed as mean ± SEM. $^{*}p < 0.05$ and $^{****}p < 0.0001$ *vs* vehicle control (one-way ANOVA with Bonferroni post hoc test). *ns*, not significant.

Figure 6.

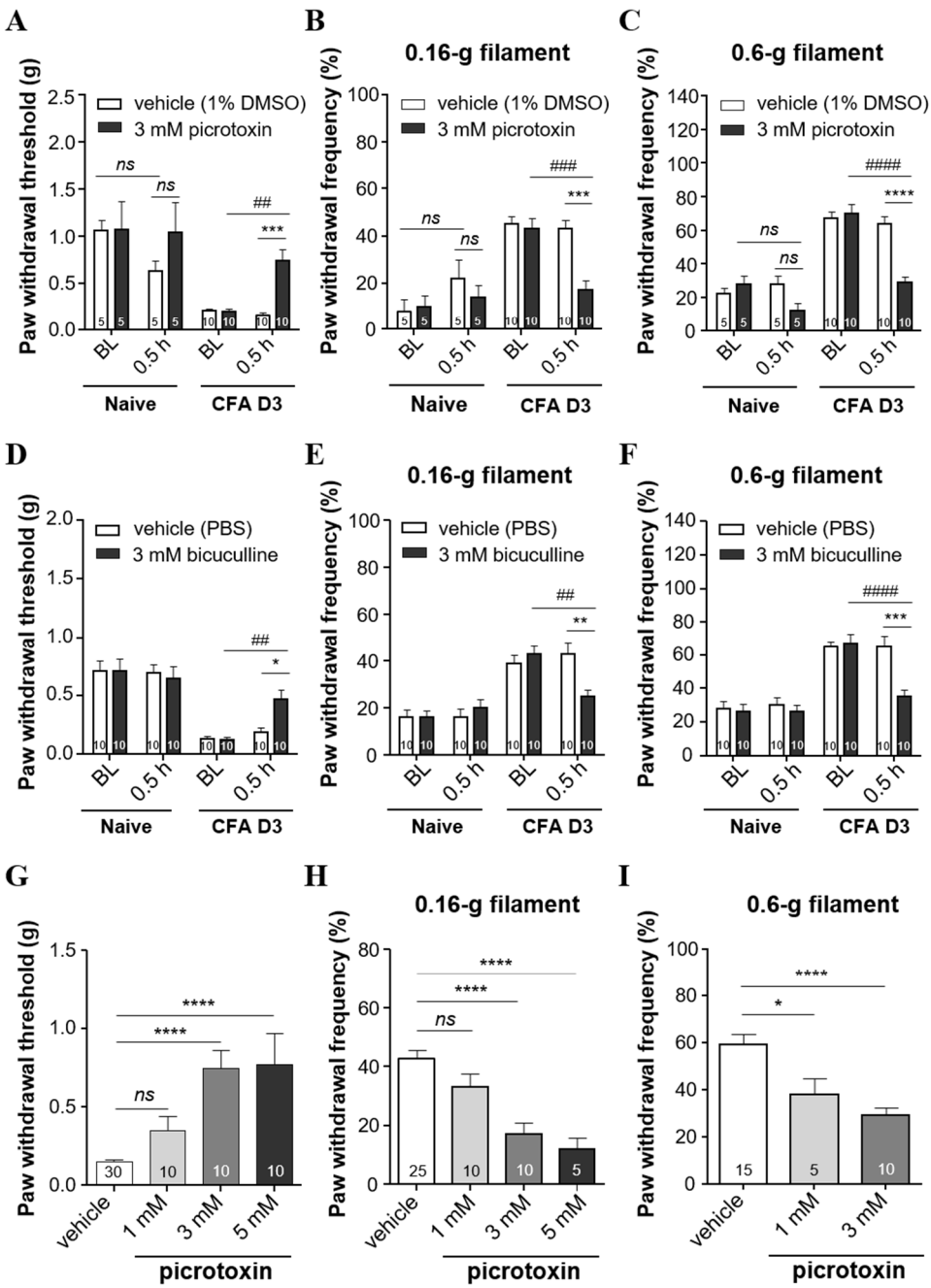
A
B
C
D
E
F
G
H
I
Paw withdrawal threshold (g)
Paw withdrawal frequency (%)
vehicle (1% DMSO)
3 mM picrotoxin
vehicle (PBS)
3 mM bicuculline
0.16-g filament
0.6-g filament
ns
##
###
####
***
****
*
**
BL
0.5 h
Naive
CFA D3
vehicle
1 mM
3 mM
5 mM
picrotoxin

Figure 6. Inhibition of CFA-induced mechanical hypersensitivity by application (i.pl.) of $GABA_AR$ antagonists

(**A-F**) Quantification of the paw withdrawal threshold (**A-D**) and paw withdrawal frequency of CFA-injected mice at D3 (CFA D3) or in naïve mice, in response to the 0.16-g (**B-E**) or 0.6-g (**C-F**) von Frey filaments, before (baseline, BL) or 0.5 h after picrotoxin (3 mM, 10 µL), bicuculline (3 mM, 10 µL), or vehicle (1% DMSO in PBS or PBS, respectively, 10 µL) i.pl. injection. All groups consisted of 5-10 mice, as indicated. Data are expressed as mean ± SEM. $^{*}p < 0.05$, $^{**}p < 0.01$, $^{***}p < 0.001$, $^{****}p < 0.0001$ (two-way ANOVA with Bonferroni post hoc test). $^{\#\#}p < 0.01$, $^{\#\#\#}p < 0.001$, $^{\#\#\#\#}p < 0.0001$ (one-way ANOVA with Bonferroni post hoc test). *ns*, not significant.

Figure 7.

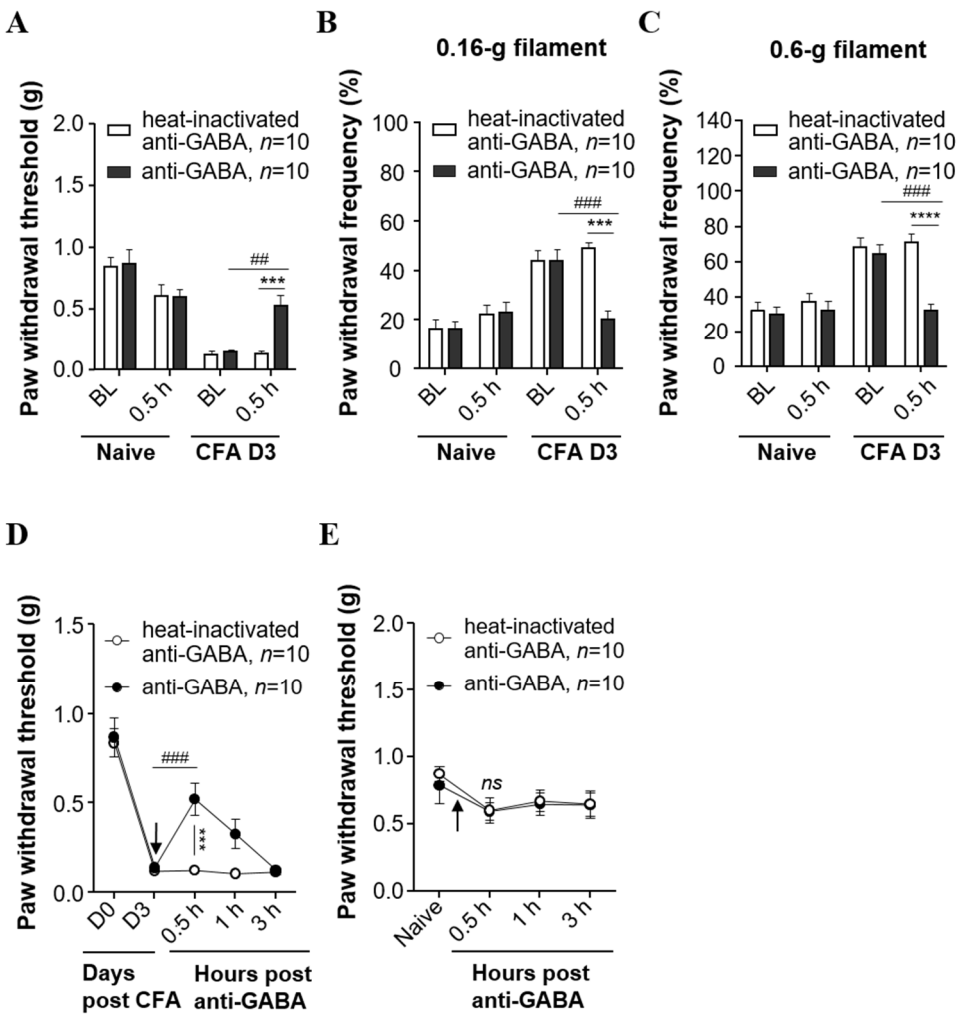
A
B
C
0.16-g filament
0.6-g filament
Paw withdrawal threshold (g)
Paw withdrawal frequency (%)
heat-inactivated anti-GABA, n=10
anti-GABA, n=10
BL
0.5 h
Naive
CFA D3
##
***
###
****
D
E
D0
D3
1 h
3 h
Days post CFA
Hours post anti-GABA
Naive
ns

Figure 7. Reversal of CFA-induced mechanical hypersensitivity by application (i.pl.) of GABA specific antibody

(**A-C**) Quantification of the paw withdrawal threshold (**A**) and paw withdrawal frequency of CFA-injected mice at D3 (CFA D3) or in naïve mice, in response to the 0.16-g (**B**) or 0.6-g (**C**) von Frey filaments, before (baseline, BL) or 0.5 h after regular or heat-inactivated anti-GABA antibody (1/100 dilution, 10 μL, i.pl.). (**D-E**) Quantification of changes in the paw withdrawal threshold over time observed after i.pl. injection of anti-GABA antibody in CFA D3 (**D**) or naïve mice (**E**). Data are expressed as mean ± SEM; $n = 10$ mice; $^{***}p < 0.001$, $^{****}p < 0.0001$ (two-way ANOVA with Bonferroni post hoc test). $^{\#\#}p < 0.01$, $^{\#\#\#}p < 0.001$ (one-way ANOVA with Bonferroni post hoc test).

Figure 8.

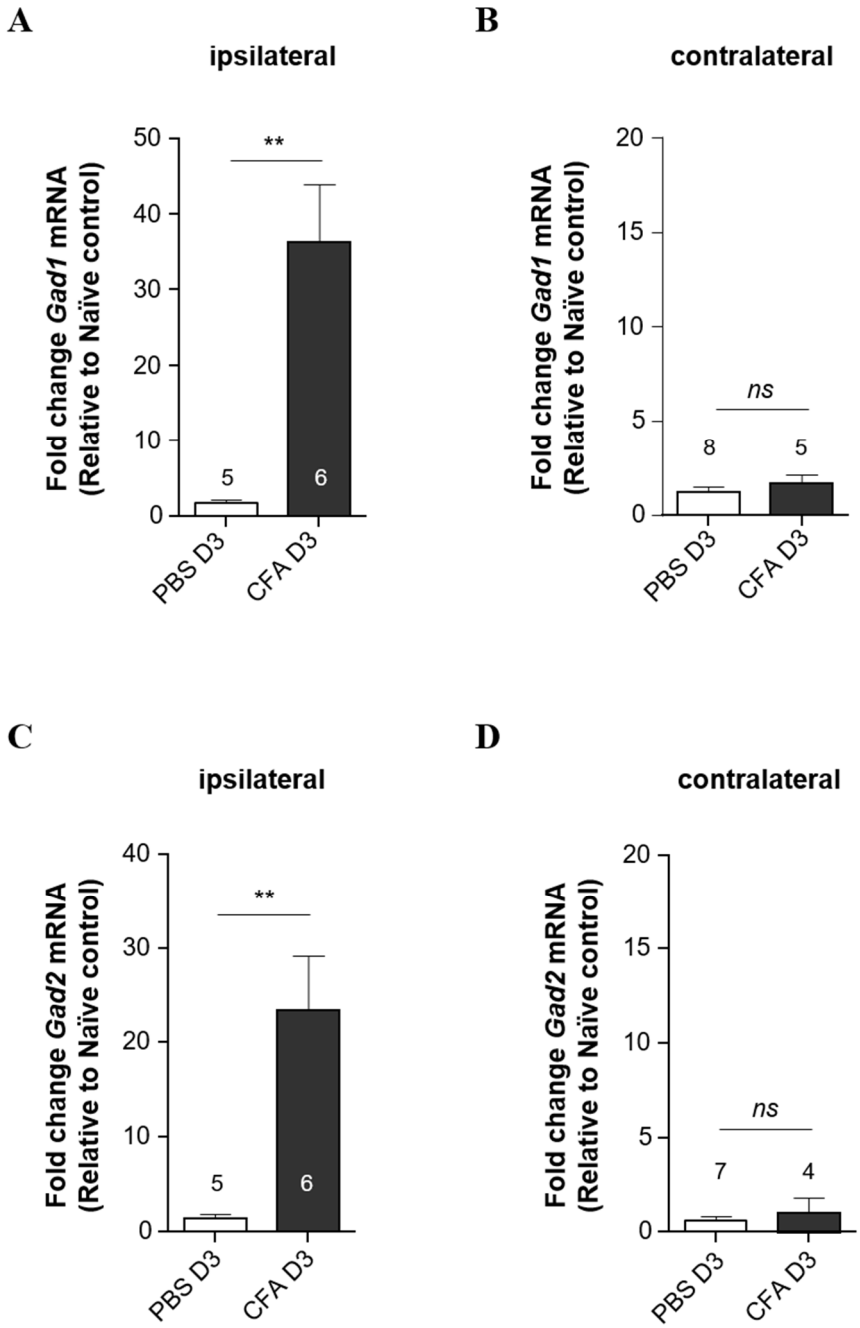
A
ipsilateral
Fold change Gad1 mRNA (Relative to Naïve control)
50
40
30
20
10
0
**
5
6
PBS D3
CFA D3
B
contralateral
Fold change Gad1 mRNA (Relative to Naïve control)
20
15
10
5
0
ns
8
5
PBS D3
CFA D3
C
ipsilateral
Fold change Gad2 mRNA (Relative to Naïve control)
40
30
20
10
0
**
5
6
PBS D3
CFA D3
D
contralateral
Fold change Gad2 mRNA (Relative to Naïve control)
20
15
10
5
0
ns
7
4
PBS D3
CFA D3

Figure 8. Upregulation of *Gad1* and *Gad2* expression in the hind paw tissue following CFA-induced inflammation

(**A-D**) RT-qPCR shows increases in *Gad1* and *Gad2* mRNA expression levels in the ipsilateral (**A-C**) but not contralateral (**B-D**) hind paw tissue in CFA-injected mice at D3 (CFA D3). Bar graphs indicate fold changes of mRNAs relative to Naïve control. All groups include 4-8 mice, as indicated. Data are expressed as mean ± SEM. $^{**}p < 0.01$ (Unpaired t-test, two-tailed). *ns*, not significant.

Figure 9.

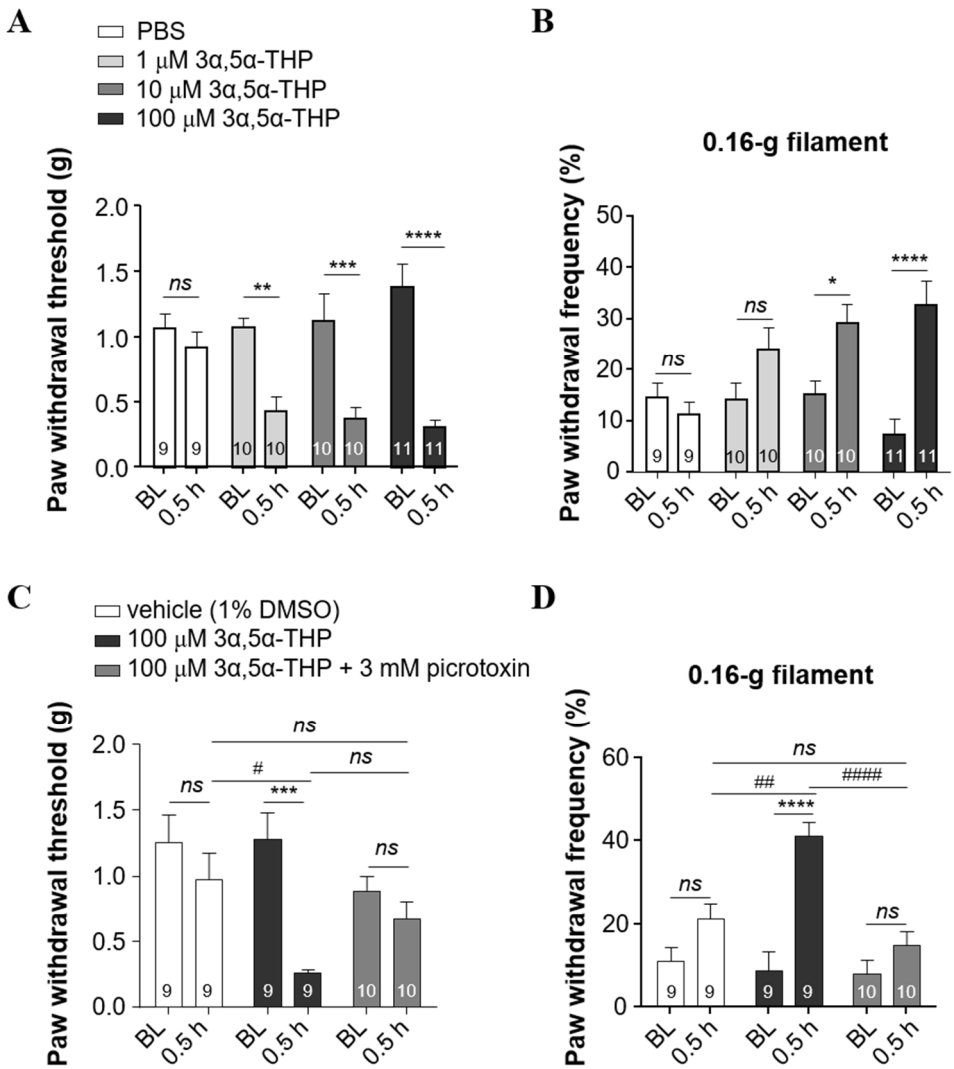
A
PBS
1 μM 3α,5α-THP
10 μM 3α,5α-THP
100 μM 3α,5α-THP
Paw withdrawal threshold (g)
ns
**
***
****
BL
0.5 h
B
0.16-g filament
Paw withdrawal frequency (%)
ns
*
****
C
vehicle (1% DMSO)
100 μM 3α,5α-THP
100 μM 3α,5α-THP + 3 mM picrotoxin
Paw withdrawal threshold (g)
#
***
D
0.16-g filament
Paw withdrawal frequency (%)
##
####
****

Figure 9. Effect of positive $GABA_AR$ modulator on mechanical allodynia in naïve mice

(**A-B**) Quantification of the paw withdrawal threshold **(A)** and paw withdrawal frequency (**B**) of naïve mice injected with 5α-pregnan-3α-ol-20-one (3α,5α-THP; 1, 10, and 100 mM, 20 µL, i.pl.) or vehicle (PBS, 20 µL, i.pl.) in response to the 0.16-g von Frey filament. (**C-D**) Quantification of the paw withdrawal threshold (**C**) and paw withdrawal frequency (**D**) of naïve mice injected with vehicle (1% DMSO in PBS, 20 µL, i.pl.), 3α,5α-THP (100 mM, 20 µL, i.pl.), or 3α,5α-THP (100 mM) and the $GABA_AR$ antagonist picrotoxin (3 mM, 20 µL, i.pl.), in response to the 0.16-g von Frey filament. All groups n = 9 to 11 mice. Data are expressed as mean ± SEM. $^{*}p < 0.05$, $^{**}p < 0.01$, $^{***}p < 0.001$, $^{****}p < 0.0001$ (two-way ANOVA with Bonferroni post hoc test). $^{\#}p < 0.05$, $^{\#\#}p < 0.01$, $^{\#\#\#\#}p < 0.0001$ (one-way ANOVA with Bonferroni post hoc test). *ns*, not significant.

DISCUSSION

In chapter 1, I demonstrated the functional role of peripheral $GABA_AR$ and endogenous GABA at inflamed tissue in persistent inflammatory hypersensitivity. Firstly, the CFA-induced persistent spontaneous and mechanical hypersensitivity were alleviated by i.pl. injection of the $GABA_AR$ antagonists, picrotoxin and bicuculline. Secondly, i.pl. injection of the GABA specific antibody reduced mechanical hypersensitivity, suggesting a contribution of endogenous GABA in persistent inflammatory hypersensitivity. Thirdly, potentiation of the cutaneous peripheral $GABA_AR$ signaling by the $GABA_AR$ positive modulator 3α,5α-THP induced mechanical allodynia in naïve mice in a dose-dependent manner. Finally, mRNA expression levels of *Gad1* (GAD 67) and *Gad2* (GAD 65), were upregulated in the inflamed hind paw tissue upon CFA injection.

GABA can activate both ionotropic $GABA_AR$ and metabotropic $GABA_BR$ expressed in primary afferent neurons. Activation of $GABA_BR$ exhibits an inhibitory effect on DRG and TG neurons (Si et al. 1997, Takeda et al. 2004). Furthermore, $GABA_BR$ attenuates TRPV1 sensitization by inflammatory mediators via a non-canonical pathway (Hanack et al. 2015). In contrast, there is evidence suggesting that a shift in the role of $GABA_AR$-mediated signaling from inhibition (Du et al. 2017, Yamamoto and Yaksh 1993, 1991) to excitation (Anseloni and Gold 2008, Bravo-Hernandez et al. 2014, Carlton, Zhou, and Coggeshall 1999, Jang et al. 2017, Zhu, Dua, and Gold 2012, Zhu, Lu, and Gold 2012) would contribute to persistent pain hypersensitivity. In addition, potentiation of dorsal root reflex activity by

neurogenic inflammation in Aδ- and C-fibers, as well as the swelling in inflamed tissue, is inhibited by spinal administration of $GABA_AR$ antagonists (Lin, Wu, and Willis 1999, Willis 1999). Although intrathecal administration of $GABA_AR$ antagonists induces mechanical allodynia in naïve mice (Anseloni and Gold 2008, Yamamoto and Yaksh 1993), these results show that cutaneous application of $GABA_AR$ antagonists induces neither mechanical allodynia nor spontaneous pain (**Fig. 5, 6**). However, the analgesic effects of $GABA_AR$ antagonists by i.pl. injection in the CFA-induced persistent inflammatory pain model are consistent with a previous work that reported the analgesia after spinal injection of the $GABA_AR$ antagonist gabazine in the CFA-induced inflammation (Anseloni and Gold 2008). These complex effects of $GABA_AR$-mediated signaling on nociceptive functions seem to be influenced by the regulation of $[Cl^-]_{in}$ in primary afferents under physiological (Price et al. 2009, Sung 2000) or pathological states (Anseloni and Gold 2008, Zhu, Dua, and Gold 2012, Zhu, Lu, and Gold 2012). These results suggest that peripheral $GABA_AR$-mediated nociceptive signaling has a crucial role in persistent inflammatory hypersensitivity.

It has been demonstrated that CFA produces a valid persistent inflammation in rodents, thus leading to increased stimulus-evoked pain hypersensitivity (Gao et al. 2010, Ren 1999, Ren and Dubner 1993). Even though spontaneous pain may be a more significant clinical issue for patients than stimulus-evoked pain (Mogil 2009, Vierck, Hansson, and Yezierski 2008), little is known as to whether the non-evoked ongoing pain is present in the CFA-induced inflammatory pain model. Ongoing and spontaneous pain can be measured by examining animal behavior upon pain induction, including paw licking, flinching, or biting, as well as spontaneous foot lifting

(Allchorne et al. 2012, Choi et al. 1994, Djouhri et al. 2006, Gregory et al. 2013, Mogil and Crager 2004, Tappe-Theodor and Kuner 2014, Xiao and Bennett 2007). Interestingly, I demonstrated that the paw licking and flinching behavior strongly develops in CFA-injected mice at D3 to D7 (**Fig. 5A**). Moreover, I showed that CFA-induced spontaneous/ongoing nociceptive behavior is drastically inhibited by the local administration of $GABA_AR$ antagonists, at inflamed tissue. This suggests that peripheral $GABA_AR$ signaling appears to be a critical component of spontaneous pain in this model (**Fig. 5C, D**). It has also revealed overexpression of the GABA synthesizing enzymes at inflamed tissue (**Fig. 8**), implying increased production of endogenous GABA under inflammatory conditions.

Since activation of GABA-mediated signaling in peripheral neurons requires a sufficient amount of GABA and the functional expression of $GABA_AR$, I used an IgG polyclonal anti-GABA antibody to functionally block endogenous GABA directly at inflamed tissue. In several studies, the administration of neutralizing antibodies for cytokines (Liu et al. 2016) or chemokines (Cao et al. 2014, Llorian-Salvador et al. 2016, Zhang et al. 2013) has been employed to block their functions in mouse pain models. It has shown that i.pl. application of anti-GABA increases the mechanical threshold in the CFA-induced inflammatory pain model but not in naïve mice, suggesting that endogenous GABA plays a functional role in persistent inflammatory hypersensitivity (**Fig. 7**). The anti-GABA antibody activity was validated by whole-cell patch clamp recordings of GABA-induced currents, which were significantly reduced by co-application of anti-GABA in cultured DRG neurons (data not shown).

Several recent reports have reported that non-neuronal cells, such as

mammalian glial cells (Lee, McGeer, and McGeer 2011, Lee, Schwab, and McGeer 2011, Lee et al. 2010, Magnaghi 2007), macrophages (Bhat et al. 2010), and fibroblasts (Ito et al. 2007, Kono et al. 2001), can produce and release GABA. I also found that GAD 65/67 immunoreactivity was increased in dermal fibroblasts of the inflamed hind paw (data not shown). Although observation suggests that dermal fibroblasts may produce GABA in inflamed tissue, it cannot be excluded that resident or infiltrating immune cells, like macrophages or neutrophils, release endogenous GABA during persistent inflammation. In addition, some reports claim that GABA or GAD is present in virtually all peripheral afferent neurons including those of DRG and TG neurons (Du et al. 2017, Hanack et al. 2015, Hayasaki et al. 2006). Therefore, further studies are required to address the source of endogenous GABA activating the peripheral $GABA_A$ receptors localized on the peripheral cutaneous nerve endings under persistent inflammation conditions.

Based on these results, targeting peripheral $GABA_AR$-mediated signaling can effectively attenuate both spontaneous pain and mechanical hypersensitivity during persistent inflammatory conditions. In addition, those analgesic effects of picrotoxin (**Fig. 5C, 6A-C**) are more significant than bicuculline (**Fig. 5D, 6D-F**), even though I employed similar dose of antagonists, based on other studies with formalin models in rodents (Carlton, Zhou, and Coggeshall 1999, Jang et al. 2017). It has been widely accepted that picrotoxin is a non-competitive antagonist of $GABA_AR$, whereas bicuculline is a competitive antagonist (Johnston 2013, Olsen 2006). This suggests that the resulting inhibition from bicuculline can be influenced by endogenous GABA concentration in the inflamed site. Furthermore, picrotoxin is now known to act upon $GABA_CRs$ (also known as $GABA_ARs$

containing ρ subunits) and glycine receptors (Johnston 2013), whereas bicuculline is not able to affect $GABA_CR$. Since it has been demonstrated that GABAcRs (Lee, Charbonnet, and Gold 2012, Maddox et al. 2004) and glycine receptors (Wang et al. 2018) are expressed in DRG neurons, these results may imply the presence of $GABA_CR$ in peripheral nerve endings. Therefore, kinetic mechanisms of inhibitors and the subunit composition should be confirmed in further studies for the development of drugs targeting $GABA_AR$. Although I observed strong analgesic effects in the behavioral test using GABA signaling blockade, peripheral $GABA_AR$-mediated signaling is still one of the contributors that can sufficiently modulate the inflammatory pain threshold in CFA-injected mice.

Since GABA and $GABA_ARs$ are present not only in the CNS but also in the PNS, their systemic modulation may induce convulsions or adverse effects. Therefore, non-CNS acting $GABA_AR$ antagonists or localized therapeutic approaches need to be developed for targeting peripheral $GABA_AR$. Recently, several humanized IgG monoclonal antibodies against ligands or their receptors have been applied to selective prevention of pain (Li, Zheng, and Chen 2017, Pellesi, Guerzoni, and Pini 2017). Targeting specific subunits of $GABA_AR$ to be expressed in peripheral endings can also be a feasible therapeutic application. Therefore, I suggest that functional blockade of peripheral GABA or $GABA_A$ receptors by such antibodies may be a novel therapeutic approach for treating persistent inflammatory pain.

In conclusion, it is verified in chapter 1 that peripheral $GABA_AR$ has a critical role in potentiating CFA-induced hypersensitivity and revealed that endogenous GABA is produced by the inflamed tissue. Therefore, peripheral $GABA_AR$ signaling in inflamed tissue may be a novel potential therapeutic

target for alleviating persistent inflammatory pain.

CHAPTER 2:
Cellular Mechanisms of TRPM8 Channels Contributing to Dentin Hypersensitivity

* This chapter has been reproduced from the article published by Pa Reum Lee, Jeong-Yun Lee, Han-Byul Kim, Jin-Hee Lee, Seog Bae Oh. TRPM8 Mediates Hyperosmotic Stimuli-Induced Nociception in Dental Afferents. Journal of Dental Research, 2020, Jan;99(1):107-114. doi: 10.1177/0022034519886847.

ABSTRACT

Hyperosmolar sweet foods onto exposed tooth dentin evoke sudden and intense dental pain, called dentin hypersensitivity. However, it remains unclear how hyperosmolar stimuli excite dental primary afferent (DPA) neurons and thereby lead to dentin hypersensitivity. This study elucidated whether TRPM8, which is well known as a cold temperature- or menthol-activated receptor, additionally mediates nociception in response to hyperosmolar stimuli in adult mouse DPA neurons, which are identified by a fluorescent retrograde tracer: DiI. Single-cell reverse transcription polymerase chain reaction revealed that TRPM8 was expressed in subsets of DPA neurons and that TRPM8 was highly colocalized with TRPV1 and Piezo2. Immunohistochemical analysis also confirmed TRPM8 expression in DPA neurons. By using Fura-2-based calcium imaging, application of hyperosmolar sucrose solutions elicited calcium transients in subsets of the trigeminal ganglion neurons, which was significantly abolished by a selective TRPM8 antagonist: N-(3-Aminopropyl)-2-[(3-methylphenyl)methoxy]-N-(2-thienylmethyl)benzamide (AMTB) hydrochloride. When I further examined changes of c-fos expression (a neuronal activation marker) in the spinal trigeminal nucleus after hyperosmolar stimulation onto exposed tooth dentin, c-fos mRNA and protein expression levels were increased and were also significantly reduced by AMTB, especially in the spinal trigeminal interpolaris-caudalis transition zone (Vi/Vc). Taken together, these results provide strong evidence that TRPM8 to be expressed in DPA neurons might mediate dental pain as a hyperosmosensor in adult mice.

INTRODUCTION

Dentin hypersensitivity is sudden, sharp, and intense dental pain, occurring when tooth dentin is exposed, and it typically disturbs patients during eating and drinking (Dababneh, Khouri, and Addy 1999). Dentin hypersensitivity results from various thermal, chemical, mechanical, and osmotic external stimuli (Cook et al. 1997, Dababneh, Khouri, and Addy 1999, Chung, Jung, and Oh 2013) that are conveyed by dental primary afferent (DPA) neurons innervating tooth pulp. Diverse molecular transducers that include transient receptor potential (TRP) channels and Piezo2 channel have been identified in DPA neurons that respond to thermal, chemical, and mechanical stimuli (Kim, Chung, et al. 2011, Won et al. 2017, Hossain et al. 2019).

Osmotic stimuli are known to evoke dentin hypersensitivity by inducing dentinal fluid movement (i.e. by the hydrodynamic theory; Brännström and Astroem 1964, Anderson and Matthews 1967, Chung, Jung, and Oh 2013). Based on this mechanism, several studies have identified hypo-osmosensors or mechanoreceptors that are activated by cell swelling, such as TRPV1 (Sato et al. 2013), TRPV2 (Gibbs, Melnyk, and Basbaum 2011, Sato et al. 2013), TRPV4(Sato et al. 2013), TRPM7 (Won et al. 2018), and TRPA1 (Tsumura et al. 2013), in dental tissues of rodents. Indeed, sweet foods with high osmolarity (e.g., soft drinks containing sugar with 678 to 817 mOsm/kg; Feldman and Barnett 1995) also frequently evoke dentin hypersensitivity (Sood et al. 2016); however, little is known about how sweet substances excite DPA neurons and thereby evoke dentin hypersensitivity.

The TRPM8 (transient receptor potential cation channel, subfamily M, member 8), which detects cold temperature or menthol in peripheral sensory neurons (McKemy, Neuhausser, and Julius 2002), has been reported to play a crucial role in dental pain evoked by cold stimuli in DPA neurons (Park et al. 2006, Kim et al. 2015, Hossain et al. 2019). Recently, it was demonstrated that the TRPM8 acts as a polymodal channel that is also sensitive to extracellular hyperosmolarity in corneal afferent neurons and mediates eye blinking in mice (Quallo et al. 2015, Bereiter et al. 2018). Therefore, I hypothesized that TRPM8 might serve as a hyperosmosensor in DPA neurons and contribute to the dentin hypersensitivity.

In the present study, I thus examined the expression patterns of TRPM8 in DPA neurons from adult mice via single-cell reverse transcription polymerase chain reaction (scRT-PCR) and immunohistochemical analysis. I also verified whether TRPM8 responds to hyperosmolar sucrose solution in the trigeminal ganglion (TG) neurons via Fura-2-based calcium imaging and whether TRPM8 in DPA neurons mediates upregulation of c-fos expression as a marker of hyperosmolarity-induced nociception in the spinal trigeminal nucleus (TN).

MATERIALS AND METHODS

Animals

All experiments were performed with a total of 64 C57BL/6 male mice (5 to 7 weeks old). All surgical and experimental procedures were approved by the Institutional Animal Care and Use Committee (IACUC) at Seoul National University. Mice were housed 2 to 6 per cage in a temperature-controlled room (23 ± 1℃, 12 h light-dark cycle) and were maintained with free access to food and water. This study conformed to the ARRIVE guidelines (Animal Research: Reporting In Vivo Experiments) for preclinical animal studies.

Retrograde labeling and primary culture of DPA neurons

By modifying methods described previously (Eckert, Taddese, and McCleskey 1997, Won et al. 2017), the dentin and tooth pulp of the maxillary first molars on both sides of the jaw were exposed with a low-speed dental drill and a round bur in mice, anesthetized with an intraperitoneal (i.p.) injection of pentobarbital (50 to 80 mg/kg). Crystals of 1,1′-Dioctadecyl-3,3,3′,3′-tetramethylindocarbocyanine perchlorate (DiI; Molecular Probes) were filled into the maxillary molar, and then the dental cavity was sealed with the dental cement (#21, GC Fuji II, GC Corporation) according to the manufacturer's instructions. Two weeks post-labeling, TG tissues were harvested in cold Ca^{2+}-/ Mg^{2+}-free Hank's Balanced Salt Solution (HBSS, Life technologies) and were cultured as previously described (Lee et al. 2018), except for trypsinization with 0.16% trypsin for 7 min at 37℃. TG neurons

were prepared a day prior to the single-cell reverse transcription polymerase chain reception and the calcium imaging experiment.

Single-cell reverse transcription polymerase chain reaction (scRT-PCR)

Before collection, neurons were examined for DiI signals (red) and isolectin B_4-FITC conjugate (Sigma) positivity (green) under a fluorescence microscope as previously described (Won et al. 2017). Neurons were collected randomly irrespective of cell body diameters with micromanipulation. Complementary DNAs (cDNAs) of collected neurons were synthesized by reverse transcriptase (superscript III, Invitrogen) according to the manufacturer's instructions and were used for nested PCR amplifications with separate primer pairs (*Trpm8*, *Trpv1*, *Piezo2*, *Tas1r2*, *Calca*, and *Gapdh*, **Table 2**). All primers were designed as exon junction primers to avoid residual genomic DNA contamination. The first-round PCR was performed in 25 μL of the reaction buffer (2X Platinum Green Hot Start PCR Master Mix, Invitrogen) containing 3 μL of RT product and 0.2 μM outer primers, followed by PCR reactions of 20 cycles according to the manufacturer's instructions. For the second-round PCR, the reaction buffer (25 μL) contained 2 μL of the products from the first-round PCR and 0.8 μM inner primers. The PCR condition was kept same as the first-round PCR except for increment of the cycle number to 35 cycles. Only for *Gapdh* primer, 6 μL RT products and 0.8 μM inner primers were used with same protocol for the second-round PCR. All PCR products were then displayed on SafePinky (GenDEPOT)-stained 1.5% agarose gel.

Calcium imaging

Cultured neurons were loaded with 2 μM Fura-2 AM (Molecular Probes) for 40 min in serum-free media at 37℃. Experimental procedures were performed as previously described (Park et al. 2006, Quallo et al. 2015, Won et al. 2018). To suppress baseline TRPM8 activity in the range of 307 to 310 mOsm/kg (Quallo et al. 2015), I used lower osmolar bath solution (274 ± 1.87 mOsm/L) containing 120 mM NaCl, 2 mM $CaCl_2$, 1 mM $MgCl_2$, 5 mM KCl, 10 mM glucose, and 10 mM HEPES and buffered to pH 7.41 ± 0.01 with NaOH. Hyperosmolar sucrose solution was made by adding sucrose (6.6% w/v [weight/volume]) to the bath solution (final osmolarity, 489 ± 6.42 mOsm/L). Images of cells were captured every 1 s, and calcium transients were measured by the fluorescence ratio (F340/F380) using MetaFluor software (version 7.8.13.0; Molecular Devices). Living neurons were identified by 50 mM KCl or 10 μM ionomycin-induced calcium transients. Hyperosmolarity-sensitive neurons that displayed at least two reproducible calcium transients, with ≥ 7% of the maximal amplitude by 50 mM KCl, following three sequential applications of hyperosmolar sucrose solution, were used for the analysis. Both bath solution and hyperosmolar sucrose solution were made fresh, and the osmolality was measured by freezing point depression using an osmometer (Advanced Instruments, Inc.) before every experiments.

Hyperosmolar stimulation to the teeth

The dentin of the right maxillary first molar in each mouse was exposed with a low-speed dental drill and a round bur in mice under pentobarbital anesthesia (50 to 80 mg/kg, i.p.). The stimulation with the following solutions was repetitively applied to the exposed tooth dentin at least 15 times for 30

min by means of a 31G insulin syringe. The iso-osmotic phosphate-buffered saline (PBS) solution (302 ± 1.32 mOsm/L, 15 μL) for vehicle, the hyperosmolar sucrose solution in PBS solution (5.72% w/v; final osmolarity, 478 ± 1.22 mOsm/L, 15 μL), and AMTB (30 μM, 15 μL), which was included in hyperosmolar sucrose solutions, were prepared on the day of the experiment.

Quantitative reverse transcription polymerase chain reaction (RT-qPCR)

Mice were sacrificed 1 h after hyperosmolar stimulation. The brainstem was coronally sliced and was ranged from -8.5 mm (Vc) to -7.5 mm (Vi/Vc) caudal to bregma with a mouse brain slicer (Zivic instruments). The TN regions were harvested with 1-mm biopsy punches (Kai medical) from coronal sections and were immediately submerged in RNAlater solution (Invitrogen) at 4℃. The total RNA was extracted by using the Direct-zol RNA miniprep Kit (Zymo research), and 200 to 250 ng of the total RNA was used for cDNA synthesis with the QuantiTect Reverse Transcription kit (Qiagen) according to the manufacturer's instructions. For quantitative PCR, each sample containing cDNAs (10 ng) was run in triplicate with PowerUp SYBR Green PCR Master Mix Kit (Applied Biosystems) and was performed using a StepOnePlus Real-Time PCR system (Applied Biosystems) under the following conditions: 50℃ for 2 min, 95℃ for 2 min, 40 cycles of 95℃ for 3 sec, and 60℃ for 30 sec, followed by a dissociation stage. The primer pairs for *c-fos* and *Gapdh* are indicated in the **Table 2**. All experimental groups relative to the Naïve control group were calculated by the ΔΔCT method with GAPDH as the reference gene as previously described (Lee et al. 2018).

Immunohistochemistry

The harvested TG tissues were fixed overnight in 4% paraformaldehyde in PBS (PFA; T&I), then transferred to 30% sucrose in PBS at 4℃. Serial frozen transverse sections (thickness: 15 μm) were mounted on SuperFrost Plus Slides (Thermo scientific) and were stored at -20℃ for later use. Sections were washed with PBS and were blocked with blocking solution (1% bovine serum albumin (BSA) in 0.2% tween 20 in PBS) for 2 h, followed by incubation of rabbit anti-TRPM8 (1/100 dilution in blocking solution, Cat. ACC-049, Alomone Labs) overnight at 4℃. Next day, sections were washed with PBS and were subsequently stained with donkey anti-rabbit Alexa Fluor 647 (1:200, 0.05% tween 20 in PBS, Molecular Probes) for 2 h at room temperature (RT). NeuroTrace 500/525 green fluorescent Nissl stain (1/100 dilution in PBS, Molecular Probes) was incubated for 20 min to specifically identify neuronal cell body size and then was washed with 0.1% tween 20 (Bio-Rad) in PBS. All sections were mounted on slides with Mowiol 4-88 embedding medium (Sigma) and were examined by confocal microscope (LSM 700; Carl Zeiss).

For c-fos immunostaining, mice were sacrificed 2 h after hyperosmolar stimulation, and frozen whole brainstem tissues, which were fixed with 4% PFA, were transversely cut (thickness, 40 μm). I determined three TN regions by serial sections, including the spinal trigeminal subnucleus caudalis (Vc; -0.16 to 0 mm caudal to the obex; obex = 0 mm), the spinal trigeminal subnucleus interpolaris-caudalis transition zone (Vi/Vc; 0.16 to 0.32 mm rostral to the obex), and the spinal trigeminal interpolaris (Vi; 0.48 to 0.64 mm rostral to the obex). All c-fos immunostaining procedures were prepared as previously described (Lee et al. 2017). Free-floating sections were washed

with PBS, were immersed into 0.3% H_2O_2 (in distilled H_2O) for 30 min for quenching, and were blocked with 5% normal goat serum (NGS) in 0.3% PBST (triton X-100 in PBS) for 1 h at RT, sequentially. Sections were incubated with rabbit anti-c-fos (1/1000 dilution in 1% NGS in 0.3% PBST; Calbiochem) for 3 days at 4℃, were washed with PBS, and were incubated with biotinylated goat anti-rabbit (1/200 dilution in PBS; Vector Laboratories) for 2 h at RT. Sections were processed with Vectastain ABC kit (Vector Laboratories) for 1 h and DAB kit (Vector Laboratories). After dehydration steps, all sections were mounted on silane-coated slide grass (Muto Pure Chemicals Co., LTD) with hardening mounting medium (Sigma) and were examined under bright-field microscope (DM5000B, Leica).

Compounds

Icilin (Tocris) stock solution (10 mM in DMSO), N-(3-Aminopropyl)-2-[(3-methylphenyl)methoxy]-N-(2-thienylmethyl)benzamide (AMTB) hydrochloride (Tocris) stock solution (10 mM in distilled H_2O), ionomycin (Tocris) stock solution (5 mM in DMSO), and gadolinium (III) chloride hexahydrate (Sigma) stock solution (1 M in distilled H_2O) were stored at -20 ℃ before use in the experiment. Sucrose (D(+)-Saccharose) was purchased from Sigma. 1,1'-dioctadecyl-3,3,3',3'-tetramethylindocarbocyanine perchlorate (DiI) was purchased from Molecular Probes. PBS, pH 7.4 was purchased from Life Technologies. All other chemicals were purchased from VWR Chemicals or Sigma.

Data analysis and statistics

To analyze cell body diameters (μm) for cultured DPA neurons, mean vertical and horizontal lengths were measured under bright-field microscope. All subsequent immunohistochemical analyses were measured with ImageJ software (National Institutes of Health). To identify TRPM8 labeling of DiI-labeled DPA neurons, each neuron was counted as being either TRPM8 positive neuron or TRPM8 negative neuron based on its cross-sectional area (μm^2) of TRPM8 labeling according to guidelines (Jensen 2013).

The c-fos-positive cells in the brainstem sections were counted by an experimenter who was unaware of which treatment each animal had received, as previous described (Lee et al. 2017). Briefly, the TN regions were confirmed by serial sectioning of brainstem tissues, and one to two adjacent sections with the highest expression of c-fos in three TN regions corresponding to the Vc, the Vi/Vc, or the Vi per each mouse, were selected and were analyzed. The image of selected sections was converted to grey scale (8 bit), subtracted background (30 pixels), enhanced (30%), and sharpened. Intensity threshold (0.2%) was adjusted, and then the positive particles were automatically detected only within the different regions.

Data in figures are presented as mean ± SEM. All statistics were performed by Prism software (version 6.01; GraphPad). Statistical significance was achieved by one-way analysis of variance (ANOVA) with Bonferroni post hoc test. Differences with p values < 0.05 were regarded as statistically significant.

TABLES

Table 2. List of primers used

Target Gene (bp)	Outer Primer Sequences	Inner Primer Sequences	GeneBank No.
Trpm8 (300, 130)	(F) GTACATAGGCGAGGTGGTGAGA (R) CTGGTGCGCTCAGAGATGTACT	(F) CATGGTCTCCAACAGGGACAC (R) CAGCAGGTGGGTATGGTTGTT	NM_134252.3
Trpv1 (293, 115)	(F) CATCTTCACCACGGCTGCTTA (R)AGAACACCATGGAAGCCACAT	(F) GCGACCATCCCTCAAGAGTT-3' (R) ATACTCCTTGCGATGGCTGA	NM_001001445.2
Piezo2 (232, 160)	(F) GTCGCAACACGGAATAGCAT (R) TCAGGTTGAGAACCCACCAC	(F) ATTGCTGGCAATGACACAGA (R) TGTCTCTGAACAAAATGATGGTG	NM_001039485.4
Tas1r2 (364, 156)	(F) TCGACCCTGTTCTACACAACCT (R) ACATGCCAGATCTCCCTGAGTA	(F) CATCACCGAGTCCTTTAACAACG (R) AGCTGCCATGGATAGACGATTT	NM_031873.1
Calca (242, 156)	(F) GCCTTTGAGGTCAATCTTGG (R) CCTTCACCACACCTCCTGAT	(F) CACTCTCAGTGAAGAAGAAGTTCG (R) GTCACACAGGTGGCAGTGTT	NM_001289444.1 NM_001033954.3
Gapdh (282 bp)		(F) CCAGAACATCATCCCTGCAT-3' (R) GCATCGAAGGTGGAAGAGTG-3'	NM_001289726.1 NM_008084.3
c-fos (100 bp)		(F) GGTGAAGACCGTGTCAGGAG-3' (R) CCTTCGGATTCTCCGTTTCTCT-3'	NM_010234.3

RESULTS

Localization of TRPM8 in DPA neurons

I first determined TRPM8 expression in DPA neurons via immunohistochemical analysis. DiI-labeled DPA neurons from the maxillary first molar were distributed only in the maxillary (V_2) region, not in the ophthalmic (V_1) and mandibular (V_3) regions of the TG (**Fig. 10Aa**), consistent with our recent study (Won et al. 2017). All DiI-labeled cells turned out to be neuronal cells with Nissl staining (**Fig. 10Ab–Ad**). I found that 28% (*n* = 16 of 57) of DiI-labeled DPA neurons were colabeled with TRPM8 (**Fig. 10B, C**). The 75% (*n* = 12 of 16) of the $TRPM8^+$ DPA neurons and 75% (*n* = 43 of 57) of the total DPA neurons were distributed within a range of medium-sized neurons (**Fig. 10C**), consistent with previous reports in rats (Fried et al. 1989, Pan et al. 2003, Kvinnsland et al. 2004, Fried, Sessle, and Devor 2011).

Molecular characterization of *Trpm8*-expressing DPA neurons

I then examined the *Trpm8* mRNA expression profiles of DiI-labeled DPA neurons via scRT- PCR by comparing with potential markers for DPAs: TRPV1, IB_4, and PIEZO2. TRPV1 is heat receptor and is expressed exclusively in unmyelinated C-fibers (Hossain et al. 2019), and IB_4 positivity indicates non-peptidergic C-fibers (Stucky and Lewin 1999). However, PIEZO2 is the mechanosensitive receptor expressed in predominantly myelinated A-fibers (Won et al. 2017). All DPA neurons were IB_4 negative (**Fig. 11A**), which is consistent with previous studies (Kvinnsland et al. 2004, Le Pichon and Chesler 2014, Chen et al. 2017), and 12.5% (*n* = 5 of 40) of

DPA neurons expressed *Trpm8* mRNA (**Fig. 11A, B**). Interestingly, thermosensitive *Trpv1* and mechanosensitive *Piezo2* were highly co-expressed in the majority of *Trpm8* mRNA-expressing DPA neurons (80%, n = 4 of 5, **Fig. 11C**) and in medium-sized DPA neurons (**Fig. 11D**).

Hyperosmolar sucrose solution activates TRPM8 in TG neurons

Since TRPM8 is a Ca^{2+}-permeable cation channel (McKemy, Neuhausser, and Julius 2002), I verified whether hyperosmolarity activates TRPM8 in TG neurons via calcium imaging. Hyperosmolar sucrose solution elicited calcium transients in subpopulations (8.2%, n = 24 of 294) of TG neurons, which were also responsive to icilin, a TRPM8 agonist (**Fig. 12A, F**). Three sequential applications of hyperosmolar sucrose solution produced comparable and reproducible calcium transients (**Fig. 12B, C**), and I found that second calcium transients were significantly abolished by pretreatment with AMTB, a selective TRPM8 antagonist, in a dose-dependent manner in icilin-responsive neurons (**Fig. 12D, E**). Populations of hyperosmolar-sensitive neurons within TG neurons were also decreased by AMTB in a dose-dependent manner (**Fig. 12F**).

The Vi/Vc region is critical for hyperosmolarity-induced nociception from DPA neurons

The immediate early gene c-fos mRNA (Sawamura et al. 1999) or protein (Hunt, Pini, and Evan 1987) expression, which is trans-synaptically regulated by noxious stimulation of sensory afferents, has been widely used as a neuronal marker of nociception in the spinal dorsal horn or the spinal TN (Harris 1998). I found that the *c-fos* mRNA expression levels were

significantly upregulated after hyperosmolar stimulation onto the exposed tooth dentin in the ipsilateral TN as compared with vehicle and that their enhancements were also significantly inhibited by AMTB (**Fig. 13A, B**), while. its expression levels were not changed in the contralateral side. Changes in c-fos expression were then analyzed at the protein level in the ipsilateral subnuclei of TN corresponding to the Vc, Vi/Vc, or Vi, respectively. The number of c-fos-positive neurons was increased after hyperosmolar stimulation as compared with vehicle in the Vi/Vc, which was also inhibited by AMTB (**Fig. 13E, F**). However, c-fos expression was not changed in neither the Vc (**Fig. 13C, D**) nor the Vi (**Fig. 13G, H**). Taken together, these results suggest that the Vi/Vc region may be critical for the transmission of hyperosmolarity-induced nociception, mediated by TRPM8, in teeth.

Figure 10.

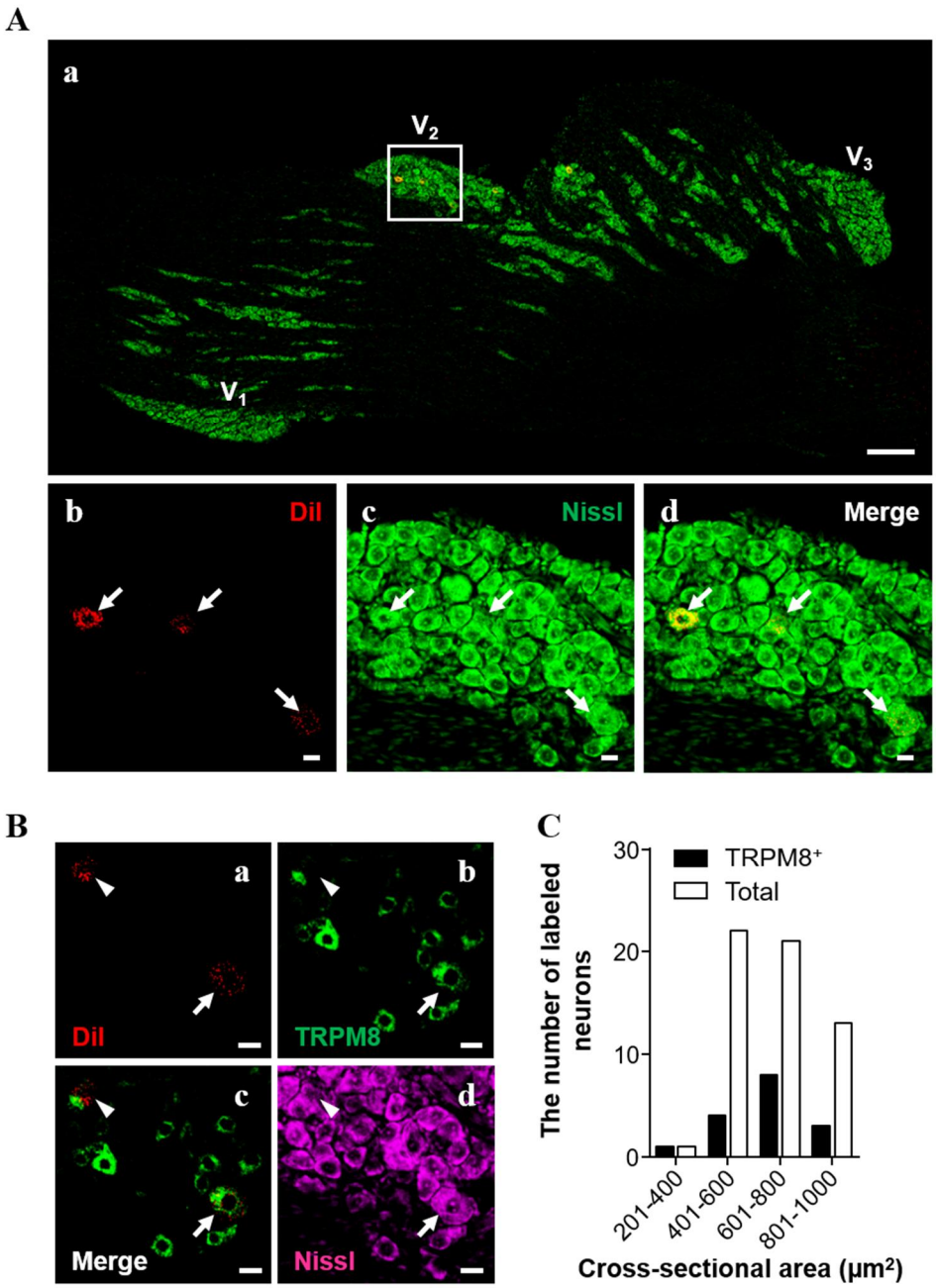
A
a
V2
V3
V1
b
DiI
c
Nissl
d
Merge
B
a
DiI
b
TRPM8
c
Merge
d
Nissl
C
TRPM8+
Total
The number of labeled neurons
30
20
10
0
201-400
401-600
601-800
801-1000
Cross-sectional area (μm²)

Figure 10. Expression of TRPM8 in DPA neurons

(**Aa**) Representative image shows DiI-labeled DPA neurons (red) and Nissl-stained somata of neuronal cells (green) in the TG. Scale bar: 200 μm. (**Ab-Ad**) Inset in panel Aa is the high-magnification images. Arrows indicate DiI-labeled DPA neurons. Scale bars: 20 μm. (**Ba-Bd**) TRPM8 (green) was expressed in DiI-labeled DPA neurons (red), which were stained by Nissl (violet). Arrows show $TRPM8^{+}$ DPA neurons, and arrowheads indicate $TRPM8^{-}$ DPA neurons. Scale bars: 20 μm. (**C**) The majority was within a range of medium-sized (401 to 800 μm^2) $TRPM8^{+}$ DPA neurons (201 to 400 μm^2, $n = 1$; 401 to 600 μm^2, $n = 4$; 601 to 800 μm^2, $n = 8$; 801 to 1,000 μm^2, $n = 3$) and total DPA neurons (201 to 400 μm^2, $n = 1$; 401 to 600 μm^2, $n = 22$; 601 to 800 μm^2, $n = 21$; 801 to 1,000 μm^2, $n = 13$). $n = 5$ mice.

Figure 11.

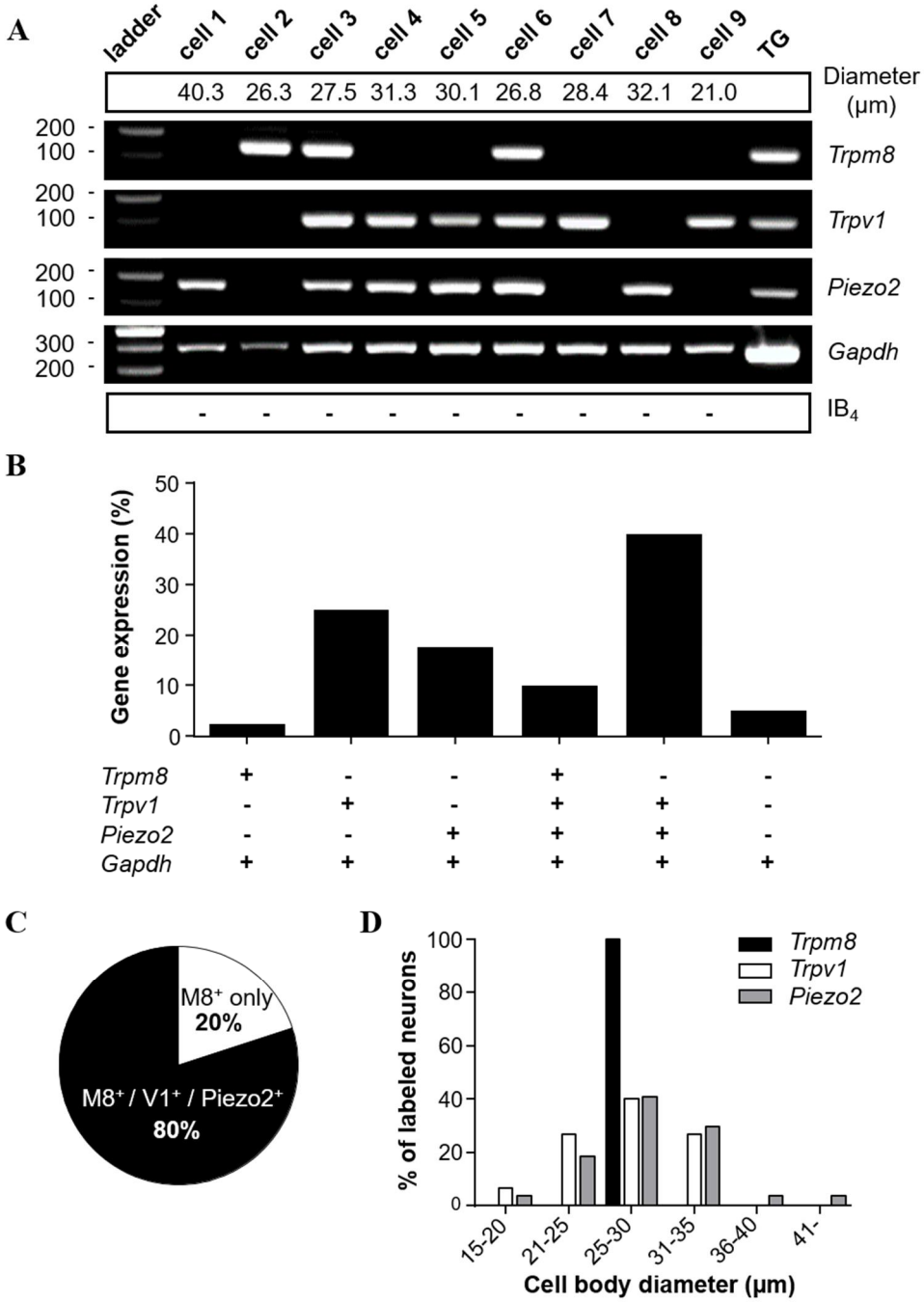
A
ladder
cell 1
cell 2
cell 3
cell 4
cell 5
cell 6
cell 7
cell 8
cell 9
TG
Diameter (μm)
40.3 26.3 27.5 31.3 30.1 26.8 28.4 32.1 21.0
200
100
Trpm8
Trpv1
Piezo2
300
200
Gapdh
IB4
B
Gene expression (%)
50
40
30
20
10
0
Trpm8 + - - + - -
Trpv1 - + - + + -
Piezo2 - - + + + -
Gapdh + + + + + +
C
M8+ only
20%
M8+ / V1+ / Piezo2+
80%
D
% of labeled neurons
100
80
60
40
20
0
Trpm8
Trpv1
Piezo2
15-20
21-25
25-30
31-35
36-40
41-
Cell body diameter (μm)

Figure 11. Characterization of *Trpm8*-expressing DPA neurons

(**A**) Representative agarose gels show 9 individual DPA neurons for each scRT-PCR product and total TG tissue as positive control. Predicted sizes for selected markers: *Trpm8* (130 bp), *Trpv1* (115 bp), *Piezo2* (160 bp), and *Gapdh* (282 bp). (**B**) Additional scRT-PCR analysis indicates that the expressional profile of collected DPA neurons revealed $Trpm8^{+}$ only (2.5%, n = 1), $Trpv1^{+}$ only (25%, n = 10), $Piezo2^{+}$ only (17.5%, n = 7), $Trpm8^{+}Trpv1^{+}Piezo2^{+}$ (10%, n = 4), $Trpv1^{+}Piezo2^{+}$ (40%, n = 16), or $Trpm8^{-}Trpv1^{-}Piezo2^{-}$ (5%, n = 2). n = 40 neurons from 11 mice. (**C**) Pie graph representation of $TRPM8^{+}$ DPA neurons. (**D**) Size distribution of *Trpm8*, *Trpv1*, and *Piezo2* mRNA-expressing DPA neurons.

Figure 12.

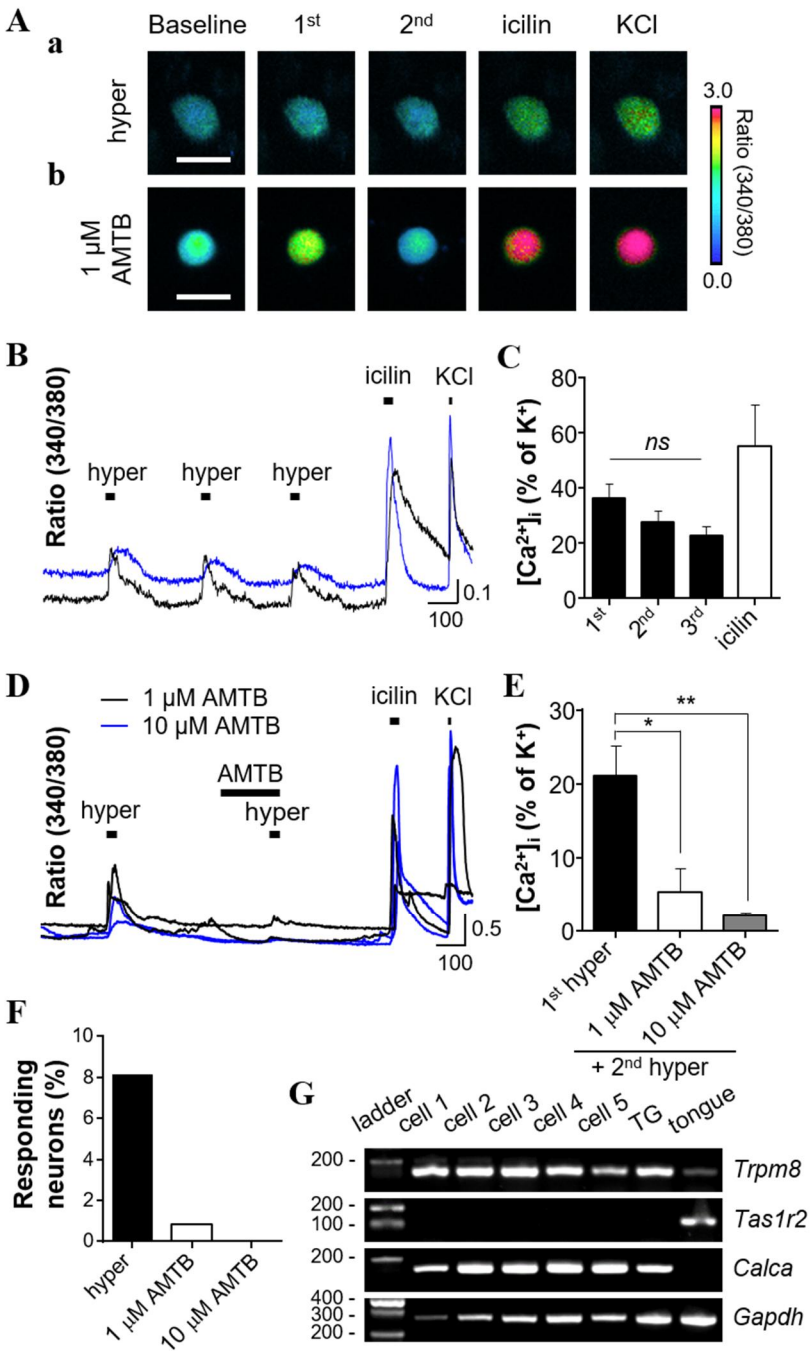
A
a
b
Baseline
1st
2nd
icilin
KCl
hyper
1 μM AMTB
3.0
0.0
Ratio (340/380)
B
Ratio (340/380)
hyper
hyper
hyper
icilin
KCl
0.1
100
C
[Ca2+]i (% of K+)
ns
1st
2nd
3rd
icilin
D
1 μM AMTB
10 μM AMTB
AMTB
hyper
hyper
icilin
KCl
Ratio (340/380)
0.5
100
E
[Ca2+]i (% of K+)
**
*
1st hyper
1 μM AMTB
10 μM AMTB
+ 2nd hyper
F
Responding neurons (%)
hyper
1 μM AMTB
10 μM AMTB
G
ladder
cell 1
cell 2
cell 3
cell 4
cell 5
TG
tongue
Trpm8
Tas1r2
Calca
Gapdh

Figure 12. Effects of hyperosmolar sucrose solution on intracellular calcium transients in TRPM8-expressing TG neurons

(**Aa-Ab**) Representative cell image of pseudocolor ratiometric $[Ca^{2+}]_i$ images in TG neurons. Scale bars: 30 μm. Representative traces (**B**) and quantitative data (**C**) of reproducible calcium transients by hyperosmolar sucrose solution (489 ± 6.42 mOsm/L) in 1 μM icilin-responding neurons, *ns* (one-way ANOVA with Bonferroni post hoc test), n = 17 neurons from 2 mice. Representative traces (**D**) and quantitative data (**E**) of dose-dependently blocked calcium transients by pretreatment with AMTB, $^{*}p < 0.05$ (one-way ANOVA with Bonferroni post hoc test, n = 9 neurons from 2 mice), $^{**}p < 0.01$ (one-way ANOVA with Bonferroni post hoc test, n = 11 neurons from 2 mice). Bars represent mean ± SEM. ANOVA, analysis of variance; *ns*, not significant. (**F**) Percentage summary of hyperosmolar-sensitive neurons that are observed in subsets of TG neurons and percentage of TG neurons remaining responsive after 1 μM (0.8%, n = 3 of 368) or 10 μM (0%, n = 0 of 366) AMTB pretreatment. (**G**) The representative gels showing scRT-PCR products from *Trpm8* mRNA-expressing DPA neurons and whole TG and tongue tissue as positive controls. Predicted sizes for selected markers *Trpm8* (130 bp), *Tas1r2* (156 bp), *Calca* (156 bp), and *Gapdh* (282 bp).

Figure 13.

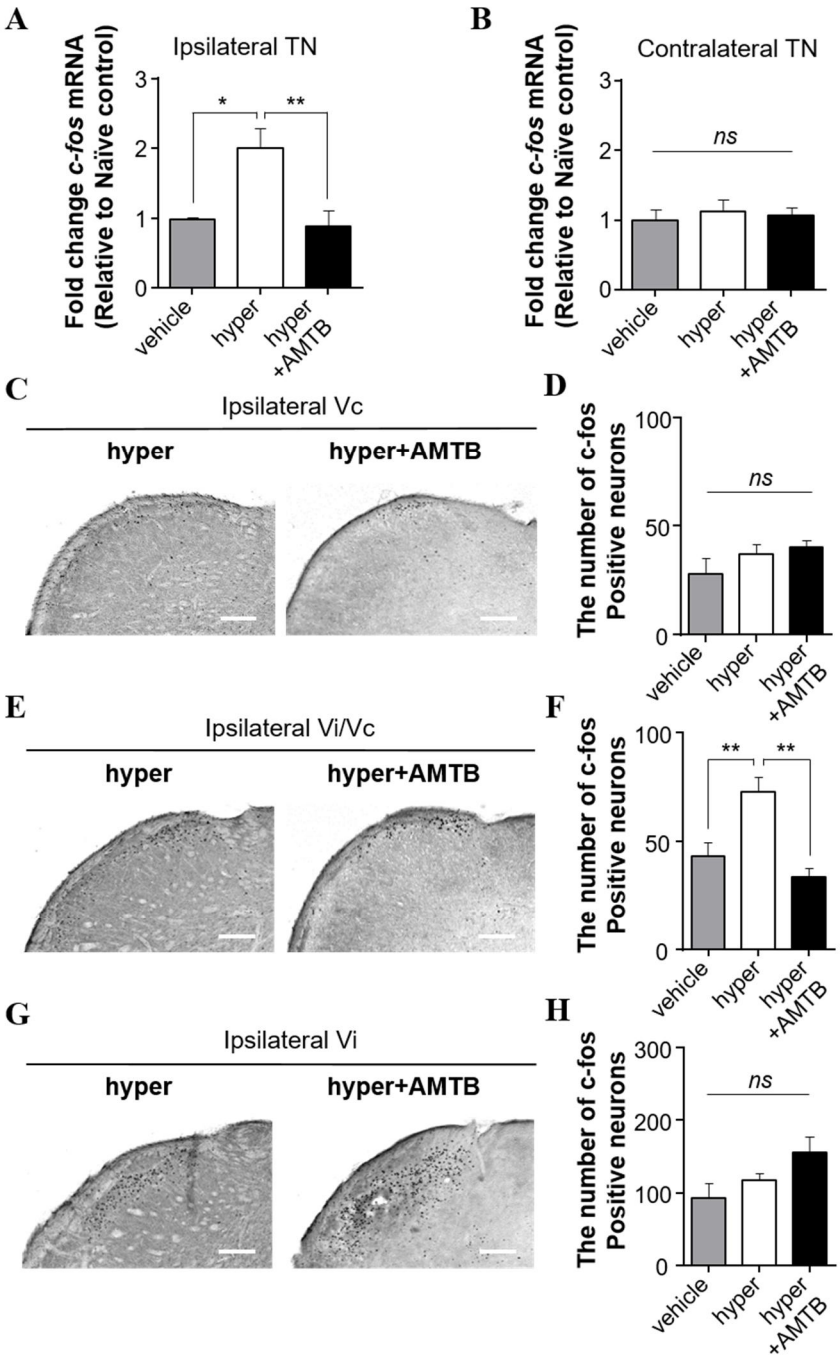
A
Ipsilateral TN
Fold change c-fos mRNA (Relative to Naïve control)
vehicle
hyper
hyper +AMTB
B
Contralateral TN
ns
C
Ipsilateral Vc
hyper
hyper+AMTB
D
The number of c-fos Positive neurons
E
Ipsilateral Vi/Vc
F
G
Ipsilateral Vi
H

Figure 13. Effects of hyperosmolar stimuli onto the exposed dentin on c-fos expression in the TN from adult mice

(**A-B**) RT-qPCR shows changes of c-fos mRNA levels in the ipsilateral TN, $^{*}p < 0.05$, $^{**}p < 0.01$ (one-way ANOVA with Bonferroni post hoc test, **A**), but not in the contralateral TN, *ns* (one-way ANOVA with Bonferroni post hoc test, **B**), of the hyper group (478 ± 1.22 mOsm/L, 15 μL) as compared with the phosphate-buffered saline vehicle group (302 ± 1.32 mOsm/L, 15 μL). Their enhancements were also significantly inhibited in the hyper + AMTB group (30 μM, 15 μL). *n* = 5 to 8 mice per each group. Bar graphs indicate fold changes in mRNAs relative to naïve controls (*n* = 4 mice, data not shown). (**C-H**) Representative images of the c-fos staining in the ipsilateral Vc (**C**), Vi/Vc (**E**), and Vi (**G**). Quantitative analysis of the c-fos expression in the Vc, *ns* (one-way ANOVA with Bonferroni post hoc test, **D**), Vi/Vc, $^{**}p < 0.01$ (one-way ANOVA with Bonferroni post hoc test, **F**), and Vi, *ns* (one-way ANOVA with Bonferroni post hoc test, **H**). *n* = one or two sections were used from the same animal. *n* = 4 to 7 mice per each group. Scale bars: 200 μm. Data are expressed as mean ± SEM. ANOVA, analysis of variance; *ns*, not significant.

Figure 14.

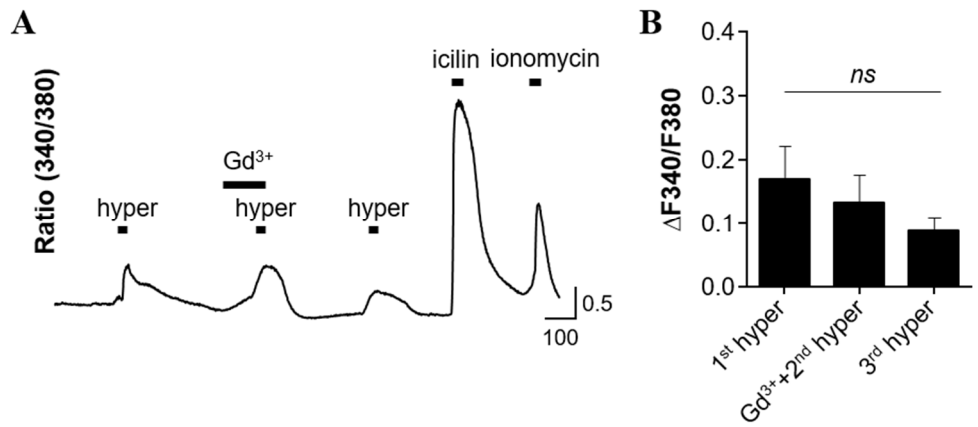
A
Ratio (340/380)
hyper
Gd3+
hyper
hyper
icilin
ionomycin
0.5
100
B
ΔF340/F380
0.4
0.3
0.2
0.1
0.0
ns
1st hyper
Gd3++2nd hyper
3rd hyper

Figure 14. A mechanosensitive ion channel blocker does not inhibit hyperosmolar sucrose solution-induced calcium transients

(**A-B**) A representative trace (**A**) and quantitative data (**B**) of reproducible calcium transients which were not blocked by 30 μM Gd^{3+} in 1 μM icilin-responding TG neurons. The delta fluorescence ratio (ΔF340/F380) was measured as the difference between the basal fluorescence ratio recorded before drug treatments and the peak fluorescence ratio, *ns* (one-way ANOVA with Bonferroni post hoc test), n = 19 neurons from 2 mice. Bars represent mean ± SEM. ANOVA, analysis of variance; *ns*, not significant.

DISCUSSION

In chapter 2, I demonstrated the following findings: TRPM8 channels were molecularly and functionally expressed in subsets of DPA neurons. TRPM8-expressing TG neurons responded to hyperosmolar stimuli, and hyperosmolar sucrose solution-induced calcium transients were blocked by AMTB in a dose-dependent manner. Hyperosmolarity-induced nociception, determined by the c-fos expression, was significantly attenuated by AMTB in the TN, critically in the Vi/Vc region. Therefore, my results suggest that TRPM8 in DPA neurons contributes to dental nociception as a hyperosmosensor in adult mice.

With respect to the labeling methods of DPA neurons, most previous studies (Cook et al. 1997, Eckert, Taddese, and McCleskey 1997, Park et al. 2006, Kim, Chung, et al. 2011, Won et al. 2017) labeled DPA neurons with crystal DiI in rats, except for a study in mice that used paste DiI (Kadala et al. 2018). I verified in the present study that DiI-labeled DPA neurons were located only in the V_2 region of the TG (**Fig. 10A**). Placing crystal DiI directly on the pulp, I could minimize pulp inflammation by preventing bleeding. Furthermore, the expression of neuronal CGRP, which is related to dentin injury and pulpal inflammation (Byers 1994), was comparable between the ipsilateral (surgical side) and contralateral (non-surgical side) TG (data not shown), suggesting that DPA neurons are less affected by pulpal inflammation in my experimental conditions. I also found that the number of accessible maxillary molar was limited to one from each side in a mouse model, even though it is possible to use up to three maxillary molars in each side of the

jaw for labeling DPA neurons in rats (Eckert, Taddese, and McCleskey 1997), and the number of DiI-labeled DPA neurons per each molar in mice was also slightly smaller than in rats (data not shown).

The population of TRPM8-expressing neurons is restricted to a relatively small population (5% to 10%) of adult DRG but higher in TG than DRG (McKemy, Neuhausser, and Julius 2002, Kobayashi et al. 2005, Le Pichon and Chesler 2014). Previous works with mutant mice expressing a green fluorescent protein under the control of the TRPM8 promoter have reported that TRPM8 is expressed in 6% (Michot, Lee, and Gibbs 2018), 13% (Kim et al. 2015), or 49% (Kadala et al. 2018) of labeled DPA neurons. In this study, it was presented that expression of TRPM8 was in subsets of DPA neurons, which were medium-sized in diameter (**Fig. 10C, 11D**).

The majority of *Trpm8* mRNA was colocalized with *Trpv1* and *Piezo2* mRNAs in DPA neurons (**Fig. 11A-C**), and *Trpm8* mRNA-expressing DPA neurons also co-expressed with *Calca* mRNA encoding CGRP (**Fig. 12**), consistent with previous reports from rats (Fried, Sessle, and Devor 2011, Won et al. 2017) and mice (Kim et al. 2015), suggesting that TRPM8 in nociceptive neurons is involved in dental pain. The preferential co-expression of *Trpm8* with *Trpv1*, *Calca*, and *Piezo2* in DPA neurons may suggest that DPA neurons have a unique sensory population of TG neurons distinct from DRG neurons. To further identify detailed molecular characteristics of DPA neurons, single-cell transcriptome analysis can be an important strategy (Nguyen et al. 2017).

The Vi/Vc, as well as the Vc, is an important region where c-fos expression increases after noxious or cold stimulation is applied to the tooth (Ren and Dubner 2011, Ahn et al. 2012, Michot, Lee, and Gibbs 2018). In this

study, c-fos-positive neurons were increased by hyperosmolar stimulation critically in the Vi/Vc region, consistent with a previous report (Michot, Lee, and Gibbs 2018), which was significantly reduced by AMTB (**Fig. 13E, F**), suggesting that hyperosmolarity-induced nociception from the tooth may be due to the activation of TRPM8 in DPA neurons. Interestingly, it was noticed that c-fos expression was about two times higher in the Vi as compared with the Vc and the Vi/Vc, even in the vehicle group (**Fig. 13H**). As the Vi receives neuronal projections from the deep oral structures, such as the temporomandibular joint and the masseter muscle (Ohya 1992), higher c-fos expression in the Vi may be due to their activation during surgery for hyperosmolar stimulation. Nevertheless, the upregulation of c-fos-positive neurons was not reduced by AMTB in the Vi (**Fig. 13G, H**), suggesting minimal involvement of TRPM8 in neuronal activation of the Vi during the surgery procedure.

It has been demonstrated that noxious cold stimulation of the tooth in mice significantly increases c-fos expression only in the Vi/Vc, not in the Vc or the Vi, and the upregulation of c-fos is not reduced by the TRPM8 knockout mice or the application of a selective TRPA1 antagonist (Michot, Lee, and Gibbs 2018). This result suggests that the TRPM8 and TRPA1 have minor effects on dental nociception following cold stimulation (Michot, Lee, and Gibbs 2018). However, an increase in osmolarity elevates the temperature threshold for TRPM8 activation to a physiologically relevant temperature (e.g., 37°C) (Quallo et al. 2015), suggesting that cold-evoked dental nociception can be affected by hyperosmolarity. To address relationships between cold and osmolarity, it remains to be elucidated how TRPM8 has polymodal roles, responding to cold temperature and hyperosmolar stimuli.

Furthermore, another issue is related to the controversy regarding menthol-evoked nociception. Menthol, derived from peppermint, acts as one of the agonists of cold-activated TRPM8 channel (Clapham 2002). Menthol has widely been used as topical pain relievers applied to the skin (Fernandez-Pena and Viana 2013). Menthol is also commonly contained in toothpaste with implications for flavors, anti-inflammatory properties, prevention of tooth decay, whitening teeth, and refreshing feelings (Nectar Lifesciences, n.d.). It has not yet been reported that the menthol produces dentin hypersensitivity in exposed tooth dentin. However, some papers have reported that very high concentrations of menthol (~40%) applied topically to the skin are noxious in human objectives (Binder et al. 2011, Wasner et al. 2004). In efforts to understand how TRPM8 activators interact with the channel, the desensitization mechanisms of TRPM8, similar to heat desensitization of TRPV1 by capsaicin, have been studied. For example, cold- and cooling agents (e.g., menthol and menthol derivatives)-evoked responses reflect Ca^{2+}-dependent desensitization (Diver, Cheng, and Julius 2019, Kuhn, Kuhn, and Luckhoff 2009). It is also contributing to our cold adaptation (Yudin et al. 2011). However, icilin (super-cooling agent) modulates TRPM8 activity through the specific ligand-binding pocket (Diver, Cheng, and Julius 2019). Due to these different mechanisms on TRPM8, its activators can lead to controversial results. Therefore, further studies are needed to address how the hyperosmolar sucrose solution interacts with TRPM8.

For this study, I used the hyperosmolar sucrose solution to mimic hyperosmolar solutions and sweet substances. It is reported that hyperosmolar solution, which is made by an increase in either NaCl or sucrose concentration, yields similar results regarding hyperosmolarity-induced calcium responses

in cultured sensory neurons, as well as at recombinant mTRPM8 receptors (Quallo et al. 2015). However, it is interesting to observe that patients experience discomfort with sweet substances more strongly and frequently as compared with salty foods. This observation implies that there is probably another mechanism for DPA neurons to transduce nociception in response to sweet stimuli. Since TRPM8 mRNA-expressing DPA neurons lacked *Tas1r2* mRNA encoding sweet taste receptor T1R2 (**Fig. 12**), this should be independent of sweet taste receptor signaling. On the other hand, NaCl solutions can be intended to treat dentin hypersensitivity via dentinal tubule occlusion. For example, a clinical study has demonstrated that the NaCl solution (3%, pH = 2.4) significantly decreases dentinal tubules' aperture and thereby reduces dentin hypersensitivity (Cuenin et al. 1991). The NaCl solution is more effective than the 3% potassium oxalate solution (3%, pH = 2.4), which have been used for treating dentin hypersensitivity (Cuenin et al. 1991). Accordingly, dentin hypersensitivity can be affected differently under hyperosmotic conditions by sucrose solution and NaCl solution.

The hydrodynamic theory has traditionally explained dentin hypersensitivity induced by sweet substance since hyperosmolar sucrose induces fluid movement in dentinal tubule (Brännström and Astroem 1964, Fried, Sessle, and Devor 2011, Chung, Jung, and Oh 2013). From the present study, I demonstrated that hyperosmolar sucrose solution could also activate TRPM8 in DPA neurons and that activation of TRPM8 in DPA neurons produced c-fos expression in the TN. These results suggest that TRPM8 contributes to dental nociception by acting as a hyperosmosensor in DPA neurons. Given that hyperosmolar solution-induced calcium transients were not blocked by pretreatment with Gd^{3+}, a mechanosensitive ion channel

blocker, in TRPM8-expressing TG neurons (**Fig. 14**), activation of TRPM8 by hyperosmolar sucrose solutions may not be due to the changes of mechanical dynamics in the cell membrane.

In conclusion, it is verified in chapter 2 the role of TRPM8 expressed by DPA neurons in the development of dental pain evoked by hyperosmolar stimuli such as sweet foods.

CHAPTER 3:
Gene-Expression Signatures of the Adult Mouse Dental Sensory System

ABSTRACT

External stimulation to the exposed dentin of teeth can cause dental pain, which is conveyed by dental primary afferent (DPA) neurons innervating tooth pulp. Since dental pain is the most likely evoked by light mechanical irritations such as brush or air puffs, there have been efforts to demonstrate mechanosensitive ion channels in DPA neurons. However, it remains elusive how these innocuous mechanical stimuli, which mostly do not activate nociceptors or evoke pain in the skin, generate pain within the tooth pulp under pathological conditions. In an effort to elucidate this observation, I performed full-length single-cell RNA sequencing (scRNA-seq) and generated whole transcriptome profiles from a total of 83 adult mouse DPA neurons. In this study, the downstream analyses revealed that six molecularly distinct subpopulations in DPA neurons. In addition, one of the largest subpopulations of DPA neurons consisted of neurons showing the high expression levels of both a low-threshold mechanosensitive *Piezo2* ion channel and a pain-related neuropeptide *Calca* encoding CGRP (calcitonin gene-related peptide). Comparing the expression of pain-related marker genes amongst *Piezo2*-expressing DPA neurons revealed that *Calca* showed the highest co-expression rate than *Trpv1* and *Tac1*. Taken together, scRNA-seq can provide insights into molecular signatures of the mouse dental sensory system. Furthermore, these results may suggest that low-threshold mechanoreceptors are involved in pain rather than touch in teeth under pathological conditions.

INTRODUCTION

External stimulation to the exposed dentin of teeth can cause dental pain, more precisely *dentin hypersensitivity*, conveyed by dental primary afferent (DPA) neurons innervating tooth pulp (Cook et al. 1997, Chung, Jung, and Oh 2013). Like most somatic afferent neurons, various sensory transducers for responding directly to noxious external stimuli, such as thermal (e.g., transient receptor potential (TRP) channels) and chemical (e.g., acid-sensing ion channels (ASICs)), have been demonstrated in DPA neurons (Chung, Jung, and Oh 2013, Hossain et al. 2019, Lee et al. 2019). However, it cannot be explained why dentin hypersensitivity is the most likely evoked by extremely light mechanical irritations, such as brushing, water spray, or air puffs so that this paradoxical phenomenon makes the dental sensory system different from nociceptive networks at other body sites (Cook et al. 1997, Fried, Sessle, and Devor 2011, Fried and Gibbs 2014). In addition, the nerve fibers are rarely expanded to the dentino-enamel junction, which is the most sensitive portion of the tooth in patients when a dental bur passes through it (Markowitz and Pashley 2015).

In this context, the *hydrodynamic theory* has first proposed by Brännström (Brännström and Astroem 1964). Brännström and his colleagues have studied the occurrence of intratubular fluid shifts *in vitro* in response to the application of hydrodynamic stimuli (e.g., thermal, evaporative, tactile, and osmotic; Brännström and Astroem 1964). Later *in vivo* animal experiments have directly demonstrated that intratubular fluid shifts excite the intradental nerves (Matthews and Vongsavan 1994, Markowitz and

Pashley 2015). In line with these studies, a paper has proposed that a particular type of low-threshold mechanoreceptors, called *algoneurons* or low-threshold nociceptors, contributes to pain rather than touch in the dental sensory system (Fried, Sessle, and Devor 2011). This neuronal type is characterized by double immunopositivity for a pain-related neuropeptide CGRP and NF200, a marker for myelinated Aβ-fibers. Parallelly, it has been demonstrated the functional expression of PIEZO2 (Won et al. 2017), ASIC3 (Ichikawa and Sugimoto 2002), and TRPV2 (Gibbs, Melnyk, and Basbaum 2011) to serve as the mechanotransducer in DPA neurons. However, it remains unclear how low-threshold mechanosensitive ion channels can generate pain within the tooth pulp under pathological conditions.

The identity of a cell can be described by the expression of marker genes or molecular characteristics of its genetic pool. An increasing number of studies have successfully applied single-cell transcriptomics to characterize a population of cells, as well as the novel differentially expressed genes within the subpopulation in the sensory neurons (Usoskin et al. 2015, Nguyen et al. 2017, Li et al. 2016, Petitpre et al. 2018, Shrestha et al. 2018, Sharma et al. 2020). Moreover, the increased read-depth of single-cell RNA sequencing (scRNA-seq) reveals variability in gene expression of genetic markers even within a single neuronal population (Sharma et al. 2020, Li et al. 2016, Shrestha et al. 2018).

In the present study, I investigated molecular subpopulation and unique gene-expression signature of DPA neurons by generating whole transcriptome profiles of DPA neurons using full-length scRNA-seq from a total of ten mouse DPA neurons. DPA neurons were composed of six molecularly distinct subpopulations (C10, C13, C4, C6, C7, and C8) annotated from trigeminal

ganglion (TG) transcriptome data (Nguyen et al. 2017); subsequent investigation of differentially expressed genes within each subpopulation revealed. I also verified the specific gene-expression in DPA neurons using *in situ* hybridization technique. These results offer insights into subtype-specific gene-expression signatures of DPA neurons to be involved in dental pain.

MATERIALS AND METHODS

Animals

All experiments were performed with a total of 14 adult (five to seven weeks old) male C57BL/6 mice. All surgical and experimental procedures were approved by the Institutional Animal Care and Use Committee (IACUC) at Seoul National University and University of Pennsylvania.

Single-cell RNA sequencing

The workflow is described in detail below and **Figure 1**.

Retrograde labeling of DPA neurons

DPA neurons retrogradely labeled with a neuronal tracer 1,1'-Dioctadecyl-3,3,3',3'-tetramethylindocarbocyanine perchlorate (DiI, Cat. D3911, Invitrogen) were prepared as described previously (Lee et al. 2020). 14 days post-labeling, DPA neurons were isolated in acute culture from the TG tissues as previously described (Lee et al. 2020) and were incubated up to four hours in a humid incubator at 37 ℃ (5% CO_2) before collection.

Collection of single neurons

A total of 96 DPA neurons from ten male mice (seven weeks old) were prepared from two independent batches of collection. Each neuron was photographed for cell body area measurements before collection. The DPA neurons were manually collected using a glass micropipette with minimizing non-neuronal contaminations.

Preparation of cDNA library and sequencing

Once the DPA neurons were separated into an individual tube, they were digested, reversed transcribed into non-stranded cDNA using poly-T primers, then amplified using SMART-Seq v4 Ultra Low Input RNA kit (Clontech) into cDNA libraries according to the manufacturer's instructions, but with the following modifications: 1) ERCC RNA Spike-In controls (1/4000000 dilution, Cat. 4456740, Invitrogen) were added at the cell lysis; 2) 18 PCR cycles were performed to amplify cDNA libraries. The libraries were diluted accordingly, then used to make DNA sequencing libraries by following Nextera XT DNA Library Preparation Kit protocol (Illumina). Then, sequencing libraries were analyzed using Bioanalyzer High Sensitivity DNA Kit (Agilent Technologies) to determine the quality of the libraries. Libraries that passed quality control filters (for size distributions) were sequenced using NextSeq 500 (Illumina) with single-end 75 base pair reads to an average of 4 million reads per sample. Reads were trimmed for adapters and poly-A sequences using in-house software and then mapped to the mouse genome (mm10) using STAR (Dobin et al. 2013). Uniquely mapped reads were used for feature quantification using VERSE (Zhu et al. 2016).

Sample quality control

Based on summary statistics from in-house software, ten samples (DPA_20, DPA_27, DPA_07, DPA_59, DPA_94, DPA_08, DPA_56, DPA_77, DPA_43, and DPA_51) with "Percent Spike-In" > 5% were removed from downstream analyses. The above samples corresponded with the sample, whose cDNA concentration after reverse transcription and amplification, was lower than

0.5 ng/μL, so three additional samples (DPA_38, DPA_54, DPA_71) with a concentration of less than 0.5 ng/μL were additionally removed. Therefore, a total of 83 samples was used in the downstream analyses.

Single-cell RNA sequencing data analysis

This paper made extensive use of the Seurat package developed by the Satija lab (Shekhar et al. 2016, Satija et al. 2015); in essence, the recommended (TransferData) methods were used to project reference data onto a query object (Stuart et al. 2019). Briefly, single-cell TG transcriptome data, to be used as the reference (Nguyen et al. 2017), provided by the Ryba lab were log normalized and center scaled; variable features were identified and were used for linear dimensional reduction (principal components analysis, PCA). As previously described, informative principal components were used for clustering, and multidimensional data were displayed in a UMAP 2-dimensional representation. Similarly, DPA transcriptome data (query) were log normalized and center scaled; variable features were identified. Next, anchors were identified in the reference data set, and a weights matrix was constructed that defined the association between each query cell and each anchor. Afterward, a binary classification matrix where the rows correspond to possible cluster identities, and the columns correspond to the anchors, where the matrix cell is 1 if the anchor pair is a member of a certain cluster, was created and multiplied to the weights matrix as mentioned above to calculate prediction scores to transfer cluster labels onto the DPA data.

The transferred cluster labels were verified with two different separate cluster analyses. First, a subset of DPA transcriptome data including only expression data for marker genes for the TG and the DRG previously reported

(Nguyen et al. 2017, Sharma et al. 2020), was log normalized and was used for non-linear dimensional reduction (t-distributed stochastic neighbor embedding, t-SNE). Upon visualization in 2-dimensions, the clusters were well separated (PVClust to be included).

In situ hybridization

The workflow is described in detail below.

Retrograde labeling of DPA neurons

For *in situ* hybridization experiments, DPA neurons were labeled with a retrograde neuronal tracer fluoro-gold (FG, Cat. 26858, Cayman Chemical). All procedures of tooth dentin and pulp exposure surgery, including anesthesia, anti-inflammatory analgesic treatment, and surgery in mice, were followed as described previously (Rossi et al. 2020). A total volume of 0.5-2 µl FG (4% in distilled water) was directly applied into an exposed dental pulp of maxillary molar (either a left side or both sides of the jaw) in mice, and then the dental cavity was sealed with the GC Fuji II dental cement (GC corporation) according to the manufacturer's instructions. Upon anesthetic recovery, animals were returned to their home cages.

Sample preparation and *in situ* hybridization using RNAscope assay

Five days post-labeling, mice were deeply anesthetized and were perfused with ice-cold PBS solution followed by ice-cold 4% paraformaldehyde in PBS solution (PFA solution). TG tissues were post-fixed in 4% PFA solution for at least 4 hours at 4°C and then were transferred to 30% sucrose solution in PBS at 4°C. Serial frozen transverse sections (thickness: 14 µm) of TG

were mounted onto superfrost plus slides and were stored at -20°C until later use. The slides were used for *in situ* hybridization using RNAscope Multiplex Fluorescent v2 assay (Advanced Cell Diagnostics) as previously described (Rossi et al. 2020) with two probes assigned a different color channel, which is either Channel 2 (C2) or Channel 3 (C3) (**Table 3**). The C2 was visualized using opal 570 (Cy3 range) dye, and the C3 was visualized using opal 690 (Cy5 range) dye. The slides were mounted with mounting medium (Vector Laboratories), and all images were acquired using a fluorescence microscope (Leica) with a 20x objective.

Data acquisition and analysis

Cell body area (μm^2) of dissociated DPA neurons was measured with ImageJ software (National Institutes of Health). For quantitative analysis of *in situ* hybridization, images were obtained separately before the RNAscope assay to acquire FG-labeled DPA neurons (DAPI range) and then after the RNAscope assay to acquire fluorescent signals (Cy3 and Cy5 range) as all FG signals disappeared after the RNAscope assay. The ImageJ software was used to adjust brightness/contrast and to merge/align the images. Each DPA neuron was counted as a positive cell when at least ten puncta dots were shown within a cell. Bar graphs were presented as mean ± SEM using the Prism software (version 6.01; GraphPad). All plots or heatmaps of scRNA-seq data were generated in RStudio (version 1.2.5033; RStudio, Inc.).

TABLES

Table 3. List of probes used

Probe Name	Cat No.	Company	GeneBank No.
RNAscope Probe-Mm-Calca-tv2tv3-C2	420361-C2	Advanced Cell Diagnostics	NM_001033954.3
RNAscope Probe-Mm-Mrgprd-C2	417921-C2	Advanced Cell Diagnostics	NM_203490.3
RNAscope Probe-Mm-Prph-C2	400361-C2	Advanced Cell Diagnostics	NM_013639.2
RNAscope Probe-Mm-Tac1-C2	410351-C2	Advanced Cell Diagnostics	NM_009311.2
RNAscope Probe-Mm-Trpv1-C2	313331-C2	Advanced Cell Diagnostics	NM_001001445.1
RNAscope Probe-Mm-Piezo2-C3	400191-C3	Advanced Cell Diagnostics	NM_001039485.4

RESULTS

Single-cell RNA sequencing (scRNA-seq) for DPA neurons

Sequential procedures for scRNA-seq of DPA neurons, including sample preparation, single-cell collection, single-cell RNA sequencing, and transcriptome analysis, were processed as described in **Fig. 15**. A total of 96 DiI-labeled DPA neurons was manually collected in the acute culture of TG tissues from ten male C57BL/6 mice (seven weeks old) for performing scRNA-seq on each collected neuron.

Molecular subpopulations of DPA neurons

A total of 83 DPA neurons' transcriptome data, which showed the average number of mapped reads (4.975 ± 1.301 million (mean ± SD) per each neuron, **Fig. 16Aa**) and detected genes (11915 ± 1112 (mean ± SD) per each neuron, **Fig 16Ab**), passed the quality control criteria (**Fig. 16Ac**, **Ad**) and was processed for downstream analysis. No noticeable correlation between the number of genes detected and the read depth was observed (**Fig. 16Aa, Ab**). Next, unbiased single-cell transcriptome cluster analysis revealed that six molecularly distinct subpopulations were found across DPA neurons (C10, C13, C4, C6, C7, and C8) corresponding to clusters previously found in the TG transcriptome data (Nguyen et al. 2017) (**Fig. 16Ba**, **Bb**). Among the clusters identified in DPA neurons, clusters C4 and C6 highly expressed both *S100b* and *Nefh*, which are well-known markers for myelinated A-fibers (**Fig.**

16Ca, **Cb**). Also, on average, neurons in clusters C4 and C6 had larger cell body area (**Fig. 16D**).

Assessment of DPA transcriptome data using selected marker genes

Next, *in situ* hybridization using the RNAscope assay in DPA neurons in order to validate my transcriptome data. I found binary high/low expression levels of *Prph* and *Mrgprd* with close correspondence between RNAscope data (**Fig. 17A, B**) and scRNA-seq data (**Fig. 17C**). In DPA transcriptome data, housekeeping genes (*Gapdh* and *Actb*) and sensory neuronal markers (*Tubb3*, *Avil*, and *Prph*) were very prominent, while the expression levels of marker genes for satellite glial cell (*Kcnj10* and *Gja1*), motor neuron (*Chat*, *Neurog2*, and *Olig2*), and taste receptor (*Tas1r1*, *Tas1r2*, and *Tas1r3*) were low in expression (**Fig. 17D**). Interestingly, DPA neurons expressing itch-related genes, such as *Mrgpra3* and *Nppb*, were rare (**Fig. 17D**). Among several mechanosensitive ion channels, the transcriptome data also showed that *Piezo2*, *Trpm7*, *Trpv2*, and *Asic3* predominantly expressed in DPA neurons (**Fig. 17E**).

Molecular gene-expression signatures of DPA neurons

To address further molecular signatures of DPA neurons, I examined the differential gene expression across subpopulations using selected markers: *Trpv1*, *Calca*, *Tac1*, *Prph*, *Piezo2*, and *Mrgprd*. Clusters C10, C7, and C8 expressed high levels of *Trpv1*, *Calca*, and *Tac1* (**Fig. 18Aa-Ac**), but low levels of *S100b* (**Fig. 16Ca**), *Nefh* (**Fig. 16Cb**), and *Piezo2* (**Fig. 18Ae**). These neurons are likely to play a role in nociception. On the other hand, cluster C4 expressed high levels of *S100b* (**Fig. 16Ca**), *Nefh* (**Fig. 16Cb**), and *Piezo2*

(**Fig. 18Ae**), but low levels of *Trpv1*, *Calca*, and *Tac1* (**Fig. 18Aa-Ac**). As the expression levels of the myelination markers and the mechanosensitive *Piezo2* ion channel are high, these neurons are likely to be myelinated mechanosensitive neurons. Only cluster C13 consisted of a DPA neuron showing high level of *Mrgprd*, which is the noxious mechanosensitive neuron (**Fig 18Af**). In addition, all clusters broadly expressed *Prph* (**Fig. 18Ad**). Interestingly, cluster C6 showed high expression levels of both *Calca* and *Piezo2* (**Fig. 18Ab, Ae**), and the proportion of this cluster was the largest (42.17%, $n = 35$ of 83 neurons, **Fig. 18B**) among DPA neuron clusters. The *in situ* hybridization assay confirmed that *Piezo2* was highly expressed in DPA neurons (95.88 ± 1.883%, **Fig. 18Ca, Cb**).

High expression of *Calca* in *Piezo2*-expressing DPA neurons

Next, to verify the co-expression of pain-related molecules and the low-threshold mechanosensitive *Piezo2* ion channel, I investigated the expression of *Calca*, *Trpv1*, and *Tac1* in *Piezo2*-expressing DPA neurons. The *in situ* hybridization analysis revealed that *Calca* had the highest co-expression rate (81%, **Fig. 19Aa-Ad**) than *Trpv1* (37.5 ± 12.5%, **Fig. 19Ba-Bd**) and *Tac1* (15.4%, **Fig. 19Ca-Cd**) in *Piezo2*-positive DPA neurons. These results suggested that *Calca* may act as a main molecule in nociceptive processing through the low-threshold mechanosensitive *Piezo2* ion channel.

Figure 15.

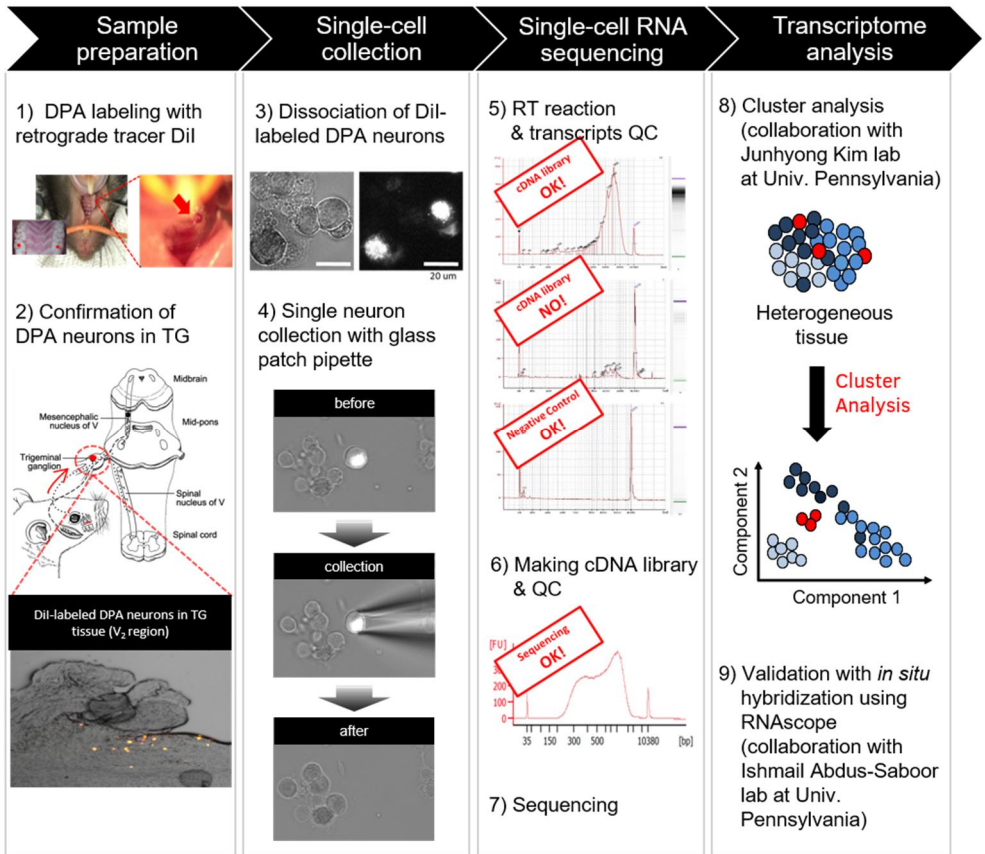
Sample preparation
Single-cell collection
Single-cell RNA sequencing
Transcriptome analysis
1) DPA labeling with retrograde tracer DiI
2) Confirmation of DPA neurons in TG
Midbrain
Mesencephalic nucleus of V
Mid-pons
Trigeminal ganglion
Spinal nucleus of V
Spinal cord
DiI-labeled DPA neurons in TG tissue (V2 region)
3) Dissociation of DiI-labeled DPA neurons
20 um
4) Single neuron collection with glass patch pipette
before
collection
after
5) RT reaction & transcripts QC
cDNA library OK!
cDNA library NO!
Negative Control OK!
6) Making cDNA library & QC
Sequencing OK!
[FU]
200
100
0
35 150 300 500 10380 [bp]
7) Sequencing
8) Cluster analysis (collaboration with Junhyong Kim lab at Univ. Pennsylvania)
Heterogeneous tissue
Cluster Analysis
Component 2
Component 1
9) Validation with in situ hybridization using RNAscope (collaboration with Ishmail Abdus-Saboor lab at Univ. Pennsylvania)

Figure 15. Single-cell RNA sequencing (scRNA-seq) workflow

Workflow for scRNA-seq following sequential steps: **1)** DPA neurons were labeled with retrograde tracer DiI from the mouse maxillary molar; **2)** 14 days post-labeling, DiI-labeled DPA neurons (soma) were confirmed in the maxillary (V_2) region of TG; **3)** DiI-labeled DPA neurons were dissociated in acute culture, and then **4)** individual cells were collected with micromanipulation under the microscope; **5)** RT and PCR (18 cycles) reactions were performed, and the quality of the whole transcripts per each DPA neuron, as well as the negative control (collection of bath solution), was checked before making cDNA library; **6)** cDNA libraries were made, and their qualities were checked before sequencing; **7)** sequencing and **8)** single-cell transcriptome analysis were performed. Detailed information (reagents, equipment, manufacturer, etc.) was described in the materials and methods section.

An illustration in 2) modified from Park 2015

Figure 16.

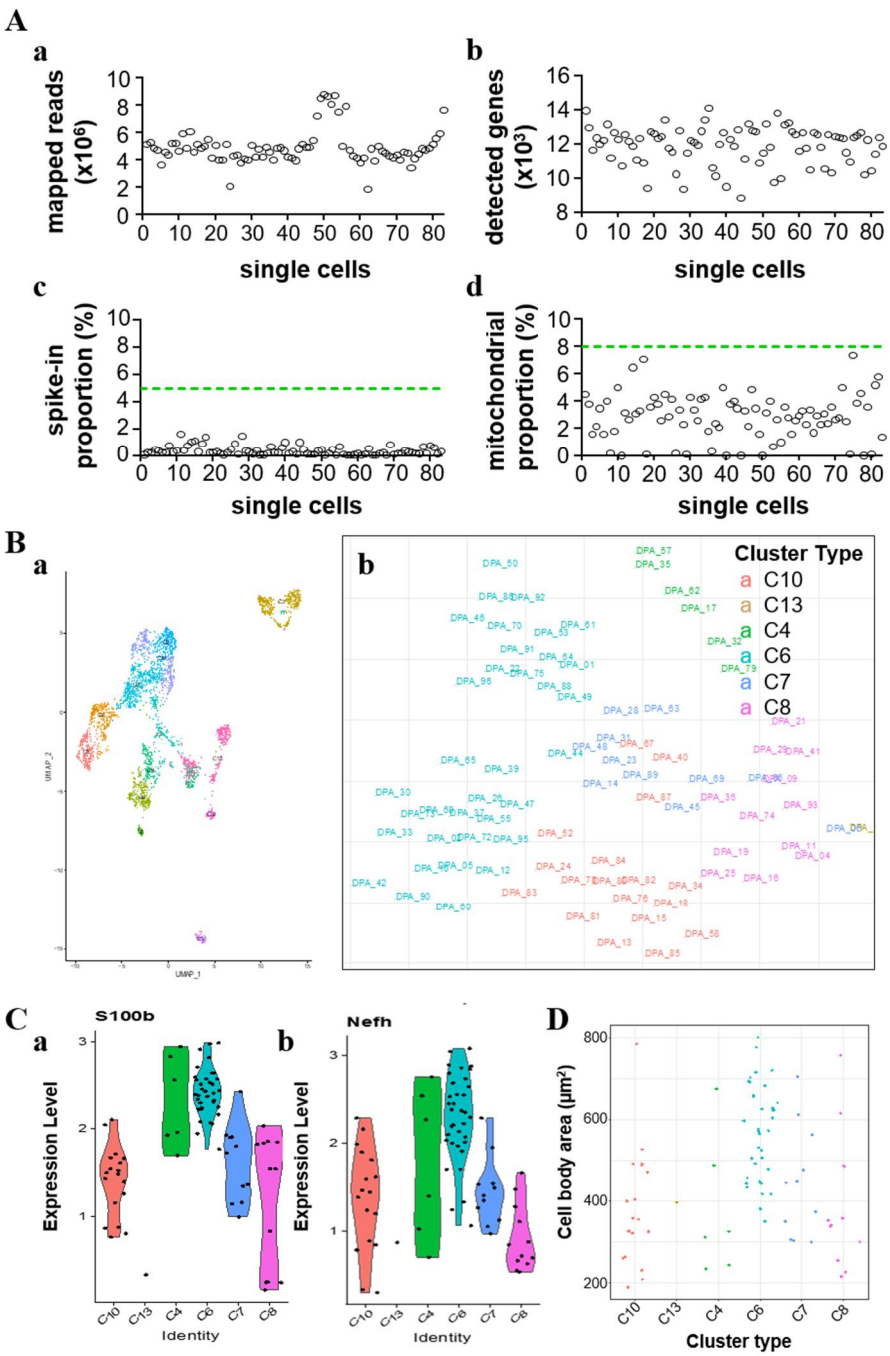
A
a
mapped reads (x10⁶)
single cells
b
detected genes (x10³)
single cells
c
spike-in proportion (%)
single cells
d
mitochondrial proportion (%)
single cells
B
a
b
Cluster Type
a C10
a C13
a C4
a C6
a C7
a C8
C
a
S100b
Expression Level
Identity
b
Nefh
Expression Level
Identity
D
Cell body area (μm²)
Cluster type

Figure 16. Subpopulations of DPA neurons detected via scRNA-seq

(**Aa-Ad**) Assessment of DPA transcriptome data and sample quality control. A total of 83 DPA neurons showed the number of mapped reads for each neuron ranged from 1.878 million to 8.826 million (**Aa**), and the number of detected genes for each neuron ranged from 8856 to 14100 (**Ab**). These neurons passed ERCC spike-in proportion (< 5%, **Ac**) and mitochondrial proportion (< 8%, **Ad**). Green dotted lines indicate the threshold value in the exclusion of the data. (**Ba-Bb**) UMAP (**Ba**) and t-SNE (**Bb**) graphs of mouse DPA neurons with dot and letter colors indicating subtype identity (C10, C13, C4, C6, C7, and C8) assigned by the TG transcriptome data (Nguyen et al. 2017). (**Ca-Cb**) Violin plots comparing the gene expression level of *S100b* (**Ca**) and *Nefh* (**Cb**) across subpopulations. (**D**) Dot plots illustrating cell body area (μm^2) of DPA neurons.

Figure 17.

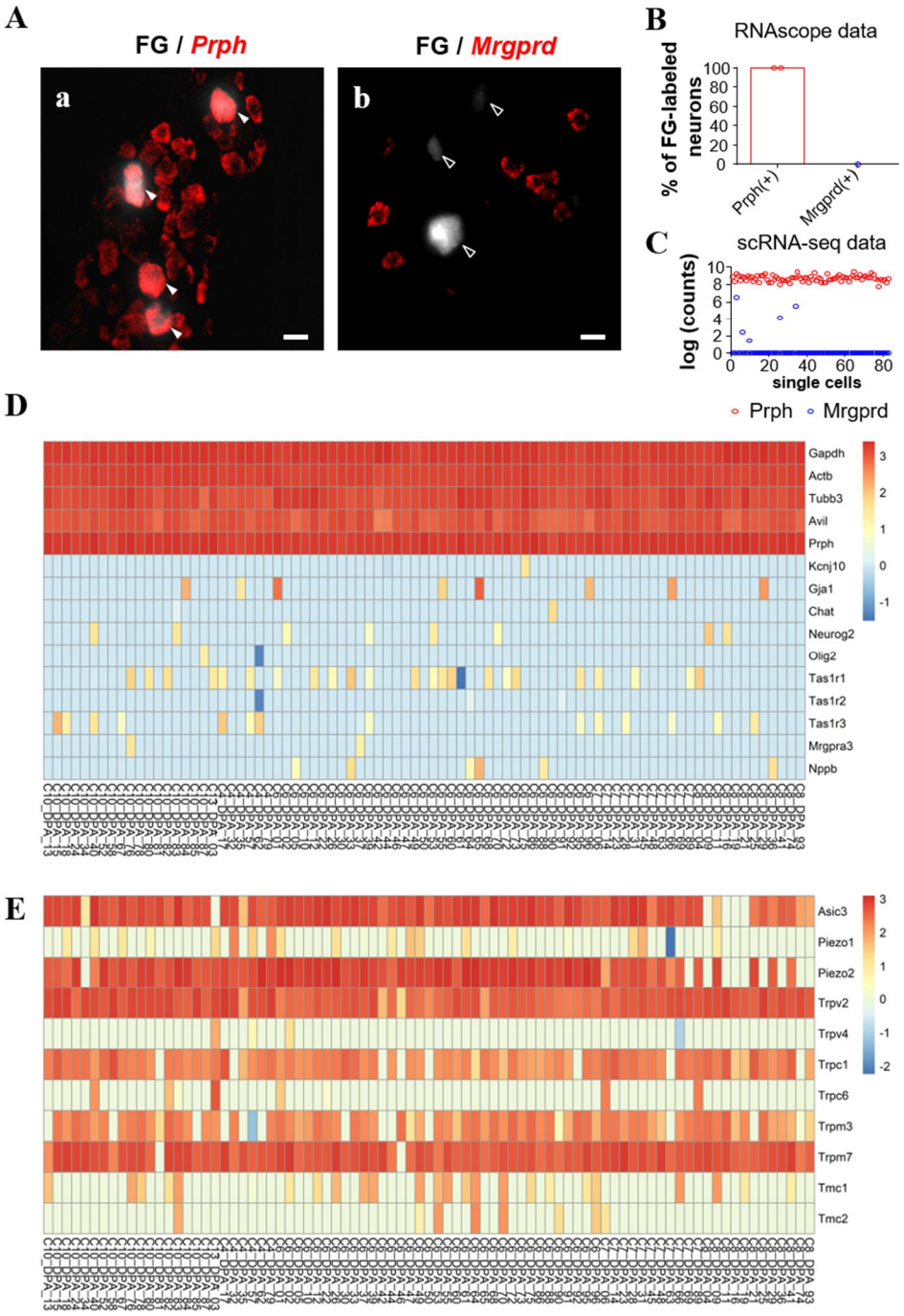
A
FG / Prph
FG / Mrgprd
a
b
B
RNAscope data
% of FG-labeled neurons
100
80
60
40
20
0
Prph(+)
Mrgprd(+)
C
scRNA-seq data
log (counts)
10
8
6
4
2
0
0
20
40
60
80
single cells
Prph
Mrgprd
D
Gapdh
Actb
Tubb3
Avil
Prph
Kcnj10
Gja1
Chat
Neurog2
Olig2
Tas1r1
Tas1r2
Tas1r3
Mrgpra3
Nppb
3
2
1
0
-1
E
Asic3
Piezo1
Piezo2
Trpv2
Trpv4
Trpc1
Trpc6
Trpm3
Trpm7
Tmc1
Tmc2
3
2
1
0
-1
-2

Figure 17. Assessment of DPA transcriptome data using selected marker genes

(**Aa-Ab**) Representative RNAscope *in situ* hybridization images for variable genes of *Prph* (red puncta, **Aa**) and *Mrgprd* (red puncta, **Ab**) in FG-labeled DPA neurons (grey). All white filled arrowheads indicate *Prph*-positive neurons, and all empty arrowheads indicate *Mrgprd*-negative neurons. Scale bars, 25 μm. (**B**) The quantitative data of *Prph* (100%, $n = 2$ mice) and *Mrgprd* (0%, $n = 1$ mouse). Bars represent mean ± SEM. (**C**) Dot plots showing gene expression of *Prph* and *Mrgprd* in scRNA-seq data, which had close correspondence with the RNAscope data. (**D**) A Heatmap showing differential gene expression with representative markers for housekeeping (Gapdh and Actb), sensory neuron (Tubb3, Avil, and Prph), satellite glial cell (Kcnj10 and Gja1), motor neuron (Chat, Neurog2, and Olig2), taste receptor (Tas1r1, Tas1r2, and Tas1r3), and itch-related genes (Mrgpra3 and Nppb) listed in the right panel. (**E**) Differentially expressed mechanosensitive ion channels illustrated in a heatmap for *Asic3*, *Piezo1*, *Piezo2*, *Trpv2*, *Trpv4*, *Trpc1*, *Trpc6*, *Trpm3*, *Trpm7*, *Tmc1*, and *Tmc2* genes across DPA neurons. Expression levels indicate log normalized counts value with DESeq2. Cell identity and subtype identity were listed in the bottom panel of each heatmap.

Figure 18.

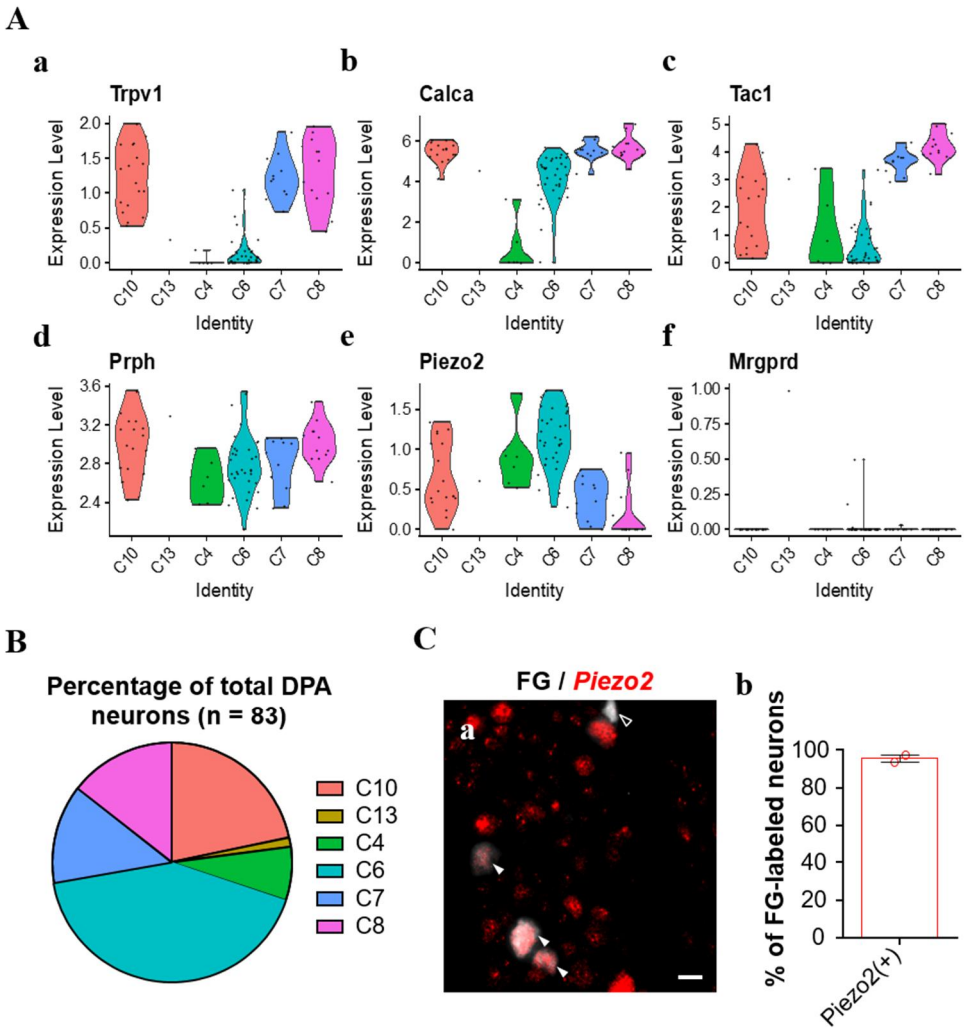
A
a
Trpv1
b
Calca
c
Tac1
d
Prph
e
Piezo2
f
Mrgprd
Expression Level
Identity
C10
C13
C4
C6
C7
C8
B
Percentage of total DPA neurons (n = 83)
C10
C13
C4
C6
C7
C8
C
FG / Piezo2
a
b
% of FG-labeled neurons
Piezo2(+)

Figure 18. Identification of the main subpopulation showing high expression levels of *Piezo2* and *Calca* in DPA neurons

(**Aa-Af**) Violin Plots illustrating the differential gene expression for *Trpv1* (**Aa**), *Calca* (**Ab**), *Tac1* (**Ac**), *Prph* (**Ad**), *Piezo2* (**Ae**), and *Mrgprd* (**Af**) across subpopulation of DPA neurons. (**B**) Pie graph showing the proportion of each subtype: C10 (21.69%, *n* = 18 of 83 neurons), C13 (1.2%, *n* = 1 of 83 neurons), C4 (7.23%, *n* = 6 of 83 neurons), C6 (42.17%, *n* = 35 of 83 neurons), C7 (13.25%, *n* = 11 of 83 neurons), and C8 (14.46%, *n* = 11 of 83 neurons). (**Ca-Cb**) Representative RNAscope *in situ* hybridization images for *Piezo2* (red puncta, **Ca**) in FG-labeled DPA neurons (grey) and quantitative data (95.88 ± 1.883%, **Cb**). *n* = 2 mice. White filled arrowheads indicate *Piezo2*-positive neurons, and an empty arrowheads indicate *Piezo2*-negative neurons. A scale bar, 25 μm.

Figure 19.

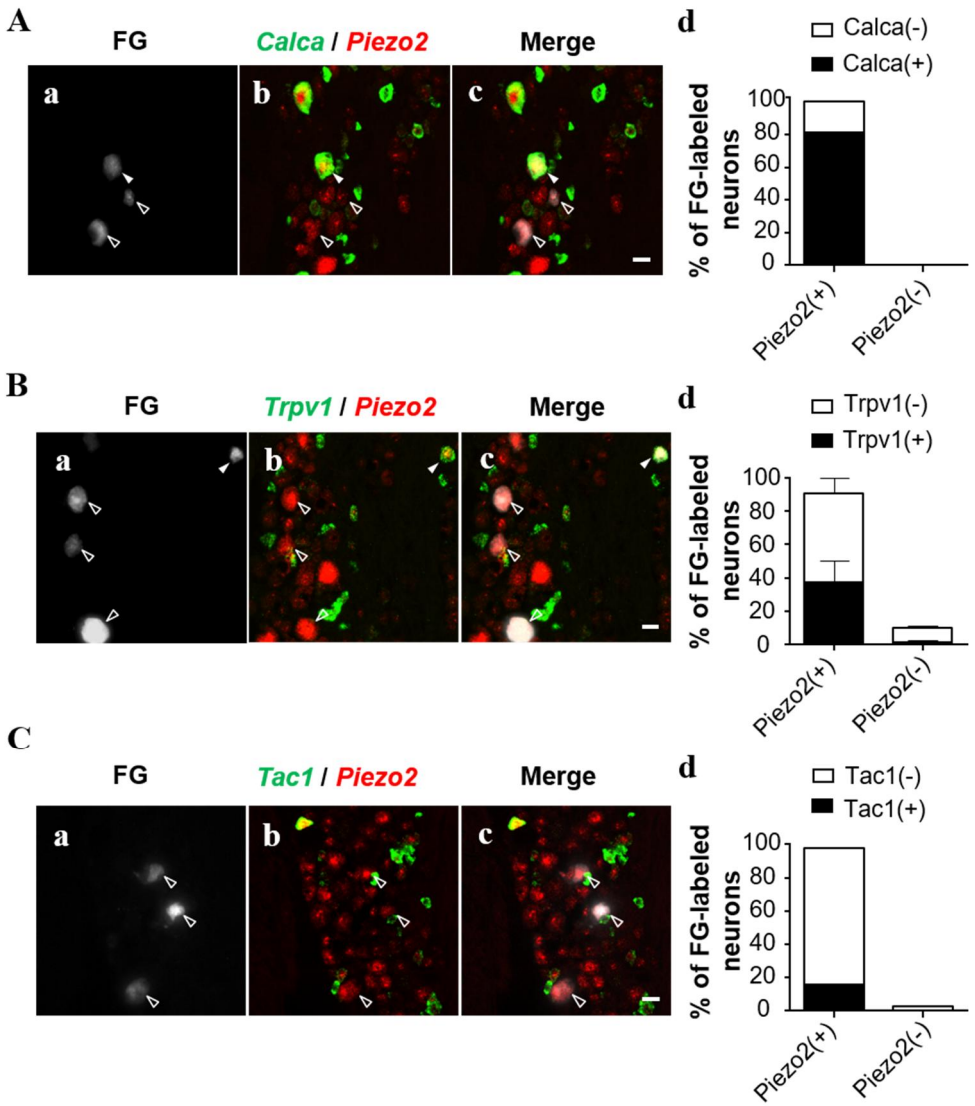
A
FG
Calca / Piezo2
Merge
a
b
c
d
Calca(-)
Calca(+)
% of FG-labeled neurons
100
80
60
40
20
0
Piezo2(+)
Piezo2(-)
B
FG
Trpv1 / Piezo2
Merge
a
b
c
d
Trpv1(-)
Trpv1(+)
% of FG-labeled neurons
100
80
60
40
20
0
Piezo2(+)
Piezo2(-)
C
FG
Tac1 / Piezo2
Merge
a
b
c
d
Tac1(-)
Tac1(+)
% of FG-labeled neurons
100
80
60
40
20
0
Piezo2(+)
Piezo2(-)

Figure 19. *Calca* is a main molecule in nociceptive processing of *Piezo2*-expressing DPA neurons

(**Aa-Ad**) Representative RNAscope *in situ* hybridization images showing co-expression of *Calca* (green puncta) and *Piezo2* (red puncta) (**Aa-Ac**) in FG-labeled DPA neurons (grey) and quantitative data (**Ad**). $n = 1$ mouse. (**Ba-Bd**) Representative RNAscope *in situ* hybridization images showing co-expression of *Trpv1* (green puncta) and *Piezo2* (red puncta) (**Ba-Bc**) in FG-labeled DPA neurons (grey) and quantitative data (**Bd**). $n = 2$ mice. (**Ca-Cd**) Representative RNAscope *in situ* hybridization images showing co-expression of *Tac1* (green puncta) and *Piezo2* (red puncta) (**Ca-Cc**) in FG-labeled DPA neurons (grey) and quantitative data (**Cd**). $n = 1$ mouse. All white filled arrowheads indicate double positive-neurons for two genes, and all empty arrowheads indicate single positive-neurons for *Piezo2* probe. Scale bars, 25 μm. Bars represent mean ± SEM.

DISCUSSION

In chapter 3, I demonstrated molecularly distinct subpopulations and gene-expression signatures in the adult mouse DPA neurons using scRNA-seq and RNAscope *in situ* hybridization. Importantly, single-cell transcriptome analysis revealed that a specific subpopulation, which highly expressed *Piezo2* as well as *Calca*, was the largest subpopulation of DPA neurons. Among pain-related molecules, *Calca* showed the highest co-expression rate than *Trpv1* and *Tac1* within *Piezo2*-expressing DPA neurons. These results suggest the possible contribution of low-threshold mechanosensitive ion channels to tooth pain.

At first, it has been considered DPA neurons all nociceptive afferents since tooth pulp only generates pain regardless of stimulation with painful or non-painful stimuli (Cook et al. 1997). In this context, several studies have attempted to identify pain-sensing receptors from pure DPA neurons (Cook et al. 1997, Eckert, Taddese, and McCleskey 1997) and to reveal the composition of nociceptive fibers (e.g., unmyelinated C-fibers and nociceptive Aδ-fibers) observed in intrapulpal nerve fibers (Lee et al. 2019, Narhi et al. 1992). However, recent electrophysiological and histological studies have revealed that most pulpal nerves are myelinated Aβ-fibers (Lee et al. 2019), remains controversial. In line with an effort to dissect cellular heterogeneity within DPA neurons, I employed single-cell transcriptomics technology. Single-cell transcriptome analysis revealed six molecular subpopulations (C10, C13, C4, C6, C7, and C8) across DPA neurons (**Fig. 16Ba, Bb**) and the variation of expression levels of myelination markers

(*S100b* and *Nefh,* **Fig. 16Ca, Cb**), correlated with their cell body size area (**Fig. 16D**). These results support that DPA neurons are composed of unmyelinated C-fibers and myelinated A-fibers, consistent with previous works (Won et al. 2017, Fried, Sessle, and Devor 2011).

Tooth pain is most likely evoked by light mechanical irritations such as brush, air puffs, or water spray (Chung, Jung, and Oh 2013). The axonal terminals of DPA neurons innervate the dentinal tubules of tooth dentin, filled with dentinal fluid. Due to this unique structure of the tooth, DPA neurons can be easily activated by the movement of dentinal fluid induced by various external stimuli; therefore, the hydrodynamic theory is the most widely accepted (Chung, Jung, and Oh 2013, Won and Oh 2019). In line with this phenomenon, a previous study proposed that a particular type of low-threshold mechanosensitive neurons, called algoneurons or low-threshold nociceptors, may contribute to pain rather than touch (Fried, Sessle, and Devor 2011). They demonstrated that most DPA neurons show double immunopositivity for a pain-related neuropeptide CGRP and NF200 as a marker for myelinated Aβ-fibers, and these neurons are characterized as algoneurons (Fried, Sessle, and Devor 2011). Furthermore, several studies reported that mechanosensitive ion channels, such as PIEZO2 (Won et al. 2017), ASICs (acid-sensing ion channels) including ASIC3 (Ichikawa and Sugimoto 2002, Chen and Wong 2013), and TRPV2 (Gibbs, Melnyk, and Basbaum 2011) expressed in DPA neurons, as well as TRPM7 in odontoblasts (Won et al. 2018), serve as the mechanotransducer of tooth pain. Consistent with these previous reports, my transcriptome data showed that mechanosensitive ion channels, such as Piezo2, Trpm7, Trpv2, and Asic3, predominantly expressed in DPA neurons (**Fig. 17E**). Interestingly, *Piezo2*

expression was broadly found in my transcriptome data (**Fig. 17E**, **18Ae**) and *in situ* hybridization results (95.88 ± 1.883%, **Fig. 18Ca, Cb**) of DPA neurons. Among the subpopulations of DPA neurons, a specific subpopulation showing the high expression level of both *Piezo2* and *Calca* was the largest subpopulation in DPA neurons (**Fig. 18B**). In addition, *Calca* showed higher expression than other pain-related marker genes *Trpv1* and *Tac1* in *Piezo2*-expressing DPA neurons (**Fig. 19**). These findings suggest that low-threshold mechanoreceptors, which are most responsive to touch or innocuous mechanical stimuli in the area of the skin, may contribute to pain at teeth under pathological conditions.

In the general pain research field, the mechanisms underlying *mechanical allodynia*, described as pain caused by innocuous mechanical stimuli under pathological conditions (Lolignier, Eijkelkamp, and Wood 2015), have also been an important topic (Hill and Bautista 2020). For example, it can be explained by CHRNA3-expressing neurons, which are mechanosensitive silent nociceptors (Prato et al. 2017). These neurons are characterized to be sensitized only by the inflammatory mediators (Prato et al. 2017). Furthermore, several papers have reported that PIEZO2-deficient mice show an impairment of nociceptive behavior in response to mechanical stimulation under inflammation or nerve injury conditions (Murthy et al. 2018), suggesting that low-threshold mechanosensitive PIEZO2 ion channels are involved in mechanical allodynia. However, more recent studies have demonstrated that PIEZO2 is associated with touch rather than pain, and PIEZO1 plays an important role in the regulation of mechanical pain (Zhang et al. 2019). However, it is still unclear since PIEZO1 shows low expression in peripheral sensory neurons (Zhang et al. 2019).

On the other hand, mechanical pain can be directly detected by specialized high-threshold mechanoreceptors. It has been demonstrated that MRGPRD-expressing C-fibers convey mechanical pain and that those neurons have a distinctive neuronal population from TRPV1-expressing C-fibers (Cavanaugh et al. 2009). Furthermore, a recent paper has identified a novel mechanosensitive ion channel called TACAN (transcript name *Tmem120a*) (Beaulieu-Laroche et al. 2020). TACAN is expressed in non-peptidergic nociceptive neurons, which are specific subsets of DRG neurons, with high expression levels of MRGPRD and purinergic receptor P2X3 (Beaulieu-Laroche et al. 2020). Strikingly, my single-cell transcriptome data and *in situ* hybridization results demonstrated that the proportion of a specific population (cluster C13) with the high expression level of *Mrgprd* was very rare (~1%, **Fig. 17B**, **18B**). These results suggest that low-threshold mechanoreceptors rather than high-threshold mechanoreceptors may play a key role in transmitting pain in teeth under pathological conditions.

In fact, a highly sensitive mechanosensory system is required for detecting stimuli through the hard shell of the tooth (Fried and Gibbs 2014). Hence, intradental low-threshold mechanoreceptors are responsible for a wide range of mechanical sensory inputs, including the texture of food, touch, pressure, vibration, and proprioception, thereby regulating occlusion, mastication, and biting (Fried and Gibbs 2014, Haggard and de Boer 2014). However, these low-threshold mechanoreceptors, which are densely innervated in the tooth pulp, make dental sensory systems distinct from nociceptive networks at other body sites in many ways when dentin is exposed (Fried and Gibbs 2014). That is, whether noxious stimulation (e.g., cold and heat) or extremely light mechanical force (e.g., brushing, air puffs,

and water spray) to exposed dentin appears as a paradoxical phenomenon that causes only pain sensation, without a mechanism for discrimination (Cook et al. 1997, Fried and Gibbs 2014, Fried, Sessle, and Devor 2011). The hydrodynamic theory can explain this where dentinal fluid shifts, regardless of stimulus modalities, excite intradental low-threshold mechanoreceptors. I thus have focused on the potential role of a neuronal population characterized by high expression of a low-threshold mechanosensitive PIEZO2 ion channel and a pain-related neuropeptide CGRP to be engaged in tooth pain in this study. However, it remains unaddressed whether activation of PIEZO2 can generate action potentials at nerve endings of DPA neurons, and nociceptive signals are transmitted to the second-order neurons via CGRP as neurotransmitters. Therefore, further studies are strongly required to investigate the functional role of PIEZO2 channels in transmitting tooth pain. I am currently working on further experiments to employ PIEZO2-specific genetic modulation with *in vitro*/*in vivo* optogenetic tools (Murthy et al. 2018) within the tooth pulp and to observe modulation of neuronal activity in the CNS level and behavioral changes. I also leave novel low-threshold mechanoreceptor candidates directly sensing pain to be open to possibility in DPA neurons.

With respect to etiology and clinical features of dentine hypersensitivity, most published papers have focused on peripheral aspects, since this pain is relatively well managed by topical application of tubular-occluding or nerve-desensitizing agents (Orchardson and Gillam 2006). However, the prevalence and the severity of dentin hypersensitivity are very variable, ranging from a minor inconvenience to the wide-ranging impact of quality-of-life in patients, so that there has been a broad spectrum of therapeutic strategies (Shiau 2012).

In clinical studies, there is an effort to investigate cerebral processes related to dentin hypersensitivity evoked by air stimuli by using the fMRI (functional magnetic resonance imaging) (Meier et al. 2012). This study has demonstrated differential activity in the anterior insular cortex (aIC) and the anterior midcingulate cortex (aMCC) of patients, suggesting that these brain regions may become clinically relevant in dentin hypersensitivity (Meier et al. 2012). Although the role of the insular cortex in modulating pain remains unknown, a clinical study has reported that two individuals with extensive lesions to the insular have substantially higher pain intensity ratings of acute experimental noxious stimuli (Starr et al. 2009). This finding may imply that the role of central nervous system plasticity in explaining the large degree of variability observed in the severity of dentin hypersensitivity (Markowitz and Pashley 2015).

CONCLUSION

Nociception experienced in the body, as well as the orofacial region, conveys by specialized peripheral sensory neurons called nociceptors, which are activated by noxious stimuli. It has been well studied for the distinct nociceptors in response to various noxious stimuli such as heat, cold, chemical, or mechanical. However, it remains unclear whether not only noxious stimuli but also innocuous or non-painful stimuli can cause pain. In an effort to elucidate this observation, I have explored the polymodal nociception that may be elicited by innocuous stimuli or endogenous mediators of inflammation with a focus on dorsal root ganglion (DRG) neurons and dental primary afferent (DPA) neurons.

In the first chapter, I demonstrated that activation of $GABA_AR$ at peripheral nerve endings of DRG neurons facilitated CFA-induced nociceptive behavior and mechanical hypersensitivity. Furthermore, the $GABA_AR$ modulated pain hypersensitivity in response to not only endogenous GABA in inflamed tissue but also endogenous positive allosteric modulation of $GABA_AR$ even in normal conditions. These results support that peripheral $GABA_AR$-mediated signaling contributes to the regulation of inflammatory pain and provides therapeutic benefits for pain management.

In the second chapter, I verified the functional expression of TRPM8 channels in DPA neurons to detect hyperosmolar stimulation, such as sweet substance with high sugar concentrations. I investigated that TRPM8 in DPA neurons mediates upregulation of c-fos expression as a marker of nociception in the CNS level by applying hyperosmolar sucrose solution to the mouse

exposed tooth dentin. Furthermore, I showed that a selective TRPM8 antagonist significantly attenuated the hyperosmolarity-induced dental nociception. These findings suggest that innocuous stimuli, such as sweet substances, can contribute to tooth pain via TRPM8 channels under pathological conditions.

In the third chapter, I introduced single-cell transcriptomics technology as an effective strategy to characterize a population of cells and to reveal rare subtypes or novel therapeutic targets in the sensory system. I used single-cell RNA sequencing (scRNA-seq) and *in situ* hybridization techniques to identify and verify gene-expression signatures in the adult mouse DPA neurons. I showed that a particular subtype, which was characterized by the high expression levels of both a low-threshold mechanosensitive *Piezo2* channel and a pain-related neuropeptide *Calca*, was the major subset of DPA neurons. This finding implies that low-threshold mechanoreceptors, which are most responsive to touch in the somatosensory system, may uniquely contribute to pain in teeth under pathological conditions. Further studies are in progress to address whether PIEZO2 plays an actual role in transmitting tooth pain and to discover other potential low-threshold mechanosensitive ion channels sensing pain in DPA neurons.

BIBLIOGRAPHY

Ahn, D. K., E. A. Doutova, K. McNaughton, A. R. Light, M. Narhi, and W. Maixner. 2012. "Functional properties of tooth pulp neurons responding to thermal stimulation." *J Dent Res* 91 (4):401-6. doi: 10.1177/0022034511435703.

Allchorne, A. J., H. L. Gooding, R. Mitchell, and S. M. Fleetwood-Walker. 2012. "A novel model of combined neuropathic and inflammatory pain displaying long-lasting allodynia and spontaneous pain-like behaviour." *Neurosci Res* 74 (3-4):230-8. doi: 10.1016/j.neures.2012.10.006.

Alvarez-Leefmans, F. J., M. Leon-Olea, J. Mendoza-Sotelo, F. J. Alvarez, B. Anton, and R. Garduno. 2001. "Immunolocalization of the Na(+)-K(+)-2Cl(-) cotransporter in peripheral nervous tissue of vertebrates." *Neuroscience* 104 (2):569-82.

Anderson, D. J., and B. Matthews. 1967. "Osmotic stimulation of human dentine and the distribution of dental pain thresholds." *Arch Oral Biol* 12 (3):417-26.

Andersson, D. A., H. W. Chase, and S. Bevan. 2004. "TRPM8 activation by menthol, icilin, and cold is differentially modulated by intracellular pH." *J Neurosci* 24 (23):5364-9. doi: 10.1523/JNEUROSCI.0890-04.2004.

Anseloni, V. C., and M. S. Gold. 2008. "Inflammation-induced shift in the valence of spinal GABA-A receptor-mediated modulation of nociception in the adult rat." *J Pain* 9 (8):732-8. doi: 10.1016/j.jpain.2008.03.004.

Beaulieu-Laroche, L., M. Christin, A. Donoghue, F. Agosti, N. Yousefpour, H. Petitjean, A. Davidova, C. Stanton, U. Khan, C. Dietz, E. Faure, T. Fatima, A. MacPherson, S. Mouchbahani-Constance, D. G. Bisson, L. Haglund, J. A. Ouellet, L. S. Stone, J. Samson, M. J. Smith, K. Ask, A. Ribeiro-da-Silva, R. Blunck, K. Poole, E. Bourinet, and R. Sharif-Naeini. 2020. "TACAN Is an Ion Channel Involved in Sensing Mechanical Pain." *Cell* 180 (5):956-967 e17. doi: 10.1016/j.cell.2020.01.033.

Belelli, D., and J. J. Lambert. 2005. "Neurosteroids: endogenous regulators of the GABA(A) receptor." *Nat Rev Neurosci* 6 (7):565-75. doi:

10.1038/nrn1703.
Belmonte, C., and F. Viana. 2009. "Nociceptor Responses." *Encyclopedia of Neuroscience*:1191-1198.
Ben-Ari, Y. 2002. "Excitatory actions of gaba during development: the nature of the nurture." *Nat Rev Neurosci* 3 (9):728-39. doi: 10.1038/nrn920.
Bereiter, D. A., M. Rahman, R. Thompson, P. Stephenson, and H. Saito. 2018. "TRPV1 and TRPM8 Channels and Nocifensive Behavior in a Rat Model for Dry Eye." *Invest Ophthalmol Vis Sci* 59 (8):3739-3746. doi: 10.1167/iovs.18-24304.
Bhat, R., R. Axtell, A. Mitra, M. Miranda, C. Lock, R. W. Tsien, and L. Steinman. 2010. "Inhibitory role for GABA in autoimmune inflammation." *Proc Natl Acad Sci U S A* 107 (6):2580-5. doi: 10.1073/pnas.0915139107.
Binder, A., M. Stengel, O. Klebe, G. Wasner, and R. Baron. 2011. "Topical high-concentration (40%) menthol-somatosensory profile of a human surrogate pain model." J Pain 12 (7):764-73. doi: 10.1016/j.jpain.2010.12.013.
Brännström, M., and A. Astroem. 1964. "A Study on the Mechanism of Pain Elicited from the Dentin." *J Dent Res* 43:619-25. doi: 10.1177/00220345640430041601.
Bravo-Hernandez, M., L. A. Feria-Morales, J. E. Torres-Lopez, C. Cervantes-Duran, R. Delgado-Lezama, V. Granados-Soto, and H. I. Rocha-Gonzalez. 2014. "Evidence for the participation of peripheral alpha5 subunit-containing GABAA receptors in GABAA agonists-induced nociception in rats." *Eur J Pharmacol* 734:91-7. doi: 10.1016/j.ejphar.2014.03.051.
Byers, M. R. 1994. "Dynamic plasticity of dental sensory nerve structure and cytochemistry." *Arch Oral Biol* 39 Suppl:13S-21S. doi: 10.1016/0003-9969(94)90183-x.
Cao, D. L., Z. J. Zhang, R. G. Xie, B. C. Jiang, R. R. Ji, and Y. J. Gao. 2014. "Chemokine CXCL1 enhances inflammatory pain and increases NMDA receptor activity and COX-2 expression in spinal cord neurons via activation of CXCR2." *Exp Neurol* 261:328-36. doi: 10.1016/j.expneurol.2014.05.014.
Carlton, S. M., S. Zhou, and R. E. Coggeshall. 1999. "Peripheral GABA(A) receptors: evidence for peripheral primary afferent depolarization." *Neuroscience* 93 (2):713-22. doi: 10.1016/s0306-4522(99)00101-3.
Carr, R. W., R. Sittl, J. Fleckenstein, and P. Grafe. 2010. "GABA increases electrical excitability in a subset of human unmyelinated peripheral

axons." *PLoS One* 5 (1):e8780. doi: 10.1371/journal.pone.0008780.
Cavanaugh, D. J., H. Lee, L. Lo, S. D. Shields, M. J. Zylka, A. I. Basbaum, and D. J. Anderson. 2009. "Distinct subsets of unmyelinated primary sensory fibers mediate behavioral responses to noxious thermal and mechanical stimuli." *Proc Natl Acad Sci U S A* 106 (22):9075-80. doi: 10.1073/pnas.0901507106.
Chen, C. C., and C. W. Wong. 2013. "Neurosensory mechanotransduction through acid-sensing ion channels." *J Cell Mol Med* 17 (3):337-49. doi: 10.1111/jcmm.12025.
Chen, G., Y. H. Kim, H. Li, H. Luo, D. L. Liu, Z. J. Zhang, M. Lay, W. Chang, Y. Q. Zhang, and R. R. Ji. 2017. "PD-L1 inhibits acute and chronic pain by suppressing nociceptive neuron activity via PD-1." *Nat Neurosci* 20 (7):917-926. doi: 10.1038/nn.4571.
Chiu, I. M., L. B. Barrett, E. K. Williams, D. E. Strochlic, S. Lee, A. D. Weyer, S. Lou, G. S. Bryman, D. P. Roberson, N. Ghasemlou, C. Piccoli, E. Ahat, V. Wang, E. J. Cobos, C. L. Stucky, Q. Ma, S. D. Liberles, and C. J. Woolf. 2014. "Transcriptional profiling at whole population and single cell levels reveals somatosensory neuron molecular diversity." *Elife* 3. doi: 10.7554/eLife.04660.
Choi, Y., Y. W. Yoon, H. S. Na, S. H. Kim, and J. M. Chung. 1994. "Behavioral signs of ongoing pain and cold allodynia in a rat model of neuropathic pain." *Pain* 59 (3):369-76. doi: 10.1016/0304-3959(94)90023-x.
Chung, G., S. J. Jung, and S. B. Oh. 2013. "Cellular and molecular mechanisms of dental nociception." *J Dent Res* 92 (11):948-55. doi: 10.1177/0022034513501877.
Clapham, D. E. 2002. "Signal transduction. Hot and cold TRP ion channels." *Science* 295 (5563):2228-9. doi: 10.1126/science.1070766.
Colburn, R. W., M. L. Lubin, D. J. Stone, Jr., Y. Wang, D. Lawrence, M. R. D'Andrea, M. R. Brandt, Y. Liu, C. M. Flores, and N. Qin. 2007. "Attenuated cold sensitivity in TRPM8 null mice." *Neuron* 54 (3):379-86. doi: 10.1016/j.neuron.2007.04.017.
Cook, S. P., L. Vulchanova, K. M. Hargreaves, R. Elde, and E. W. McCleskey. 1997. "Distinct ATP receptors on pain-sensing and stretch-sensing neurons." *Nature* 387 (6632):505-8. doi: 10.1038/387505a0.
Coull, J. A., S. Beggs, D. Boudreau, D. Boivin, M. Tsuda, K. Inoue, C. Gravel, M. W. Salter, and Y. De Koninck. 2005. "BDNF from microglia causes the shift in neuronal anion gradient underlying neuropathic pain." *Nature* 438 (7070):1017-21. doi: 10.1038/nature04223.
Cuenin, M. F., M. J. Scheidt, R. B. O'Neal, S. L. Strong, D. H. Pashley, J. A.

Horner, and T. E. Van Dyke. 1991. "An in vivo study of dentin sensitivity: the relation of dentin sensitivity and the patency of dentin tubules." *J Periodontol* 62 (11):668-73. doi: 10.1902/jop.1991.62.11.668.

Dababneh, R. H., A. T. Khouri, and M. Addy. 1999. "Dentine hypersensitivity - an enigma? A review of terminology, mechanisms, aetiology and management." *Br Dent J* 187 (11):606-11; discussion 603. doi: 10.1038/sj.bdj.4800345a.

Dhaka, A., A. N. Murray, J. Mathur, T. J. Earley, M. J. Petrus, and A. Patapoutian. 2007. "TRPM8 is required for cold sensation in mice." *Neuron* 54 (3):371-8. doi: 10.1016/j.neuron.2007.02.024.

Diver, M. M., Y. Cheng, and D. Julius. 2019. "Structural insights into TRPM8 inhibition and desensitization." *Science* 365 (6460):1434-1440. doi: 10.1126/science.aax6672.

Dixon, W. J. 1991. "Staircase bioassay: the up-and-down method." *Neurosci Biobehav Rev* 15 (1):47-50. doi: 10.1016/s0149-7634(05)80090-9.

Djouhri, L., S. Koutsikou, X. Fang, S. McMullan, and S. N. Lawson. 2006. "Spontaneous pain, both neuropathic and inflammatory, is related to frequency of spontaneous firing in intact C-fiber nociceptors." *J Neurosci* 26 (4):1281-92. doi: 10.1523/JNEUROSCI.3388-05.2006.

Dobin, A., C. A. Davis, F. Schlesinger, J. Drenkow, C. Zaleski, S. Jha, P. Batut, M. Chaisson, and T. R. Gingeras. 2013. "STAR: ultrafast universal RNA-seq aligner." *Bioinformatics* 29 (1):15-21. doi: 10.1093/bioinformatics/bts635.

Du, X., H. Hao, Y. Yang, S. Huang, C. Wang, S. Gigout, R. Ramli, X. Li, E. Jaworska, I. Edwards, J. Deuchars, Y. Yanagawa, J. Qi, B. Guan, D. B. Jaffe, H. Zhang, and N. Gamper. 2017. "Local GABAergic signaling within sensory ganglia controls peripheral nociceptive transmission." *J Clin Invest* 127 (5):1741-1756. doi: 10.1172/JCI86812.

Dubin, A. E., and A. Patapoutian. 2010. "Nociceptors: the sensors of the pain pathway." *J Clin Invest* 120 (11):3760-72. doi: 10.1172/JCI42843.

Eckert, S. P., A. Taddese, and E. W. McCleskey. 1997. "Isolation and culture of rat sensory neurons having distinct sensory modalities." *J Neurosci Methods* 77 (2):183-90. doi: 10.1016/s0165-0270(97)00125-8.

Feldman, M., and C. Barnett. 1995. "Relationships between the acidity and osmolality of popular beverages and reported postprandial heartburn." *Gastroenterology* 108 (1):125-31. doi: 10.1016/0016-5085(95)90016-0.

Fernandez-Pena, C., and F. Viana. 2013. "Targeting TRPM8 for Pain Relief."

The Open Pain Journal 6:154-164. doi: 10.2174/1876386301306010154.

Fried, K., J. Arvidsson, B. Robertson, E. Brodin, and E. Theodorsson. 1989. "Combined retrograde tracing and enzyme/immunohistochemistry of trigeminal ganglion cell bodies innervating tooth pulps in the rat." *Neuroscience* 33 (1):101-9. doi: 10.1016/0306-4522(89)90314-x.

Fried, K., and L. J. Gibbs. 2014. "Dental Pulp Innervation. " In *The Dental Pulp Biology, Pathology, and Regenerative Therapies*, edited by Michel Goldberg, 75-95. Springer, Berlin, Heidelberg.

Fried, K., B. J. Sessle, and M. Devor. 2011. "The paradox of pain from tooth pulp: low-threshold "algoneurons"?" *Pain* 152 (12):2685-9. doi: 10.1016/j.pain.2011.08.004.

Gao, Y. J., Z. Z. Xu, Y. C. Liu, Y. R. Wen, I. Decosterd, and R. R. Ji. 2010. "The c-Jun N-terminal kinase 1 (JNK1) in spinal astrocytes is required for the maintenance of bilateral mechanical allodynia under a persistent inflammatory pain condition." *Pain* 148 (2):309-19. doi: 10.1016/j.pain.2009.11.017.

Gibbs, J. L., J. L. Melnyk, and A. I. Basbaum. 2011. "Differential TRPV1 and TRPV2 channel expression in dental pulp." *J Dent Res* 90 (6):765-70. doi: 10.1177/0022034511402206.

Gold, M. S., and G. F. Gebhart. 2010. "Nociceptor sensitization in pain pathogenesis." *Nat Med* 16 (11):1248-57. doi: 10.1038/nm.2235.

Goswami, S. C., S. K. Mishra, D. Maric, K. Kaszas, G. L. Gonnella, S. J. Clokie, H. D. Kominsky, J. R. Gross, J. M. Keller, A. J. Mannes, M. A. Hoon, and M. J. Iadarola. 2014. "Molecular signatures of mouse TRPV1-lineage neurons revealed by RNA-Seq transcriptome analysis." *J Pain* 15 (12):1338-1359. doi: 10.1016/j.jpain.2014.09.010.

Gregory, N. S., A. L. Harris, C. R. Robinson, P. M. Dougherty, P. N. Fuchs, and K. A. Sluka. 2013. "An overview of animal models of pain: disease models and outcome measures." *J Pain* 14 (11):1255-69. doi: 10.1016/j.jpain.2013.06.008.

Haggard, P., and L. de Boer. 2014. "Oral somatosensory awareness." *Neurosci Biobehav Rev* 47:469-84. doi: 10.1016/j.neubiorev.2014.09.015.

Hanack, C., M. Moroni, W. C. Lima, H. Wende, M. Kirchner, L. Adelfinger, K. Schrenk-Siemens, A. Tappe-Theodor, C. Wetzel, P. H. Kuich, M. Gassmann, D. Roggenkamp, B. Bettler, G. R. Lewin, M. Selbach, and J. Siemens. 2015. "GABA blocks pathological but not acute TRPV1

pain signals." *Cell* 160 (4):759-70. doi: 10.1016/j.cell.2015.01.022.
Harris, J. A. 1998. "Using c-fos as a neural marker of pain." *Brain Res Bull* 45 (1):1-8. doi: 10.1016/s0361-9230(97)00277-3.
Hayasaki, H., Y. Sohma, K. Kanbara, K. Maemura, T. Kubota, and M. Watanabe. 2006. "A local GABAergic system within rat trigeminal ganglion cells." *Eur J Neurosci* 23 (3):745-57. doi: 10.1111/j.1460-9568.2006.04602.x.
Herbison, A. E., and S. M. Moenter. 2011. "Depolarising and hyperpolarising actions of GABA(A) receptor activation on gonadotrophin-releasing hormone neurones: towards an emerging consensus." *J Neuroendocrinol* 23 (7):557-69. doi: 10.1111/j.1365-2826.2011.02145.x.
Hill, R. Z., and D. M. Bautista. 2020. "Getting in Touch with Mechanical Pain Mechanisms." *Trends Neurosci* 43 (5):311-325. doi: 10.1016/j.tins.2020.03.004.
Hossain, M. Z., M. M. Bakri, F. Yahya, H. Ando, S. Unno, and J. Kitagawa. 2019. "The Role of Transient Receptor Potential (TRP) Channels in the Transduction of Dental Pain." *Int J Mol Sci* 20 (3). doi: 10.3390/ijms20030526.
Hu, G., K. Huang, Y. Hu, G. Du, Z. Xue, X. Zhu, and G. Fan. 2016. "Single-cell RNA-seq reveals distinct injury responses in different types of DRG sensory neurons." *Sci Rep* 6:31851. doi: 10.1038/srep31851.
Hunt, S. P., A. Pini, and G. Evan. 1987. "Induction of c-fos-like protein in spinal cord neurons following sensory stimulation." *Nature* 328 (6131):632-4. doi: 10.1038/328632a0.
Ichikawa, H., and T. Sugimoto. 2002. "The co-expression of ASIC3 with calcitonin gene-related peptide and parvalbumin in the rat trigeminal ganglion." *Brain Res* 943 (2):287-91. doi: 10.1016/s0006-8993(02)02831-7.
Institute of Medicine (US) Committee on Pain, Disability, and Chronic Illness Behavior. 1987. "The Anatomy and Physiology of Pain. " In *Pain and Disability: Clinical, Behavioral, and Public Policy Perspectives*, edited by M. Osterweis, A. Kleinman and D. Mechanic, 123-45. Washington (DC): National Academies Press (US).
Ito, K., K. Tanaka, Y. Nishibe, J. Hasegawa, and H. Ueno. 2007. "GABA-synthesizing enzyme, GAD67, from dermal fibroblasts: evidence for a new skin function." *Biochim Biophys Acta* 1770 (2):291-6. doi: 10.1016/j.bbagen.2006.09.017.
Jang, I. J., A. J. Davies, N. Akimoto, S. K. Back, P. R. Lee, H. S. Na, H. Furue,

S. J. Jung, Y. H. Kim, and S. B. Oh. 2017. "Acute inflammation reveals GABAA receptor-mediated nociception in mouse dorsal root ganglion neurons via PGE2 receptor 4 signaling." *Physiol Rep* 5 (8). doi: 10.14814/phy2.13178.

Jensen, E. C. 2013. "Quantitative analysis of histological staining and fluorescence using ImageJ." *Anat Rec (Hoboken)* 296 (3):378-81. doi: 10.1002/ar.22641.

Johnston, G. A. 2013. "Advantages of an antagonist: bicuculline and other GABA antagonists." *Br J Pharmacol* 169 (2):328-36. doi: 10.1111/bph.12127.

Julius, D. 2013. "TRP channels and pain." *Annu Rev Cell Dev Biol* 29:355-84. doi: 10.1146/annurev-cellbio-101011-155833.

Kadala, A., P. Sotelo-Hitschfeld, Z. Ahmad, P. Tripal, B. Schmid, A. Mueller, L. Bernal, Z. Winter, S. Brauchi, U. Lohbauer, K. Messlinger, J. K. Lennerz, and K. Zimmermann. 2018. "Fluorescent Labeling and 2-Photon Imaging of Mouse Tooth Pulp Nociceptors." *J Dent Res* 97 (4):460-466. doi: 10.1177/0022034517740577.

Kanaka, C., K. Ohno, A. Okabe, K. Kuriyama, T. Itoh, A. Fukuda, and K. Sato. 2001. "The differential expression patterns of messenger RNAs encoding K-Cl cotransporters (KCC1,2) and Na-K-2Cl cotransporter (NKCC1) in the rat nervous system." *Neuroscience* 104 (4):933-46. doi: 10.1016/s0306-4522(01)00149-x.

Kim, D., B. You, H. Lim, and S. J. Lee. 2011. "Toll-like receptor 2 contributes to chemokine gene expression and macrophage infiltration in the dorsal root ganglia after peripheral nerve injury." *Mol Pain* 7:74. doi: 10.1186/1744-8069-7-74.

Kim, H. Y., G. Chung, H. J. Jo, Y. S. Kim, Y. C. Bae, S. J. Jung, J. S. Kim, and S. B. Oh. 2011. "Characterization of dental nociceptive neurons." *J Dent Res* 90 (6):771-6. doi: 10.1177/0022034511399906.

Kim, Y. S., T. H. Kim, D. D. McKemy, and Y. C. Bae. 2015. "Expression of vesicular glutamate transporters in transient receptor potential melastatin 8 (TRPM8)-positive dental afferents in the mouse." *Neuroscience* 303:378-88. doi: 10.1016/j.neuroscience.2015.07.013.

Kobayashi, K., T. Fukuoka, K. Obata, H. Yamanaka, Y. Dai, A. Tokunaga, and K. Noguchi. 2005. "Distinct expression of TRPM8, TRPA1, and TRPV1 mRNAs in rat primary afferent neurons with adelta/c-fibers and colocalization with trk receptors." *J Comp Neurol* 493 (4):596-606. doi: 10.1002/cne.20794.

Kono, T., F. Nishimura, H. Sugimoto, K. Sikata, H. Makino, and Y. Murayama.

2001. "Human fibroblasts ubiquitously express glutamic acid decarboxylase 65 (GAD 65): possible effects of connective tissue inflammation on GAD antibody titer." *J Periodontol* 72 (5):598-604. doi: 10.1902/jop.2001.72.5.598.

Kuhn, F. J., C. Kuhn, and A. Luckhoff. 2009. "Inhibition of TRPM8 by icilin distinct from desensitization induced by menthol and menthol derivatives." *J Biol Chem* 284 (7):4102-11. doi: 10.1074/jbc.M806651200.

Kvinnsland, I. H., K. Luukko, I. Fristad, P. Kettunen, D. L. Jackson, K. Fjeld, C. S. von Bartheld, and M. R. Byers. 2004. "Glial cell line-derived neurotrophic factor (GDNF) from adult rat tooth serves a distinct population of large-sized trigeminal neurons." *Eur J Neurosci* 19 (8):2089-98. doi: 10.1111/j.0953-816X.2004.03291.x.

Lambert, J. J., S. C. Harney, D. Belelli, and J. A. Peters. 2001. "Neurosteroid modulation of recombinant and synaptic GABAA receptors." *Int Rev Neurobiol* 46:177-205. doi: 10.1016/s0074-7742(01)46063-6.

Le Pichon, C. E., and A. T. Chesler. 2014. "The functional and anatomical dissection of somatosensory subpopulations using mouse genetics." *Front Neuroanat* 8:21. doi: 10.3389/fnana.2014.00021.

Lee, J. Y., S. Y. Yoon, J. Won, H. B. Kim, Y. Kang, and S. B. Oh. 2017. "Sinomenine produces peripheral analgesic effects via inhibition of voltage-gated sodium currents." *Neuroscience* 358:28-36. doi: 10.1016/j.neuroscience.2017.06.024.

Lee, K., B. M. Lee, C. K. Park, Y. H. Kim, and G. Chung. 2019. "Ion Channels Involved in Tooth Pain." *Int J Mol Sci* 20 (9). doi: 10.3390/ijms20092266.

Lee, K. Y., M. Charbonnet, and M. S. Gold. 2012. "Upregulation of high-affinity GABA(A) receptors in cultured rat dorsal root ganglion neurons." *Neuroscience* 208:133-42. doi: 10.1016/j.neuroscience.2012.01.050.

Lee, M., E. G. McGeer, and P. L. McGeer. 2011. "Mechanisms of GABA release from human astrocytes." *Glia* 59 (11):1600-11. doi: 10.1002/glia.21202.

Lee, M., C. Schwab, and P. L. McGeer. 2011. "Astrocytes are GABAergic cells that modulate microglial activity." *Glia* 59 (1):152-65. doi: 10.1002/glia.21087.

Lee, P. R., J. Y. Lee, H. B. Kim, J. H. Lee, and S. B. Oh. 2020. "TRPM8 Mediates Hyperosmotic Stimuli-Induced Nociception in Dental Afferents." *J Dent Res* 99 (1):107-114. doi:

10.1177/0022034519886847.
Lee, P. R., S. Y. Yoon, H. W. Kim, J. H. Yeo, Y. H. Kim, and S. B. Oh. 2018. "Peripheral GABAA receptor-mediated signaling facilitates persistent inflammatory hypersensitivity." *Neuropharmacology* 135:572-580. doi: 10.1016/j.neuropharm.2018.04.009.
Lee, S., B. E. Yoon, K. Berglund, S. J. Oh, H. Park, H. S. Shin, G. J. Augustine, and C. J. Lee. 2010. "Channel-mediated tonic GABA release from glia." *Science* 330 (6005):790-6. doi: 10.1126/science.1184334.
Levy, R. A. 1977. "The role of GABA in primary afferent depolarization." *Prog Neurobiol* 9 (4):211-67. doi: 10.1016/0301-0082(77)90002-8.
Li, C. L., K. C. Li, D. Wu, Y. Chen, H. Luo, J. R. Zhao, S. S. Wang, M. M. Sun, Y. J. Lu, Y. Q. Zhong, X. Y. Hu, R. Hou, B. B. Zhou, L. Bao, H. S. Xiao, and X. Zhang. 2016. "Somatosensory neuron types identified by high-coverage single-cell RNA-sequencing and functional heterogeneity." *Cell Res* 26 (1):83-102. doi: 10.1038/cr.2015.149.
Li, C., S. Wang, Y. Chen, and X. Zhang. 2018. "Somatosensory Neuron Typing with High-Coverage Single-Cell RNA Sequencing and Functional Analysis." *Neurosci Bull* 34 (1):200-207. doi: 10.1007/s12264-017-0147-9.
Li, P., Y. Zheng, and X. Chen. 2017. "Drugs for Autoimmune Inflammatory Diseases: From Small Molecule Compounds to Anti-TNF Biologics." *Front Pharmacol* 8:460. doi: 10.3389/fphar.2017.00460.
Lin, Q., J. Wu, and W. D. Willis. 1999. "Dorsal root reflexes and cutaneous neurogenic inflammation after intradermal injection of capsaicin in rats." *J Neurophysiol* 82 (5):2602-11. doi: 10.1152/jn.1999.82.5.2602.
Liu, B., L. Fan, S. Balakrishna, A. Sui, J. B. Morris, and S. E. Jordt. 2013. "TRPM8 is the principal mediator of menthol-induced analgesia of acute and inflammatory pain." *Pain* 154 (10):2169-77. doi: 10.1016/j.pain.2013.06.043.
Liu, C. C., Y. J. Gao, H. Luo, T. Berta, Z. Z. Xu, R. R. Ji, and P. H. Tan. 2016. "Interferon alpha inhibits spinal cord synaptic and nociceptive transmission via neuronal-glial interactions." *Sci Rep* 6:34356. doi: 10.1038/srep34356.
Llorian-Salvador, M., M. Pevida, S. Gonzalez-Rodriguez, A. Lastra, M. T. Fernandez-Garcia, A. Hidalgo, A. Baamonde, and L. Menendez. 2016. "Analgesic effects evoked by a CCR2 antagonist or an anti-CCL2 antibody in inflamed mice." *Fundam Clin Pharmacol* 30 (3):235-47. doi: 10.1111/fcp.12182.
Lolignier, S., N. Eijkelkamp, and J. N. Wood. 2015. "Mechanical allodynia."

Pflugers Arch 467 (1):133-9. doi: 10.1007/s00424-014-1532-0.

Maddox, F. N., A. Y. Valeyev, K. Poth, A. M. Holohean, P. M. Wood, R. A. Davidoff, J. C. Hackman, and C. W. Luetje. 2004. "GABAA receptor subunit mRNA expression in cultured embryonic and adult human dorsal root ganglion neurons." *Brain Res Dev Brain Res* 149 (2):143-51. doi: 10.1016/j.devbrainres.2004.01.001.

Magnaghi, V. 2007. "GABA and neuroactive steroid interactions in glia: new roles for old players?" *Curr Neuropharmacol* 5 (1):47-64. doi: 10.2174/157015907780077132.

Magnaghi, V., M. Ballabio, A. Consoli, J. J. Lambert, I. Roglio, and R. C. Melcangi. 2006. "GABA receptor-mediated effects in the peripheral nervous system: A cross-interaction with neuroactive steroids." *J Mol Neurosci* 28 (1):89-102. doi: 10.1385/JMN:30:3:341.

Majewska, M. D. 1990. "Steroid regulation of the GABAA receptor: ligand binding, chloride transport and behaviour." *Ciba Found Symp* 153:83-97; discussion 97-106. doi: 10.1002/9780470513989.ch5.

Markowitz, K., and D. Pashley. 2015. "*The Physiological Basis of Dentin Hypersensitivity*." In *Dentine Hypersensitivity : Advances in Diagnosis, Management, and Treatment*, edited by David G. Gillam, 11-39. Springer, Cham.

Matthews, B., and N. Vongsavan. 1994. "Interactions between neural and hydrodynamic mechanisms in dentine and pulp." *Arch Oral Biol* 39 Suppl:87S-95S. doi: 10.1016/0003-9969(94)90193-7.

McKemy, D. D., W. M. Neuhausser, and D. Julius. 2002. "Identification of a cold receptor reveals a general role for TRP channels in thermosensation." *Nature* 416 (6876):52-8. doi: 10.1038/nature719.

Megat, S., P. R. Ray, D. Tavares-Ferreira, J. K. Moy, I. Sankaranarayanan, A. Wanghzou, T. Fang Lou, P. Barragan-Iglesias, Z. T. Campbell, G. Dussor, and T. J. Price. 2019. "Differences between Dorsal Root and Trigeminal Ganglion Nociceptors in Mice Revealed by Translational Profiling." *J Neurosci* 39 (35):6829-6847. doi: 10.1523/JNEUROSCI.2663-18.2019.

Meier, M. L., M. Brugger, D. A. Ettlin, R. Luechinger, A. Barlow, L. Jancke, and K. Lutz. 2012. "Brain activation induced by dentine hypersensitivity pain--an fMRI study." *J Clin Periodontol* 39 (5):441-7. doi: 10.1111/j.1600-051X.2012.01863.x.

Michot, B., C. S. Lee, and J. L. Gibbs. 2018. "TRPM8 and TRPA1 do not contribute to dental pulp sensitivity to cold." *Sci Rep* 8 (1):13198. doi: 10.1038/s41598-018-31487-2.

Mitchell, Rory, and Susan Fleetwood-Walker. 2015. "TRPM8 as a Target for Analgesia." In *TRP Channels as Therapeutic Targets*, 239-62. http://dx.doi.org/10.1016/B978-0-12-420024-1.00014-X.

Mogil, J. S. 2009. "Animal models of pain: progress and challenges." *Nat Rev Neurosci* 10 (4):283-94. doi: 10.1038/nrn2606.

Mogil, J. S., and S. E. Crager. 2004. "What should we be measuring in behavioral studies of chronic pain in animals?" *Pain* 112 (1-2):12-5. doi: 10.1016/j.pain.2004.09.028.

Muench, Kristin. 2015. "Pain in the Brain." http://www.neuwritewest.org/blog/pain-in-the-brain.

Murthy, S. E., M. C. Loud, I. Daou, K. L. Marshall, F. Schwaller, J. Kuhnemund, A. G. Francisco, W. T. Keenan, A. E. Dubin, G. R. Lewin, and A. Patapoutian. 2018. "The mechanosensitive ion channel Piezo2 mediates sensitivity to mechanical pain in mice." *Sci Transl Med* 10 (462). doi: 10.1126/scitranslmed.aat9897.

Narhi, M., E. Jyvasjarvi, A. Virtanen, T. Huopaniemi, D. Ngassapa, and T. Hirvonen. 1992. "Role of intradental A- and C-type nerve fibres in dental pain mechanisms." *Proc Finn Dent Soc* 88 Suppl 1:507-16.

Nectar Lifesciences. n.d. "Applications." Accessed June 13, 2020. http://nectarmenthol.com/applications/.

Nguyen, M. Q., Y. Wu, L. S. Bonilla, L. J. von Buchholtz, and N. J. P. Ryba. 2017. "Diversity amongst trigeminal neurons revealed by high throughput single cell sequencing." *PLoS One* 12 (9):e0185543. doi: 10.1371/journal.pone.0185543.

Ohya, A. 1992. "Responses of trigeminal subnucleus interpolaris neurons to afferent inputs from deep oral structures." *Brain Res Bull* 29 (6):773-81. doi: 10.1016/0361-9230(92)90145-n.

Olsen, R. W. 2006. "Picrotoxin-like channel blockers of GABAA receptors." *Proc Natl Acad Sci U S A* 103 (16):6081-2. doi: 10.1073/pnas.0601121103.

Olsen, R. W., and W. Sieghart. 2008. "International Union of Pharmacology. LXX. Subtypes of gamma-aminobutyric acid(A) receptors: classification on the basis of subunit composition, pharmacology, and function. Update." *Pharmacol Rev* 60 (3):243-60. doi: 10.1124/pr.108.00505.

Olsen, R. W., and W. Sieghart. 2009. "GABA A receptors: subtypes provide diversity of function and pharmacology." *Neuropharmacology* 56 (1):141-8. doi: 10.1016/j.neuropharm.2008.07.045.

Orchardson, R., and D. G. Gillam. 2006. "Managing dentin hypersensitivity."

J Am Dent Assoc 137 (7):990-8; quiz 1028-9. doi: 10.14219/jada.archive.2006.0321.

Pan, Y., E. F. Wheeler, J. M. Bernanke, H. Yang, and J. P. Naftel. 2003. "A model experimental system for monitoring changes in sensory neuron phenotype evoked by tooth injury." *J Neurosci Methods* 126 (1):99-109. doi: 10.1016/s0165-0270(03)00071-2.

Park, C. K. 2015. "Maresin 1 Inhibits TRPV1 in Temporomandibular Joint-Related Trigeminal Nociceptive Neurons and TMJ Inflammation-Induced Synaptic Plasticity in the Trigeminal Nucleus." *Mediators Inflamm* 2015:275126. doi: 10.1155/2015/275126.

Park, C. K., M. S. Kim, Z. Fang, H. Y. Li, S. J. Jung, S. Y. Choi, S. J. Lee, K. Park, J. S. Kim, and S. B. Oh. 2006. "Functional expression of thermo-transient receptor potential channels in dental primary afferent neurons: implication for tooth pain." *J Biol Chem* 281 (25):17304-11. doi: 10.1074/jbc.M511072200.

Peier, A. M., A. Moqrich, A. C. Hergarden, A. J. Reeve, D. A. Andersson, G. M. Story, T. J. Earley, I. Dragoni, P. McIntyre, S. Bevan, and A. Patapoutian. 2002. "A TRP channel that senses cold stimuli and menthol." *Cell* 108 (5):705-15. doi: 10.1016/s0092-8674(02)00652-9.

Pellesi, L., S. Guerzoni, and L. A. Pini. 2017. "Spotlight on Anti-CGRP Monoclonal Antibodies in Migraine: The Clinical Evidence to Date." *Clin Pharmacol Drug Dev*. doi: 10.1002/cpdd.345.

Petitpre, C., H. Wu, A. Sharma, A. Tokarska, P. Fontanet, Y. Wang, F. Helmbacher, K. Yackle, G. Silberberg, S. Hadjab, and F. Lallemend. 2018. "Neuronal heterogeneity and stereotyped connectivity in the auditory afferent system." *Nat Commun* 9 (1):3691. doi: 10.1038/s41467-018-06033-3.

Prato, V., F. J. Taberner, J. R. F. Hockley, G. Callejo, A. Arcourt, B. Tazir, L. Hammer, P. Schad, P. A. Heppenstall, E. S. Smith, and S. G. Lechner. 2017. "Functional and Molecular Characterization of Mechanoinsensitive "Silent" Nociceptors." *Cell Rep* 21 (11):3102-3115. doi: 10.1016/j.celrep.2017.11.066.

Price, T. J., F. Cervero, M. S. Gold, D. L. Hammond, and S. A. Prescott. 2009. "Chloride regulation in the pain pathway." *Brain Res Rev* 60 (1):149-70. doi: 10.1016/j.brainresrev.2008.12.015.

Price, T. J., K. M. Hargreaves, and F. Cervero. 2006. "Protein expression and mRNA cellular distribution of the NKCC1 cotransporter in the dorsal root and trigeminal ganglia of the rat." *Brain Res* 1112 (1):146-58.

doi: 10.1016/j.brainres.2006.07.012.
Proudfoot, C. J., E. M. Garry, D. F. Cottrell, R. Rosie, H. Anderson, D. C. Robertson, S. M. Fleetwood-Walker, and R. Mitchell. 2006. "Analgesia mediated by the TRPM8 cold receptor in chronic neuropathic pain." *Curr Biol* 16 (16):1591-605. doi: 10.1016/j.cub.2006.07.061.
Quallo, T., N. Vastani, E. Horridge, C. Gentry, A. Parra, S. Moss, F. Viana, C. Belmonte, D. A. Andersson, and S. Bevan. 2015. "TRPM8 is a neuronal osmosensor that regulates eye blinking in mice." *Nat Commun* 6:7150. doi: 10.1038/ncomms8150.
Ren, K. 1999. "An improved method for assessing mechanical allodynia in the rat." *Physiol Behav* 67 (5):711-6. doi: 10.1016/s0031-9384(99)00136-5.
Ren, K., and R. Dubner. 1993. "NMDA receptor antagonists attenuate mechanical hyperalgesia in rats with unilateral inflammation of the hindpaw." *Neurosci Lett* 163 (1):22-6. doi: 10.1016/0304-3940(93)90220-f.
Ren, K., and R. Dubner. 2011. "The role of trigeminal interpolaris-caudalis transition zone in persistent orofacial pain." *Int Rev Neurobiol* 97:207-25. doi: 10.1016/B978-0-12-385198-7.00008-4.
Rossi, H. L., L. P. See, W. Foster, S. Pitake, J. Gibbs, B. Schmidt, C. H. Mitchell, and I. Abdus-Saboor. 2020. "Evoked and spontaneous pain assessment during tooth pulp injury." *Sci Rep* 10 (1):2759. doi: 10.1038/s41598-020-59742-5.
Satija, R., J. A. Farrell, D. Gennert, A. F. Schier, and A. Regev. 2015. "Spatial reconstruction of single-cell gene expression data." *Nat Biotechnol* 33 (5):495-502. doi: 10.1038/nbt.3192.
Sato, M., U. Sobhan, M. Tsumura, H. Kuroda, M. Soya, A. Masamura, A. Nishiyama, A. Katakura, T. Ichinohe, M. Tazaki, and Y. Shibukawa. 2013. "Hypotonic-induced stretching of plasma membrane activates transient receptor potential vanilloid channels and sodium-calcium exchangers in mouse odontoblasts." *J Endod* 39 (6):779-87. doi: 10.1016/j.joen.2013.01.012.
Sawamura, S., M. Fujinaga, W. S. Kingery, N. Belanger, M. F. Davies, and M. Maze. 1999. "Opioidergic and adrenergic modulation of formalin-evoked spinal c-fos mRNA expression and nocifensive behavior in the rat." *Eur J Pharmacol* 379 (2-3):141-9. doi: 10.1016/s0014-2999(99)00463-x.
Scholz, J., and C. J. Woolf. 2002. "Can we conquer pain?" *Nat Neurosci* 5

Suppl:1062-7. doi: 10.1038/nn942.
Schuh, Cmap, B. Benso, and S. Aguayo. 2019. "Potential Novel Strategies for the Treatment of Dental Pulp-Derived Pain: Pharmacological Approaches and Beyond." *Front Pharmacol* 10:1068. doi: 10.3389/fphar.2019.01068.
Sharma, N., K. Flaherty, K. Lezgiyeva, D. E. Wagner, A. M. Klein, and D. D. Ginty. 2020. "The emergence of transcriptional identity in somatosensory neurons." *Nature* 577 (7790):392-398. doi: 10.1038/s41586-019-1900-1.
Shekhar, K., S. W. Lapan, I. E. Whitney, N. M. Tran, E. Z. Macosko, M. Kowalczyk, X. Adiconis, J. Z. Levin, J. Nemesh, M. Goldman, S. A. McCarroll, C. L. Cepko, A. Regev, and J. R. Sanes. 2016. "Comprehensive Classification of Retinal Bipolar Neurons by Single-Cell Transcriptomics." *Cell* 166 (5):1308-1323 e30. doi: 10.1016/j.cell.2016.07.054.
Shiau, H. J. 2012. "Dentin hypersensitivity." *J Evid Based Dent Pract* 12 (3 Suppl):220-8. doi: 10.1016/S1532-3382(12)70043-X.
Shrestha, B. R., C. Chia, L. Wu, S. G. Kujawa, M. C. Liberman, and L. V. Goodrich. 2018. "Sensory Neuron Diversity in the Inner Ear Is Shaped by Activity." *Cell* 174 (5):1229-1246 e17. doi: 10.1016/j.cell.2018.07.007.
Si, J. Q., Z. W. Li, H. Z. Hu, X. P. Zhou, and B. C. Guan. 1997. "Inhibitory effect of baclofen on GABA-induced depolarization and GABA-activated current in primary sensory neurons." *Neuroscience* 81 (3):821-7. doi: 10.1016/s0306-4522(97)00107-3.
Sieghart, W. 1995. "Structure and pharmacology of gamma-aminobutyric acidA receptor subtypes." *Pharmacol Rev* 47 (2):181-234.
Simon, J., H. Wakimoto, N. Fujita, M. Lalande, and E. A. Barnard. 2004. "Analysis of the set of GABA(A) receptor genes in the human genome." *J Biol Chem* 279 (40):41422-35. doi: 10.1074/jbc.M401354200.
Soghomonian, J. J., and D. L. Martin. 1998. "Two isoforms of glutamate decarboxylase: why?" *Trends Pharmacol Sci* 19 (12):500-5. doi: 10.1016/s0165-6147(98)01270-x.
Sole-Magdalena, A., M. Martinez-Alonso, C. A. Coronado, L. M. Junquera, J. Cobo, and J. A. Vega. 2018. "Molecular basis of dental sensitivity: The odontoblasts are multisensory cells and express multifunctional ion channels." *Ann Anat* 215:20-29. doi: 10.1016/j.aanat.2017.09.006.
Sood, S., M. Nagpal, S. Gupta, and A. Jain. 2016. "Evaluation of dentine

hypersensitivity in adult population with chronic periodontitis visiting dental hospital in Chandigarh." *Indian J Dent Res* 27 (3):249-55. doi: 10.4103/0970-9290.186239.

Starr, C. J., L. Sawaki, G. F. Wittenberg, J. H. Burdette, Y. Oshiro, A. S. Quevedo, and R. C. Coghill. 2009. "Roles of the insular cortex in the modulation of pain: insights from brain lesions." *J Neurosci* 29 (9):2684-94. doi: 10.1523/JNEUROSCI.5173-08.2009.

Stuart, T., A. Butler, P. Hoffman, C. Hafemeister, E. Papalexi, W. M. Mauck, 3rd, Y. Hao, M. Stoeckius, P. Smibert, and R. Satija. 2019. "Comprehensive Integration of Single-Cell Data." *Cell* 177 (7):1888-1902 e21. doi: 10.1016/j.cell.2019.05.031.

Stucky, C. L., and G. R. Lewin. 1999. "Isolectin B(4)-positive and -negative nociceptors are functionally distinct." *J Neurosci* 19 (15):6497-505. doi: 10.1523/JNEUROSCI.19-15-06497.1999.

Sung, K. W., M. Kirby, M. P. McDonald, D. M. Lovinger, and E. Delpire. 2000. "Abnormal GABAA receptor-mediated currents in dorsal root ganglion neurons isolated from Na-K-2Cl cotransporter null mice." *J Neurosci.*:7531-7538. doi: 10.1523/JNEUROSCI.20-20-07531.2000.

Takeda, M., T. Tanimoto, M. Ikeda, J. Kadoi, and S. Matsumoto. 2004. "Activaton of GABAB receptor inhibits the excitability of rat small diameter trigeminal root ganglion neurons." *Neuroscience* 123 (2):491-505. doi: 10.1016/j.neuroscience.2003.09.022.

Tappe-Theodor, A., and R. Kuner. 2014. "Studying ongoing and spontaneous pain in rodents--challenges and opportunities." *Eur J Neurosci* 39 (11):1881-90. doi: 10.1111/ejn.12643.

Thakur, M., M. Crow, N. Richards, G. I. Davey, E. Levine, J. H. Kelleher, C. C. Agley, F. Denk, S. D. Harridge, and S. B. McMahon. 2014. "Defining the nociceptor transcriptome." *Front Mol Neurosci* 7:87. doi: 10.3389/fnmol.2014.00087.

Tian, N., C. Petersen, S. Kash, S. Baekkeskov, D. Copenhagen, and R. Nicoll. 1999. "The role of the synthetic enzyme GAD65 in the control of neuronal gamma-aminobutyric acid release." *Proc Natl Acad Sci U S A* 96 (22):12911-6. doi: 10.1073/pnas.96.22.12911.

Toyoda, H., J. Yamada, S. Ueno, A. Okabe, H. Kato, K. Sato, K. Hashimoto, and A. Fukuda. 2005. "Differential functional expression of cation-Cl-cotransporter mRNAs (KCC1, KCC2, and NKCC1) in rat trigeminal nervous system." *Brain Res Mol Brain Res* 133 (1):12-8. doi: 10.1016/j.molbrainres.2004.09.015.

Tsumura, M., U. Sobhan, M. Sato, M. Shimada, A. Nishiyama, A. Kawaguchi,

M. Soya, H. Kuroda, M. Tazaki, and Y. Shibukawa. 2013. "Functional expression of TRPM8 and TRPA1 channels in rat odontoblasts." *PLoS One* 8 (12):e82233. doi: 10.1371/journal.pone.0082233.

Usoskin, D., A. Furlan, S. Islam, H. Abdo, P. Lonnerberg, D. Lou, J. Hjerling-Leffler, J. Haeggstrom, O. Kharchenko, P. V. Kharchenko, S. Linnarsson, and P. Ernfors. 2015. "Unbiased classification of sensory neuron types by large-scale single-cell RNA sequencing." *Nat Neurosci* 18 (1):145-53. doi: 10.1038/nn.3881.

Uusi-Oukari, M., and E. R. Korpi. 2010. "Regulation of GABA(A) receptor subunit expression by pharmacological agents." *Pharmacol Rev* 62 (1):97-135. doi: 10.1124/pr.109.002063.

Vierck, C. J., P. T. Hansson, and R. P. Yezierski. 2008. "Clinical and pre-clinical pain assessment: are we measuring the same thing?" *Pain* 135 (1-2):7-10. doi: 10.1016/j.pain.2007.12.008.

Wang, H. C., K. I. Cheng, P. R. Chen, K. Y. Tseng, A. L. Kwan, and L. L. Chang. 2018. "Glycine receptors expression in rat spinal cord and dorsal root ganglion in prostaglandin E2 intrathecal injection models." *BMC Neurosci* 19 (1):72. doi: 10.1186/s12868-018-0470-8.

Wasner, G., J. Schattschneider, A. Binder, and R. Baron. 2004. "Topical menthol--a human model for cold pain by activation and sensitization of C nociceptors." Brain 127 (Pt 5):1159-71. doi: 10.1093/brain/awh134.

Willis, W. D., Jr. 1999. "Dorsal root potentials and dorsal root reflexes: a double-edged sword." *Exp Brain Res* 124 (4):395-421. doi: 10.1007/s002210050637.

Won, J., H. Vang, J. H. Kim, P. R. Lee, Y. Kang, and S. B. Oh. 2018. "TRPM7 Mediates Mechanosensitivity in Adult Rat Odontoblasts." *J Dent Res* 97 (9):1039-1046. doi: 10.1177/0022034518759947.

Won, J., H. Vang, P. R. Lee, Y. H. Kim, H. W. Kim, Y. Kang, and S. B. Oh. 2017. "Piezo2 Expression in Mechanosensitive Dental Primary Afferent Neurons." *J Dent Res* 96 (8):931-937. doi: 10.1177/0022034517702342.

Won, Jonghwa, and Seog Bae Oh. 2019. "Update on dentin hypersensitivity: with the focus on hydrodynamic theory and mechanosensitive ion channels." *International Journal of Oral Biology* 44 (3):71-76. doi: 10.11620/ijob.2019.44.3.71.

Xiao, W. H., and G. J. Bennett. 2007. "Persistent low-frequency spontaneous discharge in A-fiber and C-fiber primary afferent neurons during an inflammatory pain condition." *Anesthesiology* 107 (5):813-21. doi:

10.1097/01.anes.0000286983.33184.9c.
Yamamoto, T., and T. L. Yaksh. 1991. "Spinal pharmacology of thermal hyperesthesia induced by incomplete ligation of sciatic nerve. I. Opioid and nonopioid receptors." *Anesthesiology* 75 (5):817-26. doi: 10.1097/00000542-199111000-00014.
Yamamoto, T., and T. L. Yaksh. 1993. "Effects of intrathecal strychnine and bicuculline on nerve compression-induced thermal hyperalgesia and selective antagonism by MK-801." *Pain* 54 (1):79-84. doi: 10.1016/0304-3959(93)90102-u.
Yudin, Y., V. Lukacs, C. Cao, and T. Rohacs. 2011. "Decrease in phosphatidylinositol 4,5-bisphosphate levels mediates desensitization of the cold sensor TRPM8 channels." *J Physiol* 589 (Pt 24):6007-27. doi: 10.1113/jphysiol.2011.220228.
Zhang, M., Y. Wang, J. Geng, S. Zhou, and B. Xiao. 2019. "Mechanically Activated Piezo Channels Mediate Touch and Suppress Acute Mechanical Pain Response in Mice." *Cell Rep* 26 (6):1419-1431 e4. doi: 10.1016/j.celrep.2019.01.056.
Zhang, X. L., K. Y. Lee, B. T. Priest, I. Belfer, and M. S. Gold. 2015. "Inflammatory mediator-induced modulation of GABAA currents in human sensory neurons." *Neuroscience* 310:401-9. doi: 10.1016/j.neuroscience.2015.09.048.
Zhang, Z. J., D. L. Cao, X. Zhang, R. R. Ji, and Y. J. Gao. 2013. "Chemokine contribution to neuropathic pain: respective induction of CXCL1 and CXCR2 in spinal cord astrocytes and neurons." *Pain* 154 (10):2185-97. doi: 10.1016/j.pain.2013.07.002.
Zhu, Qin, Stephen A. Fisher, Jamie Shallcross, and Junhyong Kim. 2016. "VERSE: a versatile and efficient RNA-Seq read counting tool." *bioRxiv* doi: 10.1101/053306.
Zhu, Y., S. Dua, and M. S. Gold. 2012. "Inflammation-induced shift in spinal GABA(A) signaling is associated with a tyrosine kinase-dependent increase in GABA(A) current density in nociceptive afferents." *J Neurophysiol* 108 (9):2581-93. doi: 10.1152/jn.00590.2012.
Zhu, Y., S. G. Lu, and M. S. Gold. 2012. "Persistent inflammation increases GABA-induced depolarization of rat cutaneous dorsal root ganglion neurons in vitro." *Neuroscience* 220:330-40. doi: 10.1016/j.neuroscience.2012.06.025.

국문초록

통증 감각의 말초 병태생리 기전

: 세포 기전 및 단일 세포 전사체 프로파일링에

관한 연구

신체와 구강악안면 영역에서 경험되는 통증 감각은 후근신경절(dorsal root ganglion)과 삼차신경절(trigeminal ganglion)과 같은 말초 감각 신경을 통해 중추 신경계로 전달된다. 일반적인 통증 감각은 유해감수기(nociceptor)로 불리는 특수한 말초 감각 신경의 말단에서 시작하고 이러한 유해감수기는 유해 자극에 주로 반응한다. 지금까지 열, 저온, 화학 물질 또는 기계적 자극과 같은 다양한 유해 자극에 반응하는 유해감수기에 대해서는 잘 연구되었지만 특수한 병태생리학적 상황에서는 무해한 자극도 통증을 일으킬 수 있는데, 이에 대한 기전은 아직 완전하게 규명되지 않았다. 따라서 본 학위 논문은 여러 유형의 병태생리 상태에서 무해 자극 또는 염증으로 인한 내생적 매개체(endogenous mediator)에 의해서 활성화될 수 있는 통증 감각의 기전을 세포, 분자 생물학 및 동물행동학적 수준에서 다음과 같이 탐구하고

자 했다.

첫 번째 장에서는 염증 상태에서 내생적 감마아미노 낙산(GABA)에 의해 활성화 될 수 있는 감마아미노 낙산 유형 A 수용체($GABA_AR$)의 역할을 조사했다. CFA로 유도된 염증성 통증 마우스 모델을 사용하여, 후근신경절의 말단에 발현하고 있는 감마아미노 낙산 유형 A 수용체의 활성을 줄이기 위한 선택적 억제제의 사용 또는 항-감마아미노 낙산 항체를 염증 부위에 주사하여 내생적 감마아미노 낙산을 직접적으로 차단함으로써 조절했을 때, CFA로 유도된 자발적 통증 행동(spontaneous nociceptive behavior)과 기계적 자극에 대한 통각과민(mechanical hypersensitivity)이 감소했다. 이와는 반대로 감마아미노 낙산 유형 A 수용체의 활성을 양성 입체다른자리 조절자로 증가시켰을 때는 정상 마우스에서도 기계적 자극에 대한 이질통(mechanical allodynia)이 증가했다. 이를 통해 말초 감각 신경의 감마아미노 낙산 유형 A 수용체를 매개로 하는 신호 전달이 염증성 통증 조절을 위한 새로운 치료 표적이 될 수 있음을 입증했다.

두 번째 장에서는 단 물질이 어떻게 치수유래 일차 구심성 신경(dental primary afferent neuron)을 자극하여 상아질 과민증(dentin hypersensitivity)을 유발하는지에 대한 세포 기전을 탐색했다. 설탕 농도가 높은 단 물질은 삼투압이 높기 때문에 우리가 단 음식을 섭취할 때 치아는 고삼투압 상태가 되며, 단 음식은 치통을 빈번하게 유발한다. 따라서, TRPM8 이온 채널-저온

과 멘톨 수용체로 잘 알려져 있지만 특별히 각막 신경에서는 각막의 건조와 같은 고삼투압 상태에서 눈의 깜빡임을 조절하는 것으로 보고됨-이 치수유래 일차 구심성 신경에서 고삼투압 자극에 활성화되어 통증 감각을 전달할 수 있음을 확인하고자 했다. 마우스의 치수유래 일차 구심성 신경 세포에는 TRPM8이 기능적으로 발현하고 있었으며, 살아있는 마우스의 치아 상아질을 노출시키고 고삼투압성의 설탕 용액을 적용함으로써 유발된 통증 감각이 TRPM8의 선택적 억제제에 의해서 현저하게 감소되는 것을 중추신경계 수준에서 확인했다. 따라서, 단 물질과 같은 무해한 자극이 TRPM8 채널을 통해 치통을 유발할 수 있음을 증명했다.

최근에 점점 더 많은 연구가 단일 세포 수준의 전사유전체학(single-cell transcriptomics)을 사용하여 혼합된 세포 집단 또는 복잡한 감각 신경 시스템에서 세포의 이종성, 희귀한 세포 유형, 새로운 치료 표적을 성공적으로 발견하고 있다. 세 번째 장에서는 마우스의 치수유래 일차 구심성 신경 세포에서 보이는 독특한 유전자 발현을 탐색하기 위해 단일 세포 수준의 RNA 시퀀싱(single-cell RNA sequencing) 기술과 현장혼성화(*in situ* hybridization) 조직 염색 기법을 도입했다. 단일 세포 수준의 전사체 프로파일링을 통해 치아 신경에서 여섯 개의 구별된 세포 집단(cluster)들이 존재하는 것을 발견했다. 흥미롭게도 가장 큰 집단은 약한 기계적 자극에 활성화 되는 Piezo2 이온 채널과 CGRP(칼시토닌 연관 단백질)를 부호화(encoding)하는 통증 관련

신경전달물질인 Calca의 높은 발현을 특징으로 했다. 이러한 발견은 치아의 신경세포가 피부 영역에 분포 되어 있는 다른 감각 신경과는 달리, 칫솔질 또는 공기 분사와 같은 약한 기계적 자극이 빈번하게 상아질 과민증을 발생시키는 기전을 설명하며, 이는 기존에 중요하게 제안된 유체역학 이론(hydrodynamic theory)을 입증했다. 추가적으로 나는 치통에 중요하게 관여할 수 있는 기계적 감각 이온 채널들과 본 연구의 임상적 적용에 대해서 논의했다.

주요어: 통증; 유해감수기; 기전 연구; 단일 세포 전사체 시퀀싱; 감마 아미노낙산 유형 A 수용체; TRPM8 이온 채널; 후근신경절; 치수유래 일차 구심성 신경

학번: 2015-22670